UNIVERSITY OF LILLE

Doctoral School
Submitted in partial fulfillment of the requirements

for the degree of

Doctor of Philosophy (PhD)

in Biochemistry and Molecular Biology
by

CHANYARAK SOMBUTKAYASITH

Defended on 31 October 2025

Glycan-Based Interactions of Infectious Hypodermal and Hematopoietic Necrosis Virus (IHHNV) with Host Tissues

Thesis advisors:

Prof. Yann Guérardel – Université de Lille

Prof. Wattana Weerachatyanukul – Mahidol University

Reviewers:

Assoc. Prof. Pitchanee Jariyapong – Walailak University

Dr. Soizick F. Le Guyader – IFREMER

Chair of the Committee:

Assoc. Prof. Somluk Asuvapongpatana – Mahidol University

Examiner:

Dr. Yannick Rossez – Université de Lille

Thesis conducted under a cotutelle agreement between the University of Lille (France) and Mahidol University (Thailand)

Structural and Functional Glycobiology Unit (UGSF) UMR 8576 CNRS
Faculty of Science and Technology University of Lille
Scientific City – Building C9 59655 Villeneuve-d'Ascq, France

UNIVERSITÉ DE LILLE

École Doctorale
Présentée en vue de l'obtention du grade de

Docteur de l'Université de Lille

Spécialité : Biochimie et Biologie Moléculaire
par

CHANYARAK SOMBUTKAYASITH

Soutenue le 31 octobre 2025

Interactions Glycaniques du Virus de la Nécrose Hypodermique et Hématopoïétique Infectieuse (IHHNV) avec les Tissus Hôtes

Directeurs de thèse:
Prof. Yann Guérardel – Université de Lille
Prof. Wattana Weerachatyanukul – Mahidol University
Rapporteurs:
Assoc. Prof. Pitchanee Jariyapong – Walailak University
Dr. Soizick F. Le Guyader – IFREMER
Président du Jury:
Assoc. Prof. Somluk Asuvapongpatana – Mahidol University
Examinateur:
Dr. Yannick Rossez – Université de Lille

Cette thèse a été réalisée en cotutelle entre l'Université de Lille (France) et l'Université de Mahidol (Thaïlande)

Unité de Glycobiologie Structurale et Fonctionnelle (UGSF)
UMR 8576 CNRS Faculté des Sciences et Technologies Université de Lille
Cité Scientifique – Bâtiment C9 59655 Villeneuve d'Ascq, France

TABLE OF CONTENTS

TABLE OF FIGURES

ABSTRACT

Viral disease remains a major constraint in shrimp aquaculture. Infectious hypodermal and hematopoietic necrosis virus (IHHNV) causes runt deformity syndrome in *Penaeus vannamei*, yet early host–virus contacts have been poorly defined. In this work, noninfectious IHHNV virus-like particles (IHHNV-VLPs) were produced from recombinant capsid, validated for purity, biotinylation, and ~27-nm morphology, and used as probes to map attachment and tissue targets. Whole-mount binding in post-larvae showed strong signals in gill and muscle, with minimal background in controls. Quantitative ELISA on tissue extracts (gill, muscle, hepatopancreas, stomach) and a cross-species Sf9 cell lysate ranked binding highest for gill, muscle, and Sf9. Far-Western probing revealed multiple VLP-reactive bands in gill and muscle, consistent with several candidate host glycoproteins. To define the chemical basis of binding, lectin histochemistry and lectin–ELISA were performed: ConA, AAL, and WGA gave strong signals, especially in gill. Functional assays supported a glycan requirement: pre-incubation with ConA, AAL, or WGA lowered VLP binding; enzymatic and chemical treatments (PNGase F, α-mannosidase, α-fucosidase, and periodate) reduced binding, with periodate producing the largest decrease and PNGase F/α-mannosidase producing substantial reductions. Monosaccharide blocking further decreased binding after pre-incubation with mannose or GlcNAc (gill, Sf9) and with fucose (muscle, gill). Glycomics of released glycans identified oligomannose-dominant N-glycans with core fucosylation and fucosylated O-glycans in gill, aligning with the lectin and inhibition results. Taken together, the data support a model in which IHHNV-VLPs engage high-mannose, fucose-containing, and GlcNAc-rich glycans on shrimp tissues, with gill and muscle providing the most permissive landscapes. These findings supply a mechanistic basis for glycan-focused control strategies and a practical, VLP-centered toolkit for studying shrimp–virus interactions.

IMPLICATIONS

By identifying glycan classes that promote IHHNV attachment, this thesis points to intervention routes that are compatible with hatchery practice and do not rely on antibiotics. Defined sugar "decoys" or safe marine polysaccharides could be formulated as short dips or feed additives to compete with capsid–glycan binding during vulnerable stages; gentle, surface-acting blockers modeled on ConA/AAL/WGA specificities could transiently mask high-mannose, fucosylated, or GlcNAc motifs on gill and muscle; and VLPs themselves can be repurposed as capture reagents for diagnostics that report receptor-competent particles alongside nucleic-acid tests. In parallel, breeding and nutrition programs may use glycan phenotypes as markers to reduce presentation of highly permissive motifs without compromising development. The VLP-to-glycomics workflow established here—imaging, ELISA, Far-Western, lectin profiling, enzymatic trimming, monosaccharide blocking, and mass spectrometry—offers a template for analyzing other crustacean pathogens and for translating basic glycobiology into practical disease-management tools for aquaculture.

KEYWORDS: VLP (virus-like particle), Infectious hypodermal and hematopoietic necrosis virus (IHHNV), Densovirus, glycans P. vannamei,

Acknowledgement

First and foremost, I would like to express my deepest gratitude to my two advisors, Professor Wattana Weerachatyanukul and Professor Yann Guérardel, for their invaluable guidance and support throughout my Ph.D. journey. Prof. Wattana, your guidance has shaped my critical thinking and allowed me to explore these challenging areas with confidence. Prof.Yann, I am especially thankful for your support during my stay in France. Being far away from home was often difficult and overwhelming, but your encouragement helped me to regain focus, see myself more clearly, and improve without unnecessary pressure. You are truly the best foreign professor I have ever had the privilege to work with. I would also like to thank my collaborator, Assoc. Prof. Dr. Somluk Asuvapongpatana, Orawan Thongsum, Supawich Boonkua, and Assist. Prof. Dr. Monsicha Somrit, whose help with the VLP experiments was indispensable. Without your support, it would have been nearly impossible to begin my work in this area. I am also grateful to Dr. Shin-Yi Yu, Dr. Yannick Rossez, and all the members of UGSF, Lille University. Thank you for your professionalism, kindness, and patience. On a personal note, I owe my deepest thanks to my dearest mother, whose sacrifices have allowed me to pursue my Ph.D. and follow my own path. To Rove the cat, my companion in France, thank you for being there through difficult moments.

Finally, I would like to acknowledge the support of Campus France and the Franco-Thai Scholarship, without which my invaluable experience in France would not have been possible.

This journey has been long, tiring, and at times deeply challenging. Yet, it has also been filled with joy, growth, and reward. I am profoundly grateful to everyone who has been part of it.

LIST OF ABBREVIATIONS

AAL	Aleuria aurantia lectin
BGBP	β-glucan binding protein
BSA	Bovine serum albumin
CRISPR	Clustered Regularly Interspaced Short Palindromic Repeats
CTL	C-type lectin
DAPI	4′,6-diamidino-2-phenylindole
DNA	Deoxyribonucleic acid
dp	Degree of polymerization
ELISA	Enzyme-linked immunosorbent assay
Env	Envelope glycoprotein
EVE	Endogenous viral element
FAO	Food and Agriculture Organization
FCR	Feed conversion ratio
GAG	Glycosaminoglycan
GalNAc	N-acetylgalactosamine
GlcNAc	N-acetylglucosamine
HA	Hemagglutinin
HBGA	Histo-blood group antigen
HIV	Human immunodeficiency virus
HRP	Horseradish peroxidase
HS	Heparan sulfate

IHC	Immunohistochemistry
IHHNV	Infectious hypodermal and hematopoietic necrosis virus
LGBP	Lipopolysaccharide and β-glucan binding protein
MALDI-MS	Matrix-assisted laser desorption/ionization mass spectrometry
MVB	Multivesicular body
NS	Nonstructural protein
ORF	Open reading frame
PBS	Phosphate-buffered saline
PCR	Polymerase chain reaction
PNGase F	Peptide-N-glycosidase F
PRR	Pattern recognition receptor
proPO	Prophenoloxidase
qPCR	Quantitative polymerase chain reaction
RDS	Runt deformity syndrome
SDS-PAGE	Sodium dodecyl sulfate–polyacrylamide gel electrophoresis
ssDNA	Single-stranded DNA
TEM	Transmission electron microscopy
TBS	Tris-buffered saline
TSV	Taura syndrome virus
VLP	Virus-like particle
VP	Viral capsid protein
WGA	Wheat germ agglutinin
WSSV	White spot syndrome virus

CHAPTER I

INTRODUCTION

Shrimp farming supplies a large share of the world's seafood, yet production remains vulnerable to viral disease. A persistent concern is IHHNV, a small, non-enveloped, single-stranded DNA virus that, in *Penaeus vannamei*, is better known for runt deformity syndrome than for acute mortality. Slower growth and deformities still erode harvest weight and profitability. Because crustaceans lack antibody-based adaptive immunity, the very first steps of infection—how a particle attaches to host tissue—deserve close attention. In many animal viruses, initial contact is mediated by cell-surface glycans displayed on proteins and lipids. These sugars often provide low-affinity, high-avidity footholds that concentrate virions before deeper engagement. Mannose-rich N-glycans, fucosylated motifs, and N-acetylglucosamine-containing structures are common examples. For IHHNV, direct evidence for glycan use in shrimp has been limited; clarifying whether host glycans promote attachment would explain tissue preferences and open practical, non-antibiotic routes to mitigation.

This thesis examines IHHNV attachment using IHHNV-VLPs assembled from recombinant capsid protein. The VLPs mimic the external capsid surface and can be handled safely. Tissue preference was first mapped in whole post-larvae by fluorescence labeling of biotinylated VLPs. Binding was then quantified by ELISA using coated extracts from gill, muscle, hepatopancreas, and stomach; an Sf9 insect-cell lysate was included to gauge cross-species reactivity. Putative host ligands were visualized by Far-Western blotting, with VLPs used as the probe. The glycan landscape of target tissues was profiled by lectin histochemistry and lectin-ELISA. Functional dependence was tested

in two directions: pre-occupying the capsid with lectins or simple sugars (mannose, fucose, N-acetylglucosamine), and glycans removal by enymes (PNGase F, α-mannosidase, α-fucosidase). Finally, MALDI-MS(/MS) of released N- and O-glycans provided composition-level context for the binding patterns.

The goals are straightforward: identify which shrimp tissues show the strongest VLP binding, determine which glycan classes are associated with and contribute to that binding, and perform blocking by lectins, enzymatic trimming, and monosaccharide blocking. By focusing on the first contact between particle and host, the work aims to lay a testable basis for hatchery-ready measures such as sugar decoys, safe polysaccharides, or gentle surface blockers.

CHAPTER II

OBJECTIVES

Interactions between densoviruses and their hosts, including IHHNV, remain incompletely defined. Building on evidence that many viruses exploit host glycans for initial contact, it is proposed that IHHNV uses glycans on *Penaeus vannamei* tissues as attachment determinants. Consequently, selective removal or competitive masking of those glycans should diminish viral binding and lower the risk of infection.

Specific objectives.

- Establish an IHHNV virus-like particle (VLP) capsid model to study host–tissue attachment.
- Determine which *P. vannamei* tissues display preferential binding to IHHNV-VLPs.
- Define the glycan landscape of the tissues identified as most susceptible.
- Evaluate whether glycan-focused blockade (e.g., competitive masking or removal of key motifs) reduces IHHNV-VLP attachment.

CHAPTER III

LITERATURE REVIEW

1. Introduction to Shrimp Virology and Aquaculture Impact

Shrimp aquaculture has expanded rapidly over the last four decades and now constitutes a cornerstone of global aquatic food supply. In its 2024 flagship assessment, the Food and Agriculture Organization (FAO) reported that aquaculture surpassed capture fisheries as the world's leading source of aquatic animals for the first time in 2022, producing 130.9 million tonnes of marine animals—51% of total aquatic animal output that year (including finfish, crustaceans, mollusks, and other groups) (1). This milestone reflects sustained intensification through improvements in genetics, feed formulation, aeration, and biosecurity. It is notable because crustacean aquaculture—led by the Pacific white shrimp Penaeus vannamei—is among the most valuable segments within the broader aquaculture portfolio (2). While aggregate output has increased, the industry's trajectory remains tightly constrained by infectious diseases, particularly viruses, which drive volatility in production and profitability across major producing regions. (1,3)

A defining characteristic of shrimp virology is the disproportionate impact of disease on sector performance relative to other production bottlenecks. Cross-sector evaluations of aquatic animal health consistently conclude that infectious diseases generate multi-billion-dollar annual losses and can depress adequate capacity in high-value sectors such as shrimp by up to ~40% during crisis periods (3). These estimates integrate acute epizootics, chronic performance penalties, and the cost of control measures, underscoring that disease—with viruses at the forefront—remains the principal biological constraint on the continued expansion of shrimp farming. (3)

Within this context, white spot syndrome virus (WSSV) is emblematic of rapid, high-mortality outbreaks, whereas infectious hypodermal and haematopoietic necrosis virus (IHHNV) represents a pervasive chronic threat. IHHNV is a small single-stranded DNA virus (family Parvoviridae, subfamily Hamaparvovirinae, genus Penstylhamaparvovirus) that was first recognized as a cause of severe losses in Penaeus stylirostris in Hawaii in 1981, and has since become globally distributed across shrimp-farming regions in the Americas and Asia (4–6). The biological and economic signatures of IHHNV differ by host: susceptible species (e.g., P. stylirostris) may experience high juvenile mortality, while tolerant hosts (notably P. vannamei) typically develop runt deformity syndrome (RDS)—a constellation of growth retardation and cuticular deformities that does not produce headline mortality but erodes farm revenue via lower biomass, poorer size uniformity, and downgraded product quality (4–7). This chronic phenotype explains why IHHNV can be under-appreciated in surveillance systems that focus on catastrophic die-offs, despite its substantial cumulative burden on production. (4–7)

Shrimp are intrinsically vulnerable to viral pathogens because they lack an antibody-based adaptive immune system and rely instead on innate immunity. Innate defenses encompass cellular mechanisms (phagocytosis, encapsulation, nodulation, apoptosis) mediated by circulating hemocytes, as well as humoral cascades including the prophenoloxidase (proPO) system, clotting reactions, oxidative enzymes, antimicrobial peptides (e.g., penaeidins, crustins), and an array of pattern-recognition molecules such as C-type lectins, β-glucan-binding proteins, and Toll-like receptors (8,9). Innate responses can limit replication and clear infection in some contexts; however, the absence of immunological memory means protection typically does not persist across production cycles, rendering populations susceptible to reinfection. (8,9)

The production environment exacerbates these biological vulnerabilities. Intensive pond and raceway systems expose shrimp to high animal densities, occasional water-quality stressors (e.g., fluctuations in dissolved oxygen, ammonia, temperature, and salinity), and frequent animal movements (broodstock, post-larvae) that facilitate pathogen introduction and spread. Waterborne transmission, cannibalism of dying conspecifics, contaminated equipment, and potential mechanical vectors (wild crustaceans, insects, birds) promote horizontal transmission. At the same time, the detection of pathogen nucleic acids in broodstock tissues and nauplii has raised concerns about vertical routes for several shrimp viruses (4–6,8). These ecological factors help explain why, once viruses are established in a region's metapopulation, they are rarely eradicated; instead, endemic circulation persists through inter-farm water exchange, shared hatchery sources, and wild-to-farm interfaces. (3–6,8)

For IHHNV specifically, contemporary field studies highlight its persistence at meaningful prevalence in commercial P. vannamei systems. In Ecuador and Peru, a multi-region farm survey demonstrated endemicity with farm-level prevalence ranging from 3.3% to 100%, reflecting differences in biosecurity, seed origin, and environmental conditions (6). Crucially, the study notes that linking prevalence to performance at the farm level requires careful attention to diagnostic specificity, because some polymerase chain reaction (PCR) assays may detect endogenous viral elements (EVEs)—IHHNV-like sequences integrated into shrimp genomes—leading to false-positive interpretations of active infection if target regions are not chosen appropriately (6). This issue is not merely theoretical: follow-up methodological work has documented EVE-associated false positives with specific conventional assays and advocated for EVE-aware primer/probe design, confirmatory approaches (e.g., immunohistochemistry, long-amplicon PCR), and novel CRISPR-based diagnostics that can discriminate between replicating

virus and EVE templates (10–13). Collectively, these developments are reshaping surveillance and decision-making in farms and hatcheries by lowering the risk of misclassifying stock. (10–13)

The economic consequences of viral disease extend across the shrimp value chain. At the farm level, acute epizootics (e.g., WSSV) drive direct mortality and crop failure; chronic infections (e.g., IHHNV) lengthen crop cycles, increase feed conversion ratio (FCR), and reduce size uniformity, depressing price realization at harvest. At the sector level, disease-driven production volatility disrupts processing plant utilization, export schedules, and capital flows, and can precipitate shifts in species portfolios and investment. Because many shrimp-producing nations depend on the sector for export revenue and rural livelihoods, national-scale shocks from major outbreaks have repeatedly triggered policy responses centered on biosecure seed production, movement control, and enhanced surveillance (3). Taken together, these dynamics explain why aquaculture's global growth narrative—now outpacing capture fisheries—remains conditionally tied to disease control, and why elucidating virus–host mechanisms that can be translated into practical interventions is a strategic research priority. (1,3)

From a biological mechanism standpoint, IHHNV offers a compelling case study. As a small, non-enveloped parvovirus with limited coding capacity, IHHNV must rely on precisely tuned interactions between its capsid protein (VP) and host-cell surface determinants to attach, enter, and initiate replication in target tissues of ectodermal and mesodermal origin (notably hypodermis and haematopoietic tissues) (4,5). This observation naturally raises the hypothesis—strongly supported in vertebrate parvovirology—that cell-surface glycans (e.g., sulfated glycosaminoglycans and terminal sialic acids) act as primary attachment factors that shape tissue

tropism and host range. While definitive receptor(s) for IHHNV in P. vannamei remain to be identified, the tropism patterns documented histologically and by molecular assays in farmed shrimp provide a tractable scaffold for subsequent capsid–glycan mapping using modern tools such as virus-like particles (VLPs) and glycomics. (4–6)

In summary, shrimp aquaculture is both a success story and a cautionary tale: it has achieved unprecedented production milestones, yet it remains biologically constrained by viral diseases whose impacts range from catastrophic mortality to chronic performance loss. IHHNV exemplifies the latter and illustrates the need for mechanistic understanding—particularly of glycan-mediated attachment and entry—to inform next-generation diagnostics and interventions compatible with farm realities. The sections that follow synthesize current knowledge on (i) IHHNV biology, pathogenesis, and economic relevance; (ii) detection and epidemiology; (iii) general principles of virus–host binding with emphasis on glycan recognition and capsid–glycan interactions; (iv) shrimp glycobiology and immune lectins; (v) IHHNV–shrimp interactions and evidence for glycan involvement; (vi) VLP tools and applications; and (vii) glycan-based antiviral strategies and future directions.

2. Overview of IHHNV: Biology, Pathogenesis, and Economic Relevance

Infectious hypodermal and hematopoietic necrosis virus (IHHNV) is a small, non-enveloped, single-stranded DNA (ssDNA) virus that has become one of the most persistent pathogens in penaeid shrimp aquaculture. Taxonomically, IHHNV belongs to the family Parvoviridae, subfamily Hamaparvovirinae, genus Penstylhamaparvovirus; under current nomenclature, it is formally recognized as Decapod penstylhamaparvovirus 1 [1–3]. This reclassification reflects a 2020 revision of parvovirus taxonomy that reorganized aquatic and invertebrate lineages and

clarified relationships within Hamaparvovirinae [2,3]. These changes are relevant for surveillance and diagnostics because they align older literature that used the term “penstyldensovirus” with contemporary naming conventions.

i. *Virion morphology and genomic organization*

IHHNV virions are icosahedral, approximately 22–25 nm in diameter, and non-enveloped, consistent with other parvoviruses that package a compact ssDNA genome in a T=1 capsid [4–6] (figure 3.1). The genome is ~4.1 kb and contains three open reading frames (ORFs) that encode the hallmark parvoviral proteins: NS1 and NS2 (nonstructural proteins involved in replication and regulation) and VP (capsid protein) [4,6–8] (figure 3.2). NS1 carries conserved helicase and endonuclease motifs found in parvoviruses. It is essential for rolling-hairpin replication, while VP self-assembles into the icosahedral shell and displays the external surface that engages host determinants. Although early studies largely inferred replication strategy from vertebrate parvoviruses, subsequent work in crustacean densoviruses supports a nuclear replication cycle with rolling-hairpin synthesis of complementary DNA strands and host-dependent transcription [7,8]. From a structural–functional perspective, the capsid exterior is the key interface for host range and tissue tropism, and, by analogy to vertebrate parvoviruses, is the most plausible site for glycan-mediated attachment (discussed in Section 4) (figure 3.3 and 3.4).

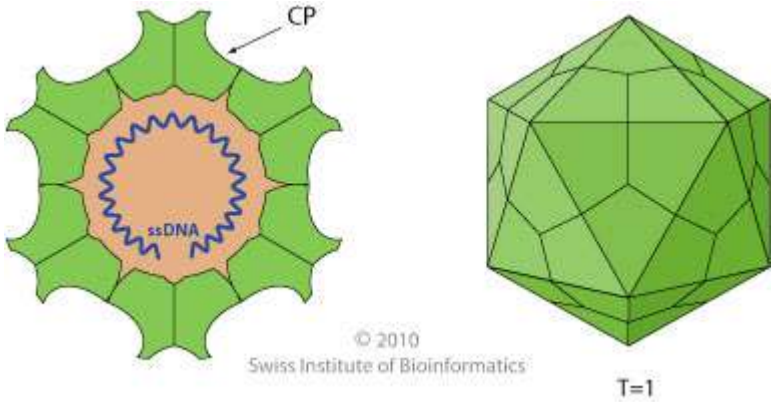

Figure 3.1. Basic virus capsid structure of Icosahedral, T=1. IHHNV is T=1 icosahedral capsid structure virus that contain ssDNA, 4.2 kb.

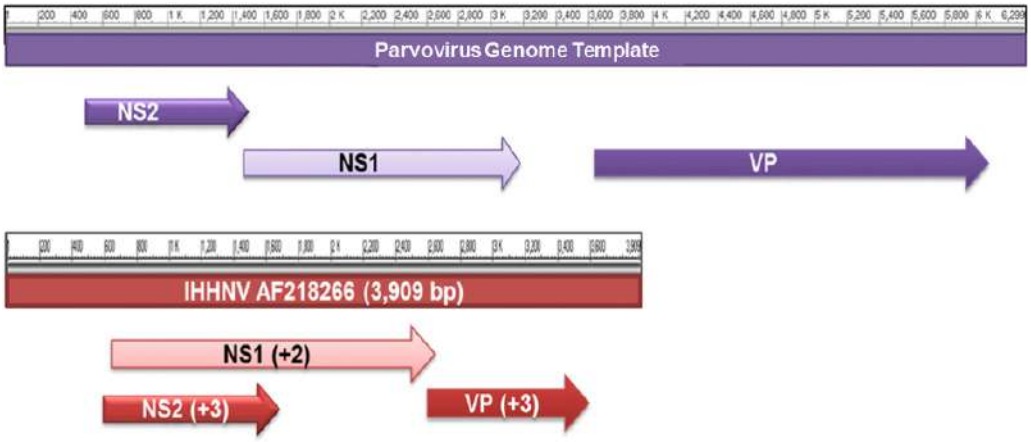

Figure 3.2. Organization of open reading frames (ORFs) in the genomes of Parvovirus genome template and IHHNV (PstDNV). The size of each ORF and the genome are depicted by their relative size. The numbers in parentheses indicate the ORF of each encoded protein

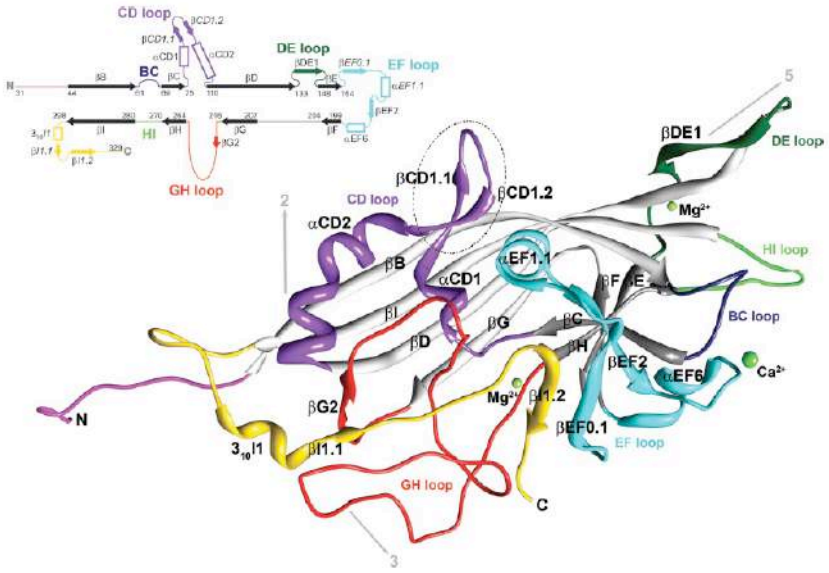

Figure 3.3. Ribbon diagram of the crystal structure of the IHHNV capsid protein. The BIDG and CHEF sheets of the eight-stranded -barrel are shown in light gray and dark gray, respectively. The surface loops connecting the strands of the -barrel are labeled by color as follows: BC loop, dark blue; CD, purple; DE, dark green; EF, cyan; GH, red; and HI, green. The N-terminal region upstream of B is shown in magenta, and the C-terminal portion downstream of I is shown in gold. The positions of icosahedral symmetry elements and their direction from the viral center are indicated by arrows. Between the conserved helical elements CD1 and CD2, the dashed circle highlights a hairpin loop insertion that is unique to the IHHNV structure. The position of secondary structural elements along the primary sequence is also presented in a schematic shown in the top left corner. Numbering corresponds to the starting residues of the -strands (solid arrows), shown black in the conserved jelly roll -barrel and colored in connecting loops. The N terminus (N) and C terminus (C) are indicated [72].

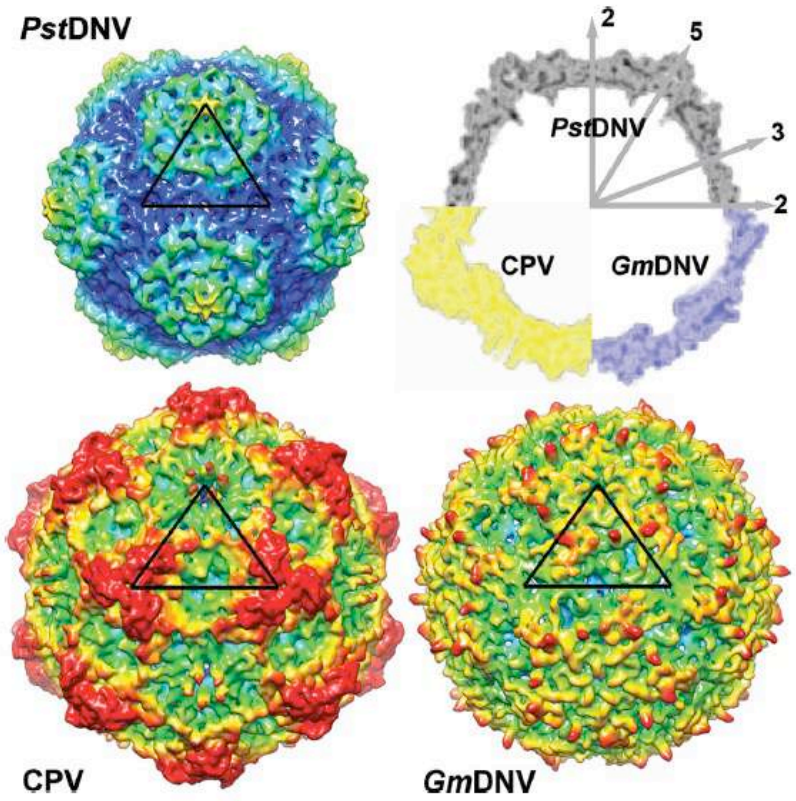

Figure 3.4. Topographic comparison of the IHHNV protein capsid with other parvoviruses. Surface renderings of 3D density maps of PstDNV, GmDNV, and CPV at 8 Å resolution, generated from atomic coordinates. One icosahedral asymmetric unit is indicated by a black triangle. The surface is colored according to the distance from the viral center (100 Å [blue], 107.5 Å [cyan], 115 Å [green], 122.5 Å [yellow], and 130 Å[red]). In the top right corner of the figure, a combination display of the equatorial slices of the density maps depicts the differences in thickness and expansion of the protein shells. The positions of icosahedral symmetry axes are indicated by the numbered gray arrows [72].

ii. *Discovery, host range, and phenotypic outcomes*

IHHNV was first recognized in Hawaii in 1981 in association with severe losses of Penaeus stylirostris (now Litopenaeus stylirostris), and within a decade it had spread through the eastern Pacific into Latin American production, later appearing in Asia and elsewhere [9–11]. The host range includes several penaeid shrimp species; clinical expression, however, is species-dependent. In susceptible hosts (e.g., L. stylirostris), IHHNV can cause acute juvenile mortalities and crop failure. By contrast, in tolerant hosts such as Pacific white shrimp (P. vannamei) and black tiger shrimp (P. monodon), IHHNV typically produces runt deformity syndrome (RDS) rather than mass mortality [4,10,12]. RDS manifests as growth retardation, cuticular deformities (e.g., bent rostrum, curved bodies), and size heterogeneity, which depresses harvest value even in the absence of overt die-offs. The chronic productivity penalty explains why farms and national surveillance systems sometimes underestimate the burden of IHHNV relative to acutely lethal viruses.

iii. *Tissue tropism and pathology*

Consistent with the original case descriptions and subsequent histopathology, IHHNV targets tissues of ectodermal and mesodermal origin, especially hypodermis and hematopoietic tissues, producing intranuclear inclusion bodies and nuclear hypertrophy (Cowdry type A inclusions) that are pathognomonic in severe cases [4,10] (figure 3.5). Classic teaching—still largely valid—is that endodermal organs (e.g., hepatopancreas) are not primary targets in natural infection; however, recent experimental work has nuanced this view. A carefully controlled feeding-challenge study in P. vannamei detected IHHNV DNA by qPCR in several tissues (pleopods, gills, muscle) and also reported hepatopancreas positivity in some conditions, sparking discussion on whether the

hepatopancreas can occasionally harbor viral DNA or whether detection reflects transient carriage rather than productive replication [13]. Parallel organ-distribution work in farmed shrimp has re-emphasized predominant tropism for hypodermal and hematopoietic tissues while acknowledging occasional detection beyond classical targets, especially under experimental challenge [14]. Together, these data warrant careful interpretation of tissue testing results (particularly with highly sensitive qPCR) and reinforce the need for localization methods (e.g., in situ hybridization, immunohistochemistry) when ascribing tissue tropism in field settings.

At the organismal level, clinical presentation varies by species and life stage. In juvenile L. stylirostris, infections can be rapidly lethal, whereas juvenile and grow-out P. vannamei typically present with stunted growth, deformities, and reduced feed efficiency with minimal acute mortality. Co-infections (e.g., with WSSV or TSV) can worsen outcomes, likely via immune modulation and compounded physiological stress, though quantifying these interactions in commercial settings remains challenging due to overlapping risk factors (stocking density, water quality). The metabolic cost of IHHNV infection has been demonstrated experimentally: a controlled study showed disturbances in metabolic rate and energy allocation in P. monodon infected with IHHNV, supporting the hypothesis that chronic growth penalties reflect systemic physiological disruption beyond tissue-specific lesions [15].

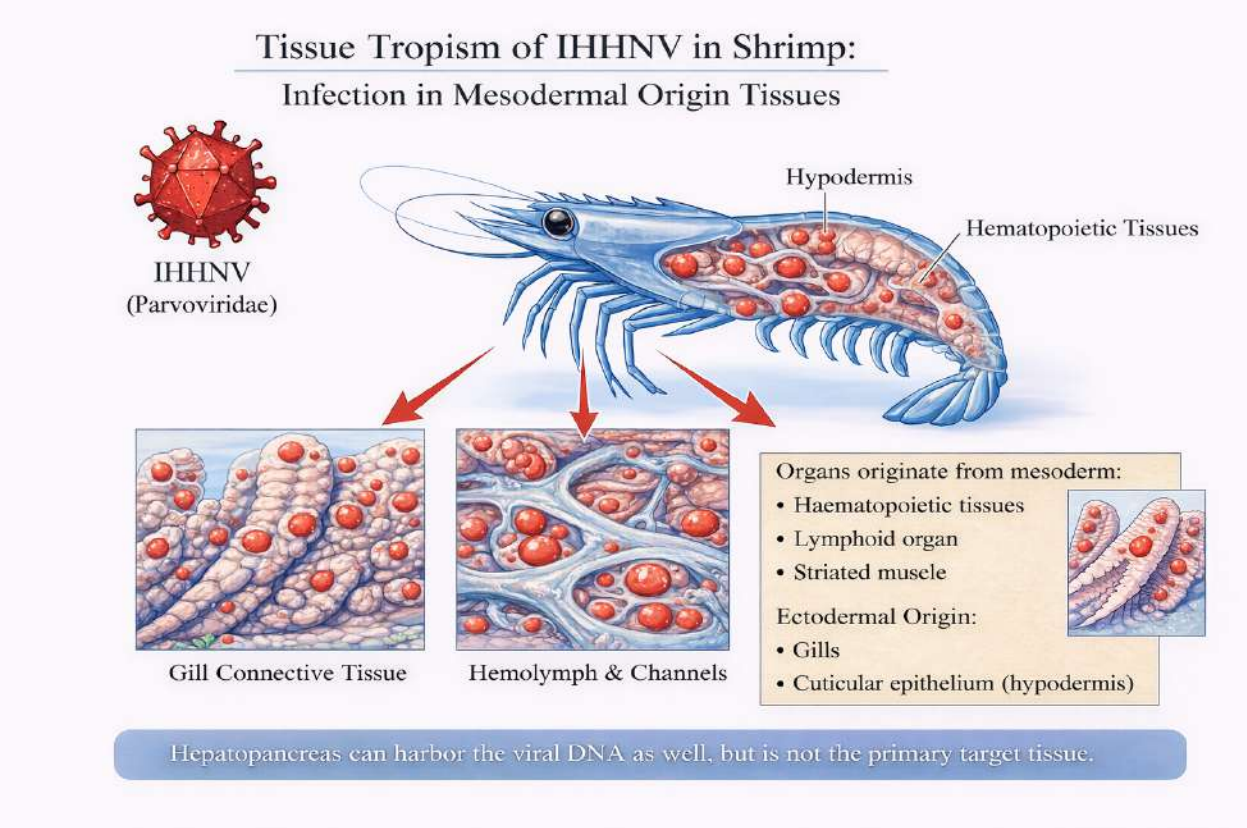

Figure 3.5. Tissue tropism of IHHNV in shrimp with emphasis on mesoderm-derived tissues. Schematic illustration showing the distribution of IHHNV in mature shrimp. The virus exhibits strong tropism toward tissues of mesodermal origin, particularly hematopoietic tissues, striated muscle, gill connective tissue, hemolymph channels, and associated connective tissues. Viral DNA may be detected in the hepatopancreas; however, it is not considered a primary target tissue for viral replication. Red inclusions represent sites of viral infection and/or viral DNA localization (Image genrated by AI).

iv. *Molecular epidemiology and detection landmarks*

Two developments have shaped the modern understanding of IHHNV epidemiology. First, the advent of real-time quantitative PCR (qPCR) enabled sensitive detection and viral load quantification across farms and regions. Early landmark assays demonstrated limits of detection

down to ~10 copies and log-linear quantification across several orders of magnitude, allowing robust comparisons of infection intensity among tissues and geographic isolates [16,17]. qPCR adoption revealed the cosmopolitan distribution of IHHNV (Americas, Asia, Oceania) and linked viral loads to clinical expression in susceptible hosts. Second, recognition of endogenous viral elements (EVEs). IHHNV-like sequences integrated into shrimp genomes exposed a diagnostic pitfall: conventional PCR can amplify EVE templates and misclassify shrimp as actively infected. Recent methods papers therefore emphasize EVE-aware primer/probe design, long-amplicon PCR or immunohistochemistry for confirmation, and CRISPR-Cas assays that discriminate replicating virus from EVE sequences [10,18,19]. These refinements are not merely technical; they alter prevalence estimates, stock movement decisions, and biosecurity policies at farm and national levels.

v. *Economic relevance: from chronic production losses to sector-level effects*

Unlike WSSV, which produces acute, visible losses, IHHNV imposes diffuse and persistent economic costs that accumulate across crops and regions. In tolerant hosts (P. vannamei, P. monodon), the hallmark RDS reduces growth rate, size uniformity, and price realization, often lengthening crop cycles and raising feed conversion ratio (FCR). These penalties can require more days to harvest for the same target size, higher feed expenditure, and downgrading at processing due to deformities—effects that scale with prevalence and stocking density. Given the macro-level view that aquatic diseases remove billions of dollars in value annually and can depress adequate capacity by up to ~40% in crisis settings, the chronic nature of IHHNV makes it a structural drag on profitability in regions where it is endemic [20]. Policy and industry responses increasingly focus on biosecure seed, EVE-aware diagnostics, and stock selection for reduced susceptibility;

however, the absence of sterilizing immunity in shrimp and the environmental stability of hamaparvoviruses mean that eradication is not a realistic goal. Consequently, risk-reduction and performance mitigation—including early diagnostic triage, compartmentalization of hatchery flows, and selective breeding—are the economically rational paths in IHHNV-endemic landscapes [10,20].

3. VIRUS–HOST BINDING MECHANISMS

i. *Principle of Non-enveloped Virus Entry into Host Cells*

Because of their structural simplicity, viruses depend on the host cell's biosynthetic machinery at nearly every stage of infection. The main purpose of entry is to deliver the viral genome into the cytosol or nucleus. The genome is initially enclosed by the viral capsid, which must undergo structural changes during the "uncoating" process before replication can begin [21].

Many non-enveloped viruses initiate infection by first binding to the plasma membrane and subsequently undergoing internalization via endocytic pathways. The principal uptake routes described include clathrin-mediated endocytosis, caveolae-mediated endocytosis, and clathrin- and caveolae-independent endocytosis [21,22] (figure 3.6). Clathrin-mediated uptake depends on sequence motifs within the cytoplasmic tails of receptors, while caveolar uptake is initiated by receptor clustering. Both processes require the GTPase dynamin, which facilitates vesicle budding from the plasma membrane [21]. The clathrin- and caveolae-independent pathways are less well characterized and may involve lipid raft domains and dynamin-dependent or independent mechanisms [21,22]. Other mechanisms, such as macropinocytosis, have also been reported for certain non-enveloped viruses [21]. After binding and internalization, some viruses trigger host signaling events, including tyrosine phosphorylation and cytoskeletal rearrangements, which

promote viral uptake and facilitate entry [21]. Once inside endosomal vesicles, the next critical step is penetration of the vesicle membrane so the genome can reach the cytoplasm. Unlike enveloped viruses, which fuse with host membranes, non-enveloped viruses disrupt the endosomal membrane through capsid-mediated mechanisms. Endosomal conditions, particularly acidic pH, play an important role in facilitating capsid rearrangements, membrane destabilization, and genome release [21,23]. In early endosomes, a mildly acidic pH (approximately 6.0–6.5) promotes dissociation of receptor–ligand complexes and sorting of cargo toward late endosomes or multivesicular bodies (MVBs), which ultimately direct materials toward lysosomal degradation [21]. For non-enveloped viruses such as parvoviruses, the icosahedral capsid provides repeating binding motifs whose multivalency generates high avidity for cell-surface ligands, overcoming the intrinsically weak affinity of individual glycan–protein contacts. Following attachment, viruses typically enter cells via clathrin-mediated endocytosis or related pathways. Acidification, proteolysis, and ionic changes in endosomes drive conformational transitions that expose internal peptides or pore-forming domains, allowing genome release [21,23]. The biophysical hallmarks of glycan-mediated adhesion include electrostatic complementarity (e.g., sulfation and carboxylation on glycans interacting with basic residues on capsids), multivalency, and sensitivity to glycan microheterogeneity [24,22,25].

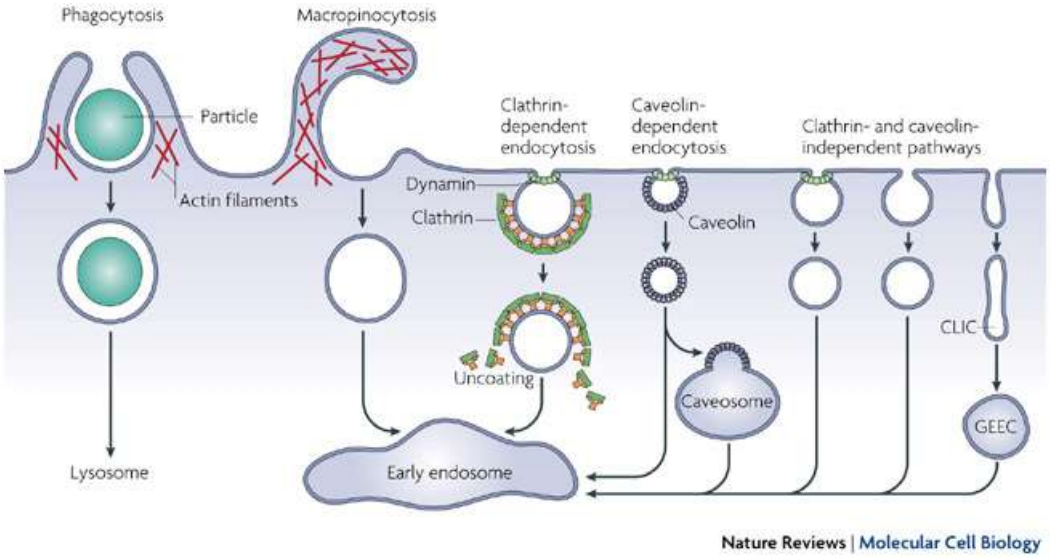

Figure 3.6. Endocytotic pathways that are essential for virus entry into host cell cytoplasm. The major routes are clathrin-mediated endocytosis and caveolae-mediated endocytosis while clathrin and caveolae-independent endocytosis and macropinocytosis are increasingly more events

ii. *Glycan recognition in representative viruses*

Influenza A virus and sialic acids

Influenza A hemagglutinin (HA) binds terminal sialic acid on host glycoconjugates, with linkage specificity correlating with host range: avian strains preferentially bind α2,3-linked sialic acids, whereas human-adapted strains preferentially bind α2,6 linkages in the upper respiratory tract **[**26**]**. Receptor switching through a small number of HA mutations can alter viral tropism and transmissibility, illustrating how glycan topology constrains epidemic potential **[**27**]**. Structural studies demonstrate that a shallow HA binding pocket interacts with the sialic acid carboxylate and glycerol side chain, and subtle changes in pocket geometry modulate linkage specificity [28,29]**.**

Human immunodeficiency virus (HIV-1) and the glycan shield

HIV-1 Env gp120 is among the most heavily glycosylated viral proteins, forming a dense "glycan shield" that masks peptide epitopes and shapes antibody responses [30]. Several broadly neutralizing antibodies (bnAbs) target composite epitopes comprising oligomannose glycans and adjacent protein structures, demonstrating that glycans can function both as immune shields and antigenic determinants [31,32]. Heparan sulfate on host cells also contributes to initial viral attachment for some HIV isolates prior to CD4 and coreceptor engagement [33].

Human noroviruses and histo-blood group antigens (HBGAs)

Many human noroviruses bind histo-blood group antigens displayed on mucins and glycolipids of the gastrointestinal tract. Strain-specific binding to A, B, H, or Lewis antigens helps explain host susceptibility patterns and outbreak epidemiology [34]. Crystallographic and glycan-array work has mapped HBGA contacts to the P domain of the capsid, with genotype-dependent binding footprints [35].

Parvoviruses

Parvoviruses display diverse glycan usage. Adeno-associated virus 2 binds heparan sulfate proteoglycans; human parvovirus B19 recognizes the globoside (P antigen) glycosphingolipid; minute virus of mice engages sialylated glycans [36,37,38]. These interactions are typically low-affinity, multivalent, and sensitive to glycan sulfation and branching. Mutation of surface loops that form the glycan-binding pocket alters tropism and transduction efficiency, underscoring the functional centrality of capsid–glycan contacts [39].

iii. *Capsid–glycan structural interactions*

Across non-enveloped viruses, capsid–glycan contacts usually involve shallow pockets or ridges created by symmetry-related loops at or near threefold/fivefold axes. X-ray and cryo-EM studies show that sulfate and carboxylate groups of glycans dock to basic residues (lysine/arginine) on

capsids, while hydrophobic patches position saccharide rings [22, 23]. Multivalency arises because 60 identical capsid subunits present repeating sites, enabling avidity-driven binding despite sub-millimolar to millimolar monovalent affinities [24]. Glycan microheterogeneity (linkage, sulfation pattern, branching) modulates binding and can create strain-specific phenotypes. Technically, glycan microarrays and saturation-transfer difference NMR provide complementary evidence for specificity and affinity, while cryo-EM with ligand soaking maps footprints at near-atomic resolution [40,41]. These principles guide hypotheses for IHHNV and inform assay design with virus-like particles (VLPs) in Sections 6 and 7 (figure 3.7).

iv. *Entry routes and endosomal cues*

Non-enveloped viruses commonly enter host cells via receptor-mediated endocytosis, with clathrin-mediated pathways being among the most extensively characterized mechanisms. Following internalization, progressive endosomal acidification, ionic changes, and host protease activity induce conformational rearrangements in viral capsid proteins. These structural transitions expose internal peptides with membrane-penetrating or pore-forming functions, enabling translocation of the viral genome into the cytosol [21,23]. Within the family *Parvoviridae*, endosomal escape is a critical step in infection. Capsid rearrangements under acidic conditions expose phospholipase A_2 (PLA_2)-like domains in the VP1 unique region, which facilitate disruption of the endosomal membrane and subsequent cytoplasmic release **[**23**]**.

After endosomal escape, parvoviruses rely on microtubule-mediated trafficking toward the perinuclear region. Nuclear entry is essential for replication, as viral DNA replication occurs in the host nucleus. Exposure of nuclear localization signals (NLS) on capsid proteins enables interaction with the importin machinery and transport through nuclear pore complexes [23,42].

Although the precise entry pathway of IHHNV in shrimp cells remains incompletely characterized, its classification within *Parvoviridae* suggests that similar endocytic uptake and acid-triggered capsid rearrangements are likely involved [12,23]. Given the high proliferative activity of hematopoietic and hypodermal cells, these tissues may provide a permissive intracellular environment that supports efficient nuclear trafficking and replication.

v. *Internalization: Endocytic Uptake Pathways*

Following viral attachment, non-enveloped parvoviruses are generally internalized via receptor-mediated endocytosis, most commonly through clathrin-dependent pathways [21,23]. Dynamin-mediated vesicle scission and actin cytoskeleton rearrangements are frequently required for successful uptake [21]. Alternative pathways, including caveolae-mediated endocytosis or macropinocytosis, have also been reported for certain viruses under specific cellular contexts [21]. Although direct experimental evidence for IHHNV internalization pathways in shrimp cells remains limited, the structural and phylogenetic similarity of IHHNV to vertebrate parvoviruses suggests that clathrin-mediated endocytosis is the most parsimonious mechanism [12,23]. Sensitivity to endosomal acidification in related parvoviruses further supports a model in which entry proceeds through endosomal compartments rather than direct plasma membrane penetration [21,23].

vi. *Endosomal Trafficking and Membrane Penetration*

Unlike enveloped viruses such as influenza virus or HIV, which achieve cytosolic entry via membrane fusion mediated by viral glycoproteins [26,30], non-enveloped viruses must penetrate the endosomal membrane through capsid-driven mechanisms. In parvoviruses, endosomal acidification triggers conformational rearrangements in the capsid that expose previously hidden

internal domains, including phospholipase A_2 (PLA_2) motifs within the VP1 unique region, which mediate membrane destabilization and facilitate endosomal escape [23].

Whether IHHNV encodes analogous membrane-penetrating domains has not been fully elucidated; however, given its classification within *Hamaparvovirinae* and structural conservation with other parvoviruses [12,23], it is reasonable to hypothesize that acidification-induced capsid rearrangements play a similar role. Experimental interrogation of IHHNV capsid dynamics under varying pH conditions, particularly using virus-like particles (VLPs), would provide valuable mechanistic insight [43,44,45].

vii. *Cytoplasmic Transport and Nuclear Import*

A defining feature of parvovirus biology is strict nuclear replication [23]. Consequently, successful infection requires trafficking of the viral genome to the nucleus. In vertebrate parvoviruses, this process involves microtubule-mediated transport toward the perinuclear region, followed by nuclear entry either through intact capsids docking at nuclear pore complexes or via partial uncoating in the cytoplasm [23]. Nuclear localization signals (NLS) present on capsid proteins and interactions with host transport machinery have been implicated in this process [23,42]. Although nuclear trafficking mechanisms have not yet been experimentally characterized for IHHNV in shrimp cells, its replication within nuclei of hypodermal and hematopoietic tissues [4,12] implies reliance on conserved nucleocytoplasmic transport pathways. Determining whether IHHNV capsids remain intact during nuclear import or undergo stepwise disassembly remains an important mechanistic gap.

viii. *Comparative Entry Strategies Across Viral Classe*

Positioning IHHNV within broader virological paradigms highlights important mechanistic distinctions. While IHHNV shares structural and genomic features with other parvoviruses [12,23],

its entry strategy contrasts with enveloped viruses such as influenza virus and HIV, which rely on membrane fusion mediated by viral envelope glycoproteins [26,30]. In contrast, many RNA viruses replicate entirely in the cytoplasm and therefore bypass nuclear import requirements, whereas IHHNV must deliver its genome into the nucleus to establish infection.

ix. *Implications for IHHNV*

Given the small T=1 parvoviral capsid, documented tissue tropism in shrimp, and the abundance of glycosaminoglycans and mucin-type glycans on shrimp epithelia and hemocytes, it is plausible that IHHNV uses glycan-mediated attachment as an initial capture step, possibly followed by engagement of a protein coreceptor [4,21,23]. This model predicts sensitivity to enzymatic deglycosylation, competition by soluble glycan analogs, and measurable binding of IHHNV VLPs to defined shrimp glycan fractions in vitro.

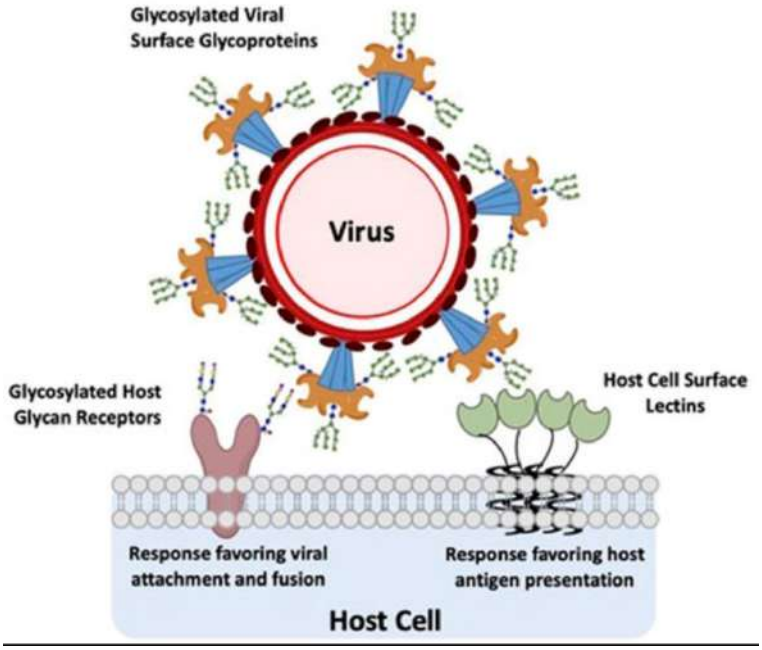

Figure 3.7. Glycan-mediated interactions between viruses and host cells.

Viral surface glycoproteins and host glycan receptors or lectins interact to drive key outcomes. These interactions can promote viral attachment and membrane fusion, supporting infection, or stimulate host immune recognition and antigen presentation. [73].

4. SHRIMP GLYCOBIOLOGY AND HOST DEFENSE

i. *Overview of shrimp glycans*

Glycans are structurally diverse carbohydrate chains covalently attached to proteins or lipids, forming glycoproteins, glycolipids, and proteoglycans that decorate the cell surface and extracellular matrix. Unlike nucleic acids and proteins, glycan biosynthesis is not template-driven; instead, it results from coordinated activity of glycosyltransferases and glycosidases within the endoplasmic reticulum and Golgi apparatus. Consequently, glycans exhibit substantial structural microheterogeneity in monosaccharide composition, linkage type, branching architecture,

sulfation pattern, and spatial presentation [40]. This diversity is biologically significant because viral attachment is often highly sensitive to fine structural differences within glycan epitopes. In crustaceans, including penaeid shrimp, cell surfaces and extracellular matrices display a repertoire of glycans comprising glycosaminoglycans (GAGs), N-linked and O-linked glycans on glycoproteins, mucin-type O-glycans in epithelial secretions, and membrane-associated glycolipids [46,47]. Although comprehensive shrimp glycomes remain less defined than mammalian systems, biochemical and histological studies confirm the presence of sulfated polysaccharides, core-fucosylated glycans, and glycan-rich mucus layers in tissues relevant to viral infection [43,46,47].

ii. *Glycosaminoglycans (GAGs)*

Glycosaminoglycans are linear, negatively charged polysaccharides composed of repeating disaccharide units typically consisting of a hexosamine (N-acetylglucosamine or N-acetylgalactosamine) linked to a uronic acid (glucuronic or iduronic acid) [40]. Their biological properties are determined largely by sulfation position and density. Sulfate groups at N-, 2-O-, 3-O-, or 6-O-positions generate polyanionic domains that can engage electrostatically with positively charged lysine and arginine clusters on viral capsid surfaces [23,40,22]. In multiple viruses, including parvoviruses, heparan sulfate functions as an initial attachment factor rather than a definitive entry receptor, concentrating virions at the cell surface prior to internalization [23,36,48]. In shrimp, heparan sulfate–like and chondroitin sulfate–like molecules have been localized within basement membranes, connective tissues, and cuticular structures [46,47]. These distributions overlap with hypodermal and hematopoietic tissues known to support IHHNV replication [4,12], supporting the hypothesis that sulfated GAGs may participate in early attachment events. Importantly, even subtle differences in sulfation pattern or chain length can

significantly alter viral binding affinity [23,24,40], suggesting that tissue-specific GAG microdomains may influence viral tropism.

iii. *N-linked glycans*

N-linked glycans are attached to asparagine residues within the consensus sequence Asn-X-Ser/Thr and share a conserved pentasaccharide core ($Man_3GlcNAc_2$) [40]. Following core assembly, they are processed into three major classes: high mannose, hybrid, and complex glycans. High-mannose structures retain terminal mannose residues, whereas complex glycans undergo further branching and extension with galactose, N-acetylglucosamine, fucose, and occasionally sialic acid residues. Core fucosylation and terminal branching patterns contribute to the formation of distinct glycosylated epitopes—defined carbohydrate motifs recognized by viral capsids or host lectins. Parvoviruses demonstrate diverse glycan usage; for example, minute virus of mice recognizes sialylated glycans, and human parvovirus B19 binds the globoside glycosphingolipid [37,38]. These examples illustrate how structural variation in terminal monosaccharides and linkage orientation can dictate viral specificity [36,37,38,39]. In marine invertebrates, including shrimp, N-glycans frequently display high mannose content and core fucosylation [43,46]. Such features may generate epitopes capable of interacting with viral capsids or modulating lectin-mediated immune recognition.

iv. *O-Linked Glycans and Mucin-Type Epitopes*

O-linked glycans are covalently attached to serine or threonine residues, most prominently within mucin glycoproteins. Mucin-type O-glycosylation typically begins with N-acetylgalactosamine (GalNAc) linked to Ser/Thr and can be elaborated into core 1 or core 2 structures [40]. These cores may be extended and terminated by galactose, fucose, N-acetylglucosamine, or sialic acid residues. Terminal carbohydrate motifs form glycosylated epitopes that are recognized with high specificity

by viral proteins. For instance, influenza A virus discriminates between α2,3- and α2,6-linked sialic acids [26,27,28,29], and noroviruses bind histo-blood group antigen epitopes defined by fucosylation patterns [30,31]. Although sialic acids are less pervasive in crustaceans compared with vertebrates, fucosylated epitopes are common in marine invertebrate glycans [46,43]. Shrimp gill and gut epithelia are coated with heavily O-glycosylated mucins that create dense glycan landscapes. These mucins may function as decoy receptors that trap viral particles; however, they may also present potential attachment sites if viral capsids exploit terminal carbohydrate motifs.

v. *Glycan Microheterogeneity and Viral Tropism*

A defining feature of glycobiology is microheterogeneity — subtle differences in linkage orientation (e.g., α versus β), branching topology, sulfation pattern, and monosaccharide composition [40]. Structural studies of capsid–glycan complexes demonstrate that even single sulfate modifications or linkage changes can dramatically alter binding affinity and specificity [22,23,24,40]. Because viral capsids present multiple identical binding sites, multivalent interactions amplify small structural differences into biologically significant variations in infectivity [24]. In the context of IHHNV, differences in glycosylation patterns among shrimp species, developmental stages, or environmental conditions may contribute to variability in susceptibility and viral load. Tissue-specific glycan expression within hypodermal and hematopoietic compartments may further shape viral tropism [4,12,46]. Comprehensive glycomic profiling of these tissues would therefore provide critical insight into the specific glycosylated epitopes that mediate viral attachment.

vi. *Lectins and Carbohydrate-Binding Proteins in Shrimp Immunity*

Shrimp rely heavily on pattern recognition receptors (PRRs), many of which are carbohydrate-binding proteins. C-type lectins (CTLs), galectins, lipopolysaccharide-binding proteins/β-glucan-

binding proteins, and hemocyanin exhibit glycan-binding activity and contribute to agglutination, opsonization, activation of the prophenoloxidase cascade, and pathogen neutralization [8,9,41,44]. CTLs in penaeids recognize mannose-, fucose-, and N-acetylglucosamine-containing motifs and are upregulated during viral challenge [41,44]. Galectins bind β-galactoside residues and may aggregate viral particles or facilitate immune clearance. Because viral capsids often exploit host glycans for attachment, PRR–glycan interactions represent a dynamic interface in which glycans can function both as viral attachment platforms and as immune recognition determinants..

5. IHHNV–SHRIMP HOST INTERACTION

i. *Tissue tropism*

Classical histopathology and in situ hybridization localize IHHNV replication in tissues of ectodermal and mesodermal origin, notably the hypodermis and hematopoietic tissues, with characteristic intranuclear inclusion bodies and nuclear hypertrophy [4,12]. In tolerant hosts such as *Penaeus vannamei*, infection is typically chronic and manifests as growth retardation and deformities (runt deformity syndrome) with relatively low acute mortality. In contrast, susceptible species such as *Litopenaeus stylirostris* may experience high juvenile mortality [3,15]. Recent experimental feeding-challenge studies have detected viral DNA and/or antigens in additional tissues, including gill, muscle, and occasionally hepatopancreas, emphasizing the importance of distinguishing transient viral presence from active replication using localization methods [11,13–15].

ii. *Experimental findings on attachment and replication*

Quantitative PCR studies reveal broad dynamic ranges of viral loads across tissues and over time, supporting persistent, low-grade replication in tolerant hosts [8,11]. Organ-distribution surveys in

commercial settings reaffirm classical tissue tropism while noting sporadic detection in non-classical tissues, particularly under stress or co-infection conditions [13]. Physiological studies indicate altered metabolic activity and energy allocation in IHHNV-infected *P. vannamei*, linking chronic infection to growth suppression [15]. Methodologically, distinguishing active replication from endogenous viral element (EVE)-derived signals requires EVE-aware assays and confirmatory approaches (e.g., long-amplicon PCR and immunohistochemistry), particularly in broodstock and seed screening [9–12].

iii. *Potential glycan involvement in viral entry*

By analogy to vertebrate parvoviruses and considering shrimp glycobiology, a plausible model is that the IHHNV capsid engages sulfated glycosaminoglycans or terminally fucosylated/sialylated glycans on epithelial or hemocyte surfaces as initial attachment factors [36,37,38,39,46]. This model predicts: (i) reduced binding following enzymatic removal of specific glycans (e.g., heparinase, neuraminidase); (ii) competition by soluble glycan analogs (e.g., heparin, chondroitin oligosaccharides, or fucosylated oligosaccharides); (iii) measurable binding of IHHNV VLPs to shrimp tissue extracts and purified glycans; and (iv) modulation of binding by ionic strength and pH, consistent with electrostatically driven interactions [36–39]. Early VLP-based assays in crustacean systems support the feasibility of these approaches, although definitive receptor identification for IHHNV in *P. vannamei* remains an open question that warrants glycomics-guided investigation.

6. VIRUS-LIKE PARTICLES (VLPs) AS A TOOL

i. *Concept and advantages*

VLPs are self-assembled structures formed by viral structural proteins that lack the genome and are thus non-infectious. They faithfully present conformational epitopes and receptor-binding surfaces, making them ideal for: (i) structural studies (e.g., cryo-EM and molecular docking); (ii) receptor discovery using glycan arrays and tissue extracts; (iii) immunogenicity testing and vaccine design; and (iv) development of binding-based diagnostics [49,50]. Because VLPs mimic the native capsid, they enable detailed investigation of viral attachment and entry mechanisms without the biosafety constraints associated with live viruses.

ii. *Production platforms and characterization*

Common VLP production platforms include baculovirus–insect cell systems, yeast, and plant-based expression systems. Correct assembly is typically confirmed using electron microscopy, dynamic light scattering, and sedimentation analyses, while antigenicity is verified using conformation-dependent antibodies when available [49,50]. For glycan-binding studies, VLPs can be fluorescently labeled or chemically biotinylated to enable quantitative analysis of interactions with immobilized or soluble glycans.

iii. *IHHNV VLP applications in binding studies*

IHHNV capsid proteins expressed in heterologous systems assemble into particles that recapitulate key surface features of the native virus. These VLPs can be applied to: (i) commercial glycan arrays for initial specificity mapping; (ii) shrimp tissue-derived glycomes (e.g., hemocyte membranes and gill mucins); and (iii) defined glycosaminoglycan oligosaccharides to determine binding affinities. Competitive inhibition assays using heparin, chondroitin sulfate, or fucosylated

oligosaccharides, combined with enzymatic pretreatment of cells or tissues, can provide mechanistic evidence for glycan-dependent viral attachment. Such findings support the rational design of glycan-based decoy molecules or feed additives (Sections 8–9) and may inform selective breeding strategies if host glycan biosynthesis correlates with viral binding phenotypes [43,45,50].

3.6.4 Beyond binding: VLPs for immunization and delivery

Although shrimp lack antibody-mediated adaptive immunity, VLPs may function as immunostimulatory agents through interactions with pattern recognition receptors (e.g., C-type lectins and galectins), thereby enhancing cellular immune responses. In other aquatic species, VLPs have demonstrated promise as safe vaccine platforms; however, in shrimp, their primary immediate application lies in their use as research tools and diagnostic reagents for binding-based capture assays [49,51].

7. COMPARATIVE VIROLOGY: COMPARISON WITH OTHER VIRUSES

i. *Glycan-dependent binding in vertebrate and invertebrate viruses*

The prominence of glycan interactions across viruses suggests evolutionary convergence on abundant and structurally diverse host ligands. Influenza virus hemagglutinin–sialic acid interactions govern species barriers and tissue tropism [26-29]; HIV exploits a dense glycan shield and heparan sulfate–mediated attachment prior to CD4 engagement [30-33]; noroviruses use histo-blood group antigens (HBGAs) as attachment determinants with strain-specific binding preferences [34,35]; and multiple parvoviruses recognize heparan sulfate, sialic acid, or glycosphingolipids [36–39]. Among aquatic viruses, glycosaminoglycan dependence has also been reported or proposed for several fish and crustacean pathogens [46,64,22,65]. These examples

provide conceptual and methodological frameworks that are directly applicable to understanding IHHNV attachment mechanisms.

ii. *Structural paradigms and experimental workflows*

Capsid–glycan binding sites identified through cryo-electron microscopy and X-ray crystallography typically involve conserved surface loops that tolerate limited sequence variation; even single amino acid substitutions can disrupt or shift glycan specificity [23,24,40,52]. For receptor identification, a stepwise experimental workflow is effective: (i) glycan array screening using VLPs; (ii) validation by biophysical binding techniques such as surface plasmon resonance or isothermal titration calorimetry; (iii) cell-based inhibition assays using glycosidases or soluble glycan analogs; (iv) mutational analysis of candidate capsid-binding residues; and (v) in vivo validation through challenge experiments and tissue localization studies. This approach minimizes false positives arising from nonspecific electrostatic interactions with polyanionic glycans [24,22]. Given the small capsid size and tissue tropism of IHHNV, these paradigms suggest prioritizing sulfated glycosaminoglycans and terminally fucosylated O-glycans as candidate attachment factors. Mutational mapping of positively charged surface residues (e.g., lysine and arginine clusters) on the IHHNV capsid, combined with glycan-binding assays, may help identify critical determinants of viral attachment. Parallel profiling of shrimp tissues for glycosaminoglycan sulfation patterns and mucin-associated glycomes will further clarify the spatial distribution of high-affinity binding sites in vivo. These insights can inform the development of targeted antiviral strategies and selective breeding approaches.

8. GLYCAN-BASED ANTIVIRAL STRATEGIES IN AQUACULTURE

i. *Rationale and scope*

Evidence across virology shows that many non-enveloped and enveloped viruses initiate infection by binding to cell-surface glycans (e.g., heparan sulfate proteoglycans, sialylated glycans, or fucosylated mucin O-glycans) before or alongside engagement of specific protein receptors [21–27,36–39]. Because IHHNV is a small parvovirus with a highly ordered capsid and a tissue tropism pattern implicating glycan-rich epithelia and hematopoietic tissues, a practical translational hypothesis is that disruption of capsid–glycan interactions can reduce viral attachment and subsequent infection in shrimp [36,37,38,39,23,46]. Glycan-targeted strategies are particularly attractive in aquaculture because (i) they can be delivered through immersion or feed, (ii) they do not require cold-chain infrastructure, and (iii) they can complement biosecurity, diagnostics, and selective breeding approaches without relying on antibody-mediated immunity [1,3,46,49–51]. This section outlines potential intervention strategies, including glycan analogs (decoys), lectin-based blockers, enzymatic or chemical glycan modification, and binding-aware diagnostics, while considering safety, regulatory, and environmental constraints [42,44,56,59–62].

ii. *Competitive inhibitors and decoy glycans*

If IHHNV utilizes glycosaminoglycans or terminally fucosylated/sialylated glycans for initial attachment, soluble glycan analogs may competitively inhibit host receptor binding and reduce viral attachment efficiency [32–35,44,55]. Extensive work in glycobiology and antiviral research demonstrates that heparin or heparan sulfate mimetics, chondroitin sulfate derivatives, and sulfated polysaccharides derived from marine organisms (e.g., fucoidan, carrageenan, and ulvan) can inhibit virus–glycan interactions in both mammalian and aquatic viruses through electrostatic and structural competition [44,56,59–62].

Candidate scaffold;

(i) Heparin and defined heparan sulfate oligosaccharides (dp6–dp18) serve as prototypical decoys for heparan sulfate–binding viruses. Synthetic or semi-synthetic heparin mimetics can be engineered to reduce anticoagulant activity while retaining antiviral binding capacity [59–62]. (ii) Marine sulfated polysaccharides (e.g., fucoidans, carrageenans, ulvans) are attractive due to scalability and cost-effectiveness; their antiviral activity often correlates with sulfation density and chain length, although activity is highly dependent on fine structural features [44,56]. (iii) Fucosylated or sialylated oligosaccharides that mimic mucin terminal epitopes may act as competitive inhibitors if IHHNV targets such glycan structures [42,44].

iii. *Lectin blockers and receptor masking*

Concept. Lectins bind specific glycans with high affinity and can mask host receptors or agglutinate viral particles, thereby reducing effective attachment. In shrimp, C-type lectins (CTLs) and galectins are key components of innate immunity and may be exploited or supplemented to interfere with viral binding [8,9,39,46]. In addition, engineered or naturally occurring lectins (e.g., from algae or cyanobacteria) that recognize heparan sulfate–like or oligomannose motifs have demonstrated antiviral activity in other systems and may be adaptable for aquaculture applications, provided that toxicity and environmental safety are carefully evaluated [52,57–59].

iv. *Enzymatic and chemical modification of surface glycans*

Concept. Glycosidases (e.g., heparinase, chondroitinase, neuraminidase, fucosidase) or sulfatases can modify or remove glycan structures on epithelial surfaces, potentially reducing viral attachment sites. In principle, controlled application in hatchery systems could reduce early-stage infection risk if IHHNV depends on such glycans [42,44].

Practical constraints. Enzymatic treatments can be costly and sensitive to environmental conditions such as temperature and salinity, and excessive activity may damage host tissues. Because glycosaminoglycans play essential roles in structural integrity and cellular signaling, over-degradation may compromise epithelial function. Therefore, such approaches are most appropriate for mechanistic validation studies and proof-of-concept applications before large-scale implementation [42,44] (figure 3.8).

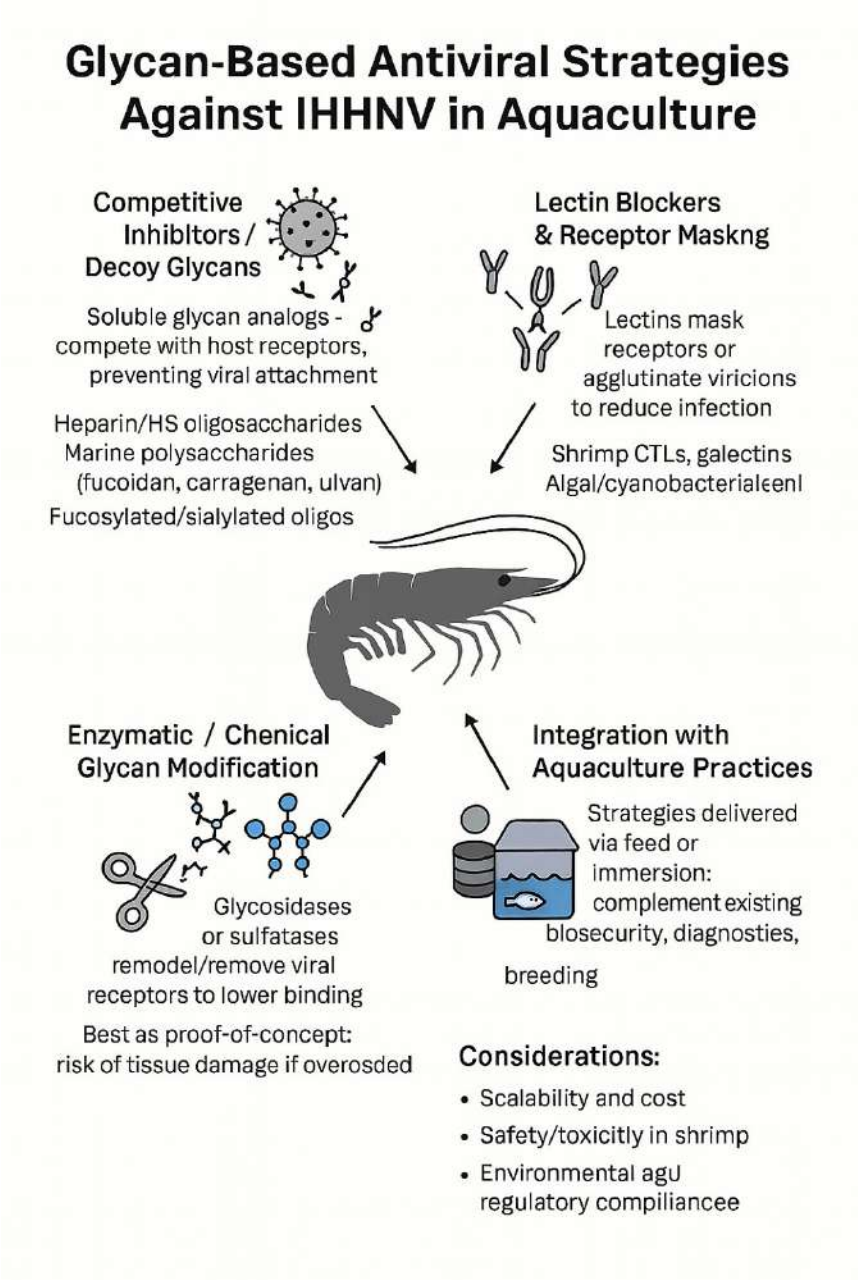

Figure 3.8. Glycan-based antiviral strategies in shrimp aquaculture.

Viruses use host cell glycans to attach and infect. Strategies to block this include adding decoy glycans to compete with viruses, using lectins to mask receptors, enzymatically modifying host glycans, and applying these tools through feed or water treatments. These approaches can support biosecurity and reduce infection risk, with attention to cost, safety, and environmental impact.

CHAPTER IV

MATERIALS AND METHODS

1. Molecular cloning and expression of IHHNV capsid proteins

The IHHNV virus capsid gene was amplified from ORF3 of the IHHNV virus genome in order to produce recombinant virus capsid (with an estimated size of 990 bp). The specific primers included IHHNV_cap_exp_F/R, designed by blast carrying the IHHNV genome from the GenBank data base (Figure 4.1). The capsid gene was amplified using a Gradient PCR Machines (Eppendorf Mastercycler® thermal cyclers). The reaction conditions of PCR were one cycle at 94ºC for 5 min, followed by one set of 94 ºC for 30 sec, 52 ºC for 1 min, and 72 ºC for 1 min with a final extension step at 72 ºC for 10 min. The PCR product was ligated into pGEM-T Easy cloning vector (Promega Inc.), and transfected into *Escherichia coli* (*E. coli*). Positive clones were selected by blue-white screening and the capsid gene was then transfered to pET-17b expression vector (Novagem Inc.) for protein expression in *E. coli* - Rosetta strain (Figure 4.2). IHHNV capsid protein was purified by using Ni-NTA Agarose beads (QUAIGEN Inc.) to bind with the His-tag sequence attached to the IHHNV capsomere protein. Purified IHHNV capsid protein was eluted from the column by an elution buffer and dialyzed against 1X Tris buffer saline (TBS) pH 7.8 at 4°C and stored with addition of anti-protease, -80ºC. This IHHNV-VLP in TBS was used for all experiments below and as antigen to stimulate rabbits for preparation of a polyclonal anti-IHHNV antibody, IgG. The anti-IHHNV capsid protein antibody was used for Western-blot analysis and immunolocalization assay.

Figure 4.1: IHHNV capsid gene (ORF3) specific primers. Top: forword primer with NdeI cutting site. **Botton:** reword priner with Histidene-tag, stop codon and XhoI cutting site.

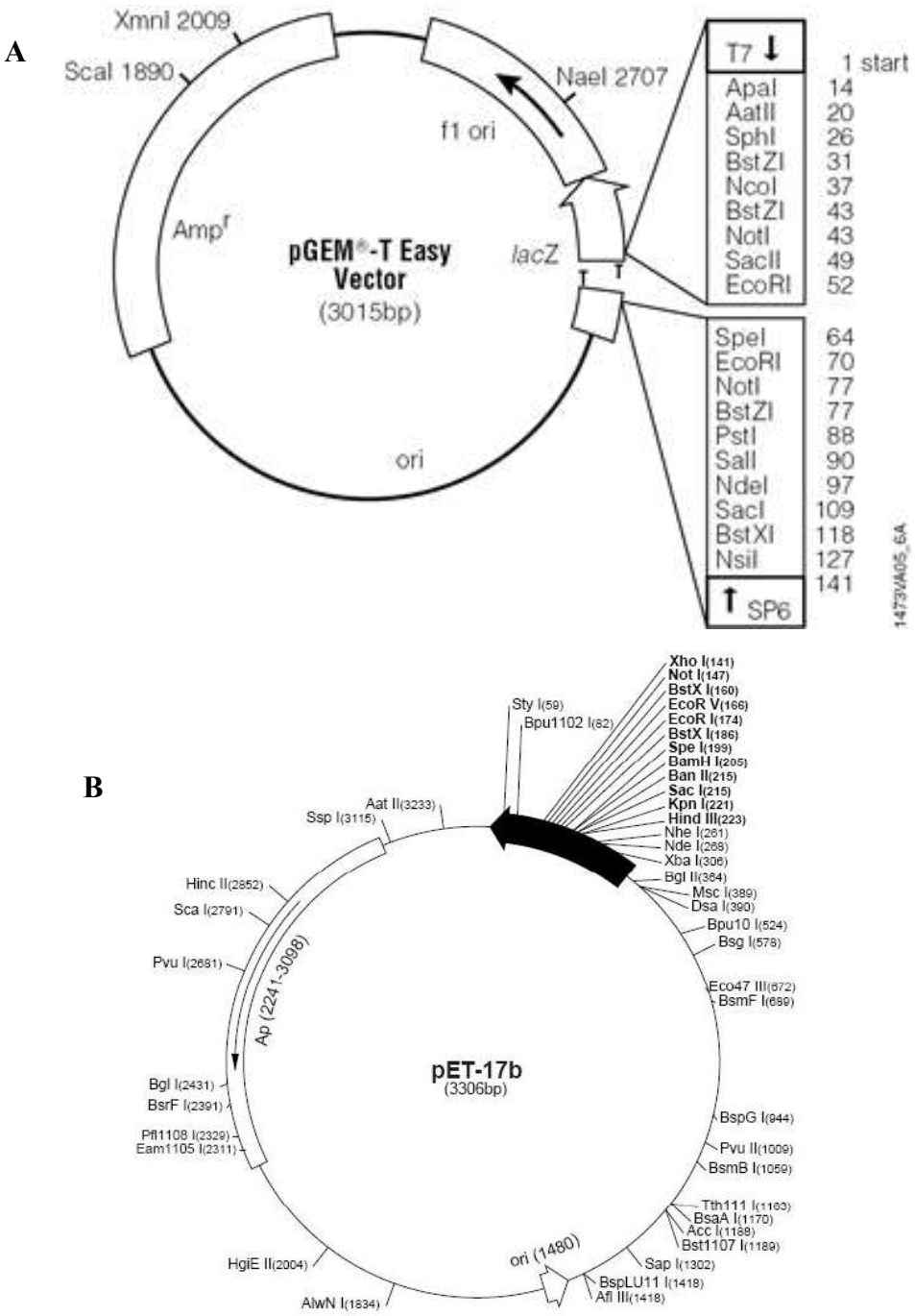

Figure 4.2: Gene mapping of pGEM-T Easy and pET-17b vecter. (A) pGEM-T Easy vector was used for amplify IHHNV capsid gene in *E. coli.* (B) pET-17b vector was used for IHHNV capsid gene expression in *E. coli* (Rosetta).

2. Protein profiling by SDS-PAGE

SDS-PAGE was performed according to Laemli's method (1970). The following sets of proteins were resolved: 1) 4-10 µg of crude extracts from E. coli cells with or without protease inhibitor cocktail (1:50 (v/v)); 2) 200-400 ng of the purified IHHNV-VLPs with the same concentration of protease inhibitor cocktail; 3) 200-400 ng of the purified IHHNV-VLPs storing in 4ºC and 25ºC at different time periods; 3) 200-400 ng of the purified IHHNV-VLPs subjected to a broad range of pH (4-9) treatments; and 5) 200-400 ng of the purified IHHNV-VLPs with 30 mU trypsin, chymotrypsin and pepsin treatments. All proteins were heated in hot plate for 5 min at 95 ºC. The denatured proteins were resolved as duplicate gels in 15% SDS-PAGE and separated in the Mini Protein electrophoresis system (Bio-Rad Laboratories) at 100 mA constant voltages for 3 h in room temperature. The separated proteins in group 2-4 were subjected to silver staining using a kit from Invitrogen (Invitrogen Co., Carlsbad, CA, USA).

3. TEM sample preparation: Negative staining

Recombinant IHHNV capsid structure was estimated by negative-stained TEM imaging. Negative staining for TEM was used to increase image quality for analysis. IHHNV-VLPs were purified and preserved in TBS, pH 7.8, at a concentration of 0.1-0.5 mg/ml. TEM samples were prepared on 200 mesh carbon-coated copper grids carrying 5 µl of IHHNV-VLP in TBS that had been, incubated on the grid for 10 seconds before side blotting. Samples were stained with 2% uranyl acetate(UA) by dropping 10 µl 2% U on sample grid and incubating for 1 min, side blotting. Completely prepared grids could be stored for 1-2 months. Prepared grids were observed using TEM with Gatan digital micrograph program at 25,000X and 50,000X.

4. Whole-mount binding of IHHNV-VLPs to Penaeus vannamei post-larvae

Biotinylated IHHNV-VLPs prepared as in Section 4.1 were used to visualize tissue binding in intact juveniles. Post-larvae were euthanized, gently decalcified (EDTA-based buffer), rinsed with PBS (pH 7.4), and incubated with biotin-IHHNV-VLP (20 µg/mL in PBS) for 48 h at 4 °C with slow rocking. Samples were washed 3× in PBS (10 min each), incubated with Alexa Fluor 488–avidin (Thermo Fisher) for 48 h at 4 °C, counterstained with DAPI (1 µL of 14.3 mM stock in 5 mL PBS; 2–5 min), mounted in anti-fade medium, and imaged on an Olympus AX123 epifluorescence microscope using identical exposure settings for control vs. VLP-treated specimens. Secondary-only controls were processed in parallel.

5. Tissue protein extraction (gill, muscle, hepatopancreas)

Gill, muscle, and hepatopancreas were dissected on ice and homogenized in a RIPA-like buffer: 0.5% (v/v) IGEPAL CA-630, 0.5% (w/v) sodium deoxycholate, 0.1% (w/v) SDS, 0.5% (v/v) Triton X-100, 1.0 mM EDTA, 0.01% (w/v) sodium azide in PBS (pH 7.4) with 1× protease inhibitors. Lysates were clarified (≥12,000 × g, 10 min, 4 °C), and the supernatants were collected. The protein concentration was measured using a colorimetric assay. Aliquots were stored at −20 °C and thawed once before ELISA.

6. ELISA quantification of IHHNV-VLP binding to tissue extracts

High-binding 96-well plates were coated overnight at 4 °C with tissue proteins (100 µg/mL or total 50 µg/well) in carbonate–bicarbonate buffer (0.1 M Na2CO3/NaHCO3, pH 9.5). After PBS-T washes (0.05–0.1% Tween-20), plates were blocked with 3% BSA in PBS-T for 1 h at room temperature. Wells were incubated overnight at 4 °C with biotin-IHHNV-VLP (same batch as Section 4.2), washed, and detected with anti-His (1:1,000) followed by goat anti-mouse HRP

(1:10,000), or with streptavidin-HRP for direct biotin formats. SureBlue TMB substrate was developed at a fixed time, reactions were stopped with acid, and absorbance was read at 452 nm. Technical replicates, plate blanks, and no-VLP controls were included.

7. Lectin–ELISA profiling of tissue glycans

To profile glycan features, coated and blocked plates (as in 4.4) were incubated with a biotinylated lectin panel (Vector Laboratories): ConA, AAL, WGA, RCA-I, UEA-I, and SNA-I (typical working 1–5 µg/mL in PBS-T with 1% BSA) for 1–2 h at room temperature. After washes, streptavidin-HRP was added, TMB was developed, and absorbance was read at 452 nm. Signals were compared across tissues run on the same plate to infer relative enrichment of mannose-, fucose-, GlcNAc-, or sialic-acid–bearing glycans (figure 4.3).

8. Lectin-blocking assay (competitive inhibition of VLP binding)

To test whether host glycans recognized by lectins participate in VLP attachment, plates coated with tissue proteins were pre-incubated overnight at 4 °C with lectins (4 µg/mL) in PBS-T/1% BSA. After washing, IHHNV-VLP (10 µg/mL) was added and processed as in Section 4.4. Specificity controls included no-lectin wells and lectins expected to bind weakly in shrimp tissues (UEA-I, SNA-I). Inhibition was expressed relative to no-lectin controls on the same plate (figure 4.3).

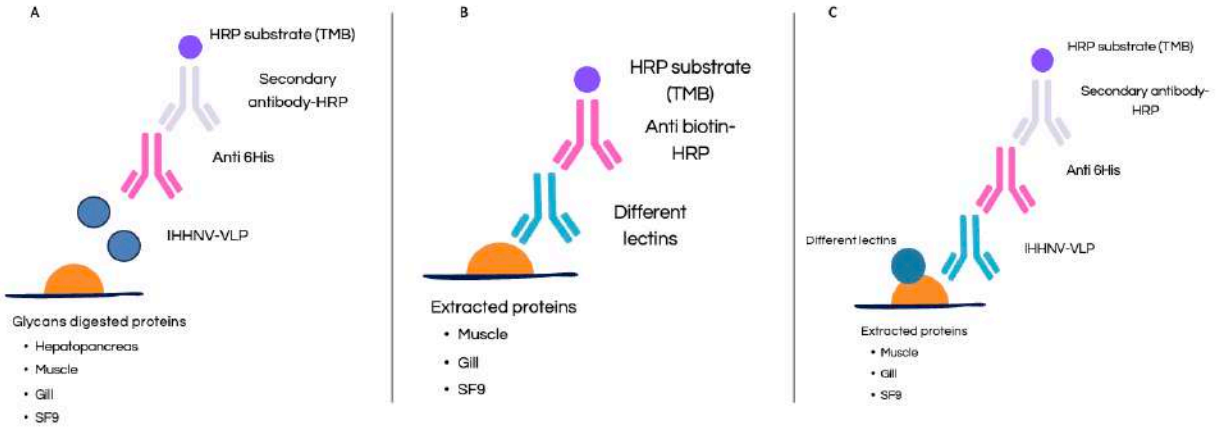

Figure 4.3 Diagram showing different schematic of ELISA assay. (A) binding of IHHNV-VLP to *P. vannamei* tissues and SF9. (B) Lectin binding on *P. vannamei* tissue. (C) Lectin blocking of IHHNV-VLP binding on P. vannamei tissues.

9. Chemical and enzymatic modification of surface glycans

To assess glycan dependence, coated plates were treated with sodium periodate (NaIO4; freshly prepared; standard vicinal-diol cleavage conditions) or with glycosidases: PNGase F (removal of N-glycans), α-mannosidase (trimming of mannose), and α-fucosidase (removal of fucose) in manufacturer-recommended buffers, overnight at 37 °C. Treated wells were thoroughly washed and immediately assayed for IHHNV-VLP binding as in Section 4.4. Buffer-only and heat-inactivated enzyme controls were included.

10. Immunohistochemistry (IHC) and lectin histochemistry on tissue sections

Frozen sections (or whole-mounts where indicated) were equilibrated to room temperature (10–20 min), rehydrated in PBS (pH 7.4, 10 min), and circumscribed with a hydrophobic barrier. Sections were blocked with 1% horse serum in PBS (30 min, room temperature) and incubated with antci-

His (1:500) in incubation buffer (1% BSA, 1% normal serum, 0.3% Triton X-100, 0.01% sodium azide in PBS) overnight at 4 °C. After 3 × 15 min PBS washes, sections were labeled with anti-mouse secondary (1:1,000) for 30–60 min at room temperature (light-protected), washed 3 × 15 min in PBS, counterstained with DAPI (as in 4.2), mounted with anti-fade medium, and imaged under constant exposure. For lectin histochemistry, sections were incubated with biotinylated ConA, AAL, WGA, RCA-I, UEA-I, and SNA-I under identical buffer conditions and detected with streptavidin conjugates before mounting and imaging. Parallel no-primary and secondary-only controls were run.

11. Protein preparation for glycomics and release of N-glycans

Lyophilized gill and muscle (50 mg per tube; duplicate tubes per tissue) were extracted in parallel with Buffer A (6 M guanidine HCl in 100 mM Tris-HCl, pH 8.5) and Buffer B (0.5% Triton X-100 in 100 mM Tris-HCl, pH 8.5) overnight at 4 °C, clarified (13,000 rpm, 10 min, room temperature), reduced with DTT (final 10 mM, 37 °C, 1 h), and alkylated with iodoacetamide (final 50 mM, 1 h, dark, room temperature). Triton extracts were precipitated with 10% TCA (−20 °C, 30 min), pelleted (13,000 rpm, 10 min, 4 °C), washed at least twice with cold acetone, air-dried, and stored at −20 °C. Guanidine extracts were dialyzed extensively against cold water and lyophilized. For N-glycan release, preparations were resuspended in 50 mM ammonium bicarbonate (200 µL), sonicated (30 min), digested with trypsin (1:100, w/w; 37 °C, 3–4 h), heat-stopped (100 °C, 5 min), and treated with PNGase F (≥1 µL; 37 °C, overnight).

12. C18 cartridge fractionation and collection of N- vs. O-glycan pools

PNGase-treated samples were loaded onto C18 cartridges pre-conditioned with 3 mL 100% acetonitrile, 3 mL 100% 1-propanol, and 5 mL 5% acetic acid (column kept acidic with additional 5% acetic acid as needed). The flow-through and 5% acetic acid wash (containing released N-

glycans) were collected and lyophilized. Bound material (peptides/de-N-glycopeptides/O-glycopeptides) was eluted stepwise with 2 mL 20% 1-propanol, then 2 mL 40%, and 2 mL 60% 1-propanol in 5% acetic acid. Pooled organic eluates were dried under nitrogen and lyophilized for O-glycan release.

13. Reductive β-elimination and cleanup of O-glycans

The pooled peptide/glycopeptide fraction was subjected to reductive β-elimination using 1 M NaBH4 in 0.05 N NaOH (400 µL; freshly prepared: 38 mg NaBH4 per mL 0.05 N NaOH) at 37 °C for 37 h (optionally 45 °C for ≥16 h). Reactions were ice-quenched dropwise with 30% acetic acid (fume hood; CO2 release), then passed through a Dowex 50W-X8 cation-exchange column pre-equilibrated with 5% acetic acid to remove salts and peptides; the flow-through (O-glycans) was lyophilized. Borate was removed by adding 10% acetic acid in methanol three times with evaporation between additions. Cleaned O-glycans were stored dry until MS.

14. MALDI-MS(/MS) analysis of N- and O-glycans

Dried N- and O-glycan samples were dissolved in LC/MS-grade water, mixed with standard MALDI matrix, spotted onto the target. MALDI-TOF and MALDI-TOF/TOF spectra were acquired on a 4800 Proteomics Analyzer (Applied Biosystems, Framingham, MA, USA) and UltrafleXtreme (Bruker, Bremen) mass spectrometers in reflection positive mode. Glycan compositions were assigned from accurate m/z and verified by MS/MS where indicated (figure 4.4).

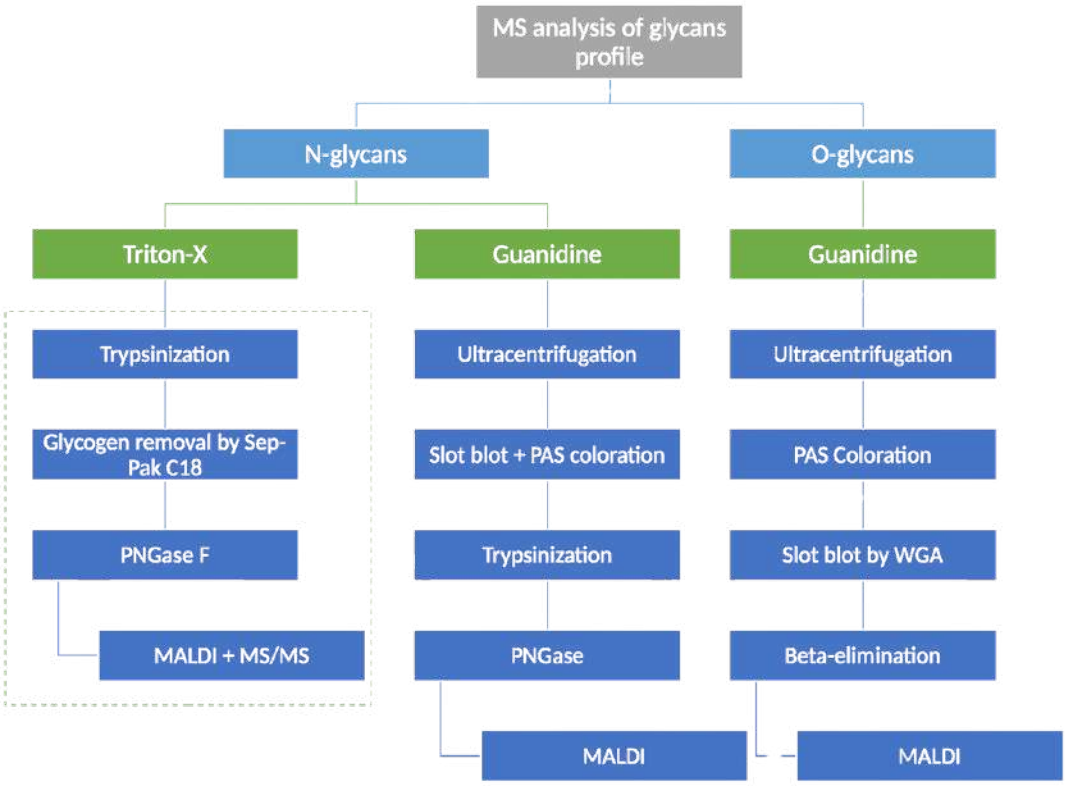

Figure 4.4 Workflow diagram outlining N- and O-glycan extraction with Triton X-100 or guanidine HCl for subsequent MS analysis.

15. **Western blot (identity and VLP checks)**

Proteins or VLPs (20–30 µg per lane) were separated by SDS–PAGE (12%), transferred to nitrocellulose (wet transfer 100–120 V, 1 h, 4 °C), and blocked with 3–5% BSA in TBST (1 h, room temperature). Membranes were probed with anti-His (1:5,000; overnight, 4 °C), washed 3 × 5–10 min in TBST, incubated with HRP-anti-mouse (1:10,000; 30–60 min, room temperature), washed, and developed with ECL (Pico) on a chemiluminescence imager. Identical exposure settings were maintained for lane-to-lane comparisons.

16. **Far Westernblot analysis**

Proteins from shrimp muscle and gill were extracted using RIPA buffer, and 20–30 μg of protein per lane was separated on a 12% SDS–PAGE gel, followed by transfer as described above. Membranes were blocked with 5% BSA in TBST for 2 h at room temperature and then incubated overnight at 4 °C with either virus-like particles (VLPs) or lectins (WGA, ConA, AAL, UEA-I; 1:5,000). After washing with 0.1% TBST (3 × 5 min), membranes were probed for detection: anti-His antibody (1:5,000; 2 h, room temperature) for VLPs or anti-biotin antibody (1:5,000; 2 h, room temperature) for lectins, followed by HRP-conjugated anti-mouse secondary antibody (1:10,000; 30–60 min, room temperature). After additional washes (3 × 5–10 min, TBST), signals were developed using ECL (Pico) and visualized on a chemiluminescence imager with identical exposure settings across lanes for comparison.

17. **Pull-down assay**

The pull-down assay using Ni-NTA–immobilized 6×His-tagged proteins as bait was adapted from a previously described method (Louche, Salcedo, & Bigot, 2017). Purified IHHNV-VLPs (200 μg), carrying a 6×His tag, were incubated with 1 ml of Ni-NTA beads (GE Healthcare, Piscataway, NJ). The IHHNV-VLP–bound beads were then exposed to shrimp gill and muscle protein extracts by passing the lysates through the resin bed. Bound proteins were eluted using buffer containing 1 mM NaCl and 250 mM imidazole. Eluted fractions, along with gill and muscle proteins alone and IHHNV-VLPs alone, were analyzed by SDS–PAGE on 12.5% polyacrylamide gels and visualized by Coomassie Brilliant Blue G-250 staining.

18. Data handling and statistics

Plate absorbance (452 nm) and imaging metadata were exported to Python 3.10.12 and analyzed with NumPy 2.0.2, Pandas 2.2.2, and SciPy 1.11.0. Multi-group comparisons (e.g., enzyme or lectin treatments vs. control) used one-way ANOVA followed by Dunnett's test ($\alpha = 0.05$). Figures were generated in Matplotlib 3.7.1 and Seaborn 0.13.2. Exact n and replicate type are reported alongside each figure.

Classical lectins can be categorized based on specific ligand motif interactions, as summarized in Table 4.1.

Table 4.1. Overview of major plant lectins; lectins employed in this study are indicated in yellow

Lectin Symbol	Lectin name	Source	Ligand motif
Mannose-binding lectins			
ConA	Concanavalin A	*Canavalia ensiformis*	α-D-mannosyl and α-D-glucosyl residues branched α-mannosidicstructures (high α-mannose type N-Glycans)
Galactose / N-acetylgalactosamine binding lectins			
RCA	*Ricinus communis* agglutinin	*Ricinus communis*	Galβ1-4GalNAcβ1-R
PNA	Peanut agglutinin	*Arachis hypogaea*	Galβ1-3GalNAcα1-Ser/Thr (T-Antigen)
N-acetylglucosamine binding lectins			
WGA	Wheat germ agglutinin	*Triticum vulgaris*	GlcNAcβ1-4GlcNAcβ1-4GlcNAc, Neu5Ac (sialic acid)
N-acetylneuraminic acid binding lectins			
SNA	Elderberry lectin	*Sambucus nigra*	Neu5Acα2-6Gal (NAc)-R (sialic acid)

MAL	*Maackia amurensis* leukoagglutinin	*Maackia amurensis*	Neu5Ac/Gcα2,3Galβ1,4Glc(NAc)
Fucose binding lectins			
UEA-I	*Ulex europaeus* agglutinin I	*Ulex europaeus*	Fucα1-2Gal-R
AAL	*Aleuria aurantia* lectin	*Aleuria aurantia*	Fucα1-2Galβ1-4(Fucα1-3/4) Galβ1-4GlcNAc, R2-GlcNAcβ1-4(Fucα1-6)GlcNAc-R1

CHAPTER V

RESULTS

1. Production and verification of IHHNV capsid and VLPs

i. *Molecular cloning and Protein purification*

Recombinant IHHNV capsid protein carrying a C-terminal hexahistidine tag was expressed in *E. coli* BL21 (DE3) using a pET-based expression vector and purified by Ni–NTA affinity chromatography. Amplification of the capsid gene produced a PCR fragment of approximately 990 bp (Figure 5.1), consistent with the expected insert size. Following elution with imidazole buffer (20 mM Tris–HCl, 250 mM imidazole, 500 mM NaCl, pH 7.4), the protein was desalted by dialysis and stored for subsequent assays. SDS–PAGE analysis revealed a single predominant band corresponding to the expected molecular weight of the capsid protein, with an estimated purity exceeding 95% (Figure 5.1). Under the described expression and purification conditions, the overall yield was approximately 2 mg of purified protein per liter of bacterial culture. Prior to use in downstream binding assays, the purified capsid protein was biotinylated. Importantly, the biotinylated capsid retained its ability to self-assemble into icosahedral virus-like particles (VLPs) with an average diameter of approximately 27 nm (Figure 5.1).

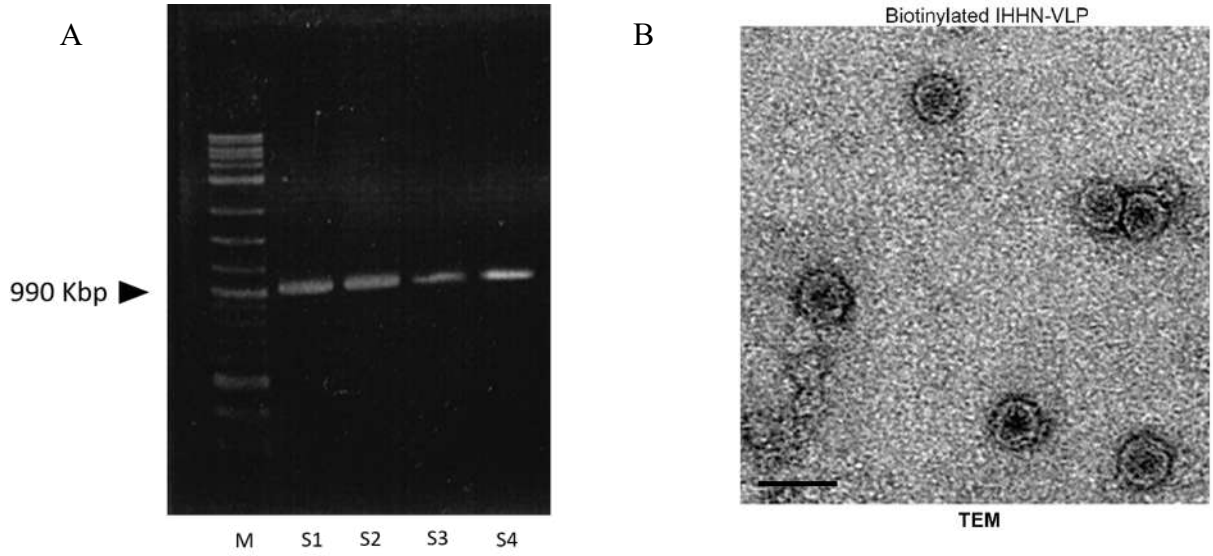

Figure. 5.1 (A) Expression of the IHHNV capsid gene**.** Gel electrophoresis showing PCR amplicons of the IHHNV capsid gene, size 990 bp, from 4 template genome preparations. (B) TEM image of IHHNV-VLP forming capsid protein

M: marker, S1: sample No.1, S2: sample No.2, S3: sample No.3, S4: sample No.4.

ii. *Capsid stability and its tolerance against many harsh conditions*

The IHHNV capsid structure showed an excellent stability against 3 conditioned tolerance tests, including 1) spontaneous-denaturation, 2) broad pH range test and 3) enzymatic digestion. The first testing condition, spontaneous-denaturation, VLP showed the stability in its protein form up to 3 months in laboratory refrigerator (4 ºC). Namely, the single, major band of 37 kDa slowly degraded into the smaller bands of 34, 30 and 27, 25 kDa since 1 week in the suspension. This

accounted for <3% of total proteins. After 2 to 3 months storage in the suspension, the major capsid protein band was rather stable – the smaller protein bands in the suspension did not increase drastically, they remained approximately <5% of the total proteins. Capsid proteins kept in 25ºC for 1 hour were also highly stable, having a similar range of protein degradation similar to those kept in the 4°C condition described above (Figure 5.2, Table 5.1).

The second condition was the broad pH range test. The results showed that IHHNV capsid protein could tolerate the drastic change of pH range, particularly in the neutral to basic condition (pH 7-9) with a very small change in protein integrity (Figure 5.3, Table 5.2). In the mild to moderate acidic condition (pH5-6), stability of capsid proteins were still of excellence – very few protein degradation in the SDS-PAGE gel was observed. However, a more protein degradation (approximately 10%) was observed in a stronger acidic condition at pH4 (Figure 5.3 and Table 5.1).

The third condition tested was enzymatic digestion test. IHHNV capsid protein showed its high stability against many hydrolytic enzymes that are well-known to be present in digestive track. For trypsin digestion test (with the optimal pH of 7.8), very little or no degraded protein bands were noted in the SDS-PAGE (Figure 4, lane Trypsin). This was in contrast with the control protein (BSA, 70 kDa) where the same amount of trypsin digestion resulted in numerous smaller banded proteins (Figure 4, lane Trypsin+BSA). Similar type of event also occurred with chymotrypsin digestion over IHHNV capsid protein, where little to no change of capsid protein was observed, whilst an apparent change in protein digestion pattern was clearly noted for positive control BSA (Figure 4, lane Chymotrypsin+BSA). The most drastic change in IHHNV capsid protein was noted in case of pepsin digestion condition where many degraded smaller banded proteins were observed (Figure 4, lane pepsin). Since the optimal pH of pepsin digestion

condition is about 3-4, we thus ruled out the effect of pH 4 that has also shown to cause IHHNV capsid degradation against pepsin digestion (table 5.2). The result showed that IHHNV capsid protein pattern that was subjected to pH4 closely resembled to that of pepsin digestion experiment. We believed that IHHNV capsid protein was favorably denatured by the low pH condition (which was herein used as the enzyme optimal buffer), rather than the additional action of pepsin enzyme (which would otherwise result in more degradation bands in the suspension.

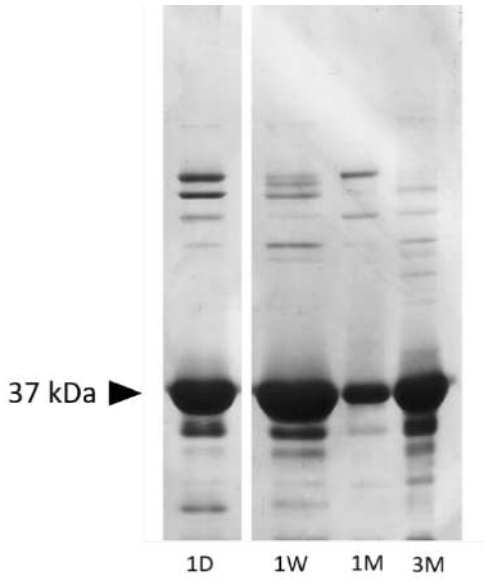

Figure 5.2: Spontaneous denaturation of IHHNV-VLP in two conditions. SDS-PAGE gel showed the result of self-denaturation periods of IHHNV capsid protein under each time condition [84].

M: marker, Cl: crude protein, FT: flow through, W: wash, E1 1D: first elute 1-day old, E2: second

Table 5.1: Summary of IHHNV capsid protein spontaneous denaturation test

Temperature / time	4ºC	25 ºC
1 day	+++	+++
1 week	+++	-
1 month	+++	-
2 months	+++	-
3 months	++	-

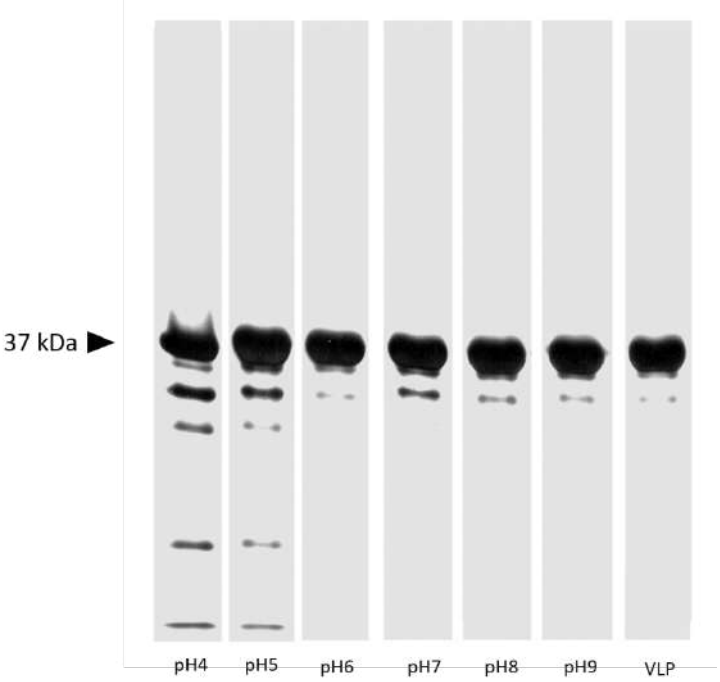

* +++ : high, ++ : medium, + : low, - : no data

Figure 5.3: Board pH range test of IHHNV capsid protein. IHHNV capsid protein was incubated in various pH conditions (pH 4-9) and resolved by SDS-PAGE followed by Coomassie blue staining [84].

M: marker, E1: positive control

Table 5.2: Summary of pH condition test

Timing / pH	2Hr
4	++
5	+++
6	+++
7	+++
8	+++
9	+++

* +++ : high, ++ : medium, + : low, - : no data

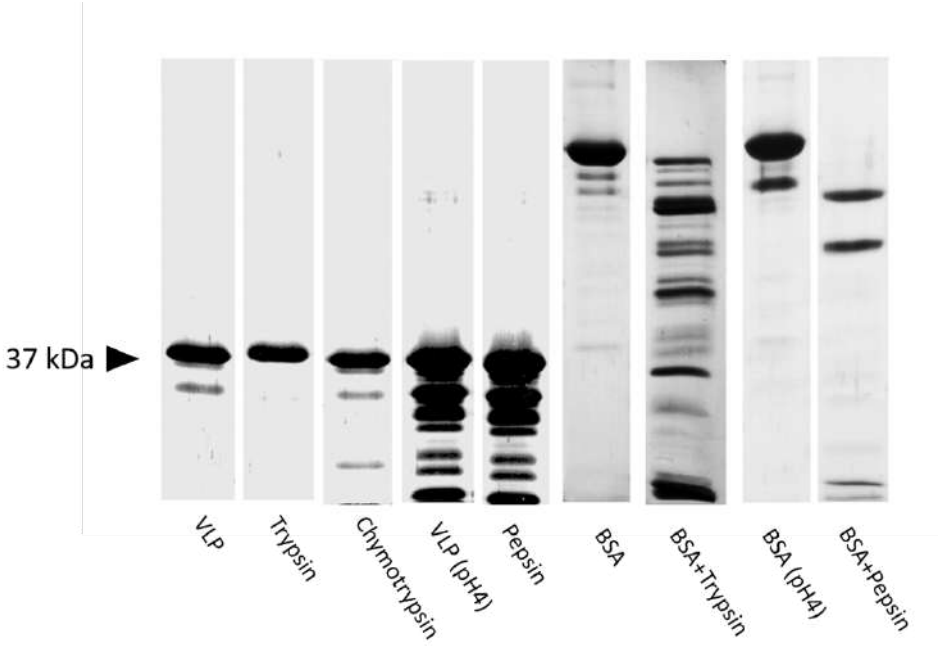

Figure 5.4: Enzymatic digestion test of IHHNV capsid protein. SDS-PAGE and Coomassie blue staining gel showed three types of enzymatic digestion test (trypsin, chymotrypsin, pepsin) over the IHHNV capsid protein versus the control protein, bovine serum albumin (BSA) [84].

Table 5.3: Summary of enzymatic digestion test

Timing / Conditions	1 Hour
Citrate buffer Control (pH4)	++
Pepsin	++
TBS buffer Control (pH7.8)	+++
Trypsin	+++
Chymotrypsin	+++

* +++ : high, ++ : medium, + : low, - : no data

**30mU enzyme concentration

iii. *Denaturation of IHHNV-VLP during its transportation*

As a part of this research dissertation is conducted in Prof. Yann Guerardel's laboratory In Lille University, France, IHHNV capsid protein and its reassembled VLP (produced massively in Thailand) were transported via air transportation. A sonicated whole lysates of E. coli containing IHHNV-VLP was shifted by FedEx service at −20 °C, which was later thawed when IHHNV purification was carried out in France. In fact, the material was received in August and was maintained at −20 °C until use. By January, denaturation of the IHHNV-VLP band was observed on Western blot under previously validated conditions (Figure 5.5, left panel), indicating the loss of the expected discrete capsid protein. This problem is periodically known to cause by the prolong storage of VLP in the extended −20 °C which might have caused a big crump of protein (seen as a white pellet in the bottom of the tube).

To solve this unexpected problem, we thus used bacterial pellets (in the cell lysates) rather than recovering VLPs from the supernatant fractions. In this regard, the cell lysate containing IHHNV capsid protein was centrifuged, and the recoverable pellet was collected and sonicated on ice. Purification was then performed using a Ni–NTA affinity column. Assessment by SDS–PAGE and Western blot showed a single band at ~37 kDa (Figure 5.5, right panel), consistent with the IHHNV capsid, and the re-purified materials were then used for the subsequent experiments.

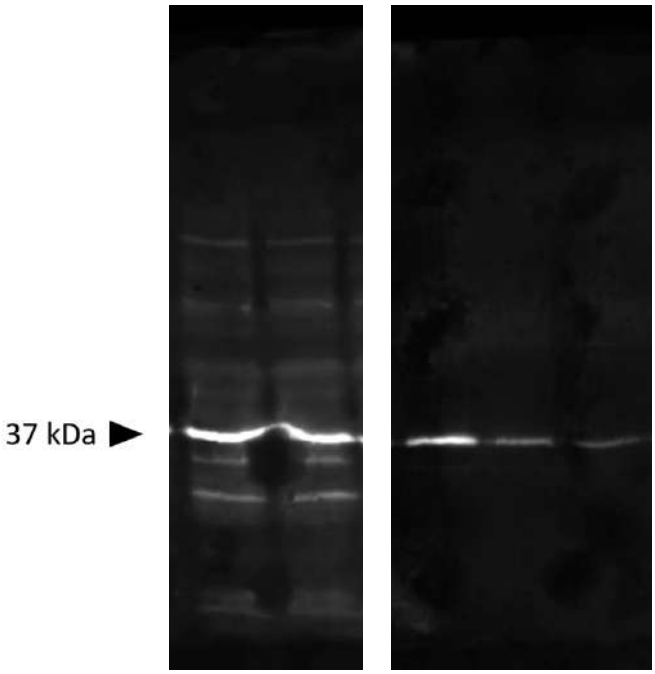

Figure 5.5: IHHNV-VLP denaturation due to transportation and its recovery from bacterial pellets. Western blot analysis showed multiple bands of anti-6X-His reactivity against degraded IHHNV-VLP obtained from the supernatant of whole lysates (left panel). Through sonication of the cell pellets, a single-banded pattern of purified IHHNV-VLP was recovered.

2. **Binding of IHHNV-VLP to P. vannamei**

i. *Whole-mount binding of IHHNV-VLPs in Penaeus vannamei*

Post-larval shrimp were incubated with biotinylated IHHNV-VLPs and were processed for whole-mount fluorescence imaging under fixed acquisition settings. Minimal background was observed in control preparations that were carried through all steps without VLPs. Strong fluorescence was observed in specimens exposed to VLPs. Signal was concentrated in the gill structures and skeletal muscle. Along the gill, labeling was observed over lamellar surfaces and margins; within the body wall, labeling was observed in organized muscle bundles. Other regions showed only weak or no signal under the same exposure. Replicate preparations that were processed on different days yielded the same tissue distribution. Within each run, control mounts remained at baseline, confirming that the signal required prior exposure to IHHNV-VLPs. Panel assignments were kept constant so that controls VLP-treated whole mounts as in Figure 5.6. To support later comparisons with plate assays, image capture parameters (objective, camera gain, exposure time) were held constant within an experiment. Under these conditions, the whole-mount data established that gill and muscle are preferential in situ targets for IHHNV-VLP binding.

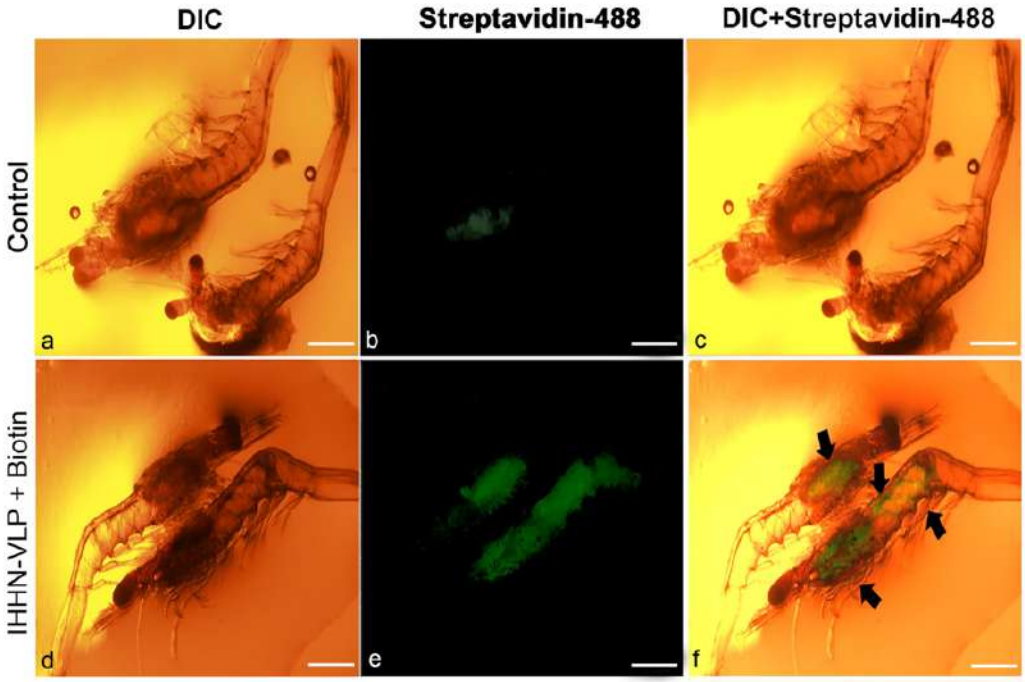

Figure 5.6. Whole-mount fluorescence of *P. vannamei* post-larvae (control), showing minimal background (a, b, and c).Whole-mount fluorescence after incubation with IHHNV-VLPs, showing strong signals localized to muscle and gill tissues, indicating tissue-specific targeting in situ (e and f).

ii. *Far western blot analysis and ELISA for quantification*

Binding of IHHNV-VLPs to indirect ELISA quantified immobilized extracts under identical coating and detection conditions (one hundred micrograms per milliliter total protein in carbonate–bicarbonate buffer, pH 9.5; TMB substrate with absorbance measured at 452 nm). An Sf9 insect-cell lysate was included to assess cross-species binding. The mean absorbance ranked as follows: gill and Sf9 showed the highest values, muscle was intermediate, hepatopancreas was lower, and stomach was the lowest. From the plotted scale, the mean optical densities were approximately 0.80 for gill, 0.78 for Sf9, 0.65 for muscle, 0.30 for hepatopancreas, and between 0.22 and 0.25 for stomach. Modest variability across replicates was indicated by the error bars, and plate blanks, together with no-VLP wells, remained at baseline. Under these settings, stronger IHHNV-VLP binding was observed for gill and Sf9, moderate binding for muscle, and weaker binding for hepatopancreas and stomach**.**

Proteins separated by SDS–PAGE were transferred to membranes, probed with IHHNV-VLPs, and detected with streptavidin–horseradish peroxidase. In the gill and muscle lanes, distinct bands were observed at about 150, 100, 75, 40, 35, and 30 kDa (Figure 5.7). The hemocyte lane displayed a broad, intense signal spanning roughly 75 to 150 kDa. The hepatopancreas lane showed a weak signal that was nevertheless slightly higher than that seen for the stomach**.** For ELISA, all tissues were analyzed on the same plate with matched blocking (3% BSA in 0.1% TBST) /washing (0.1% TBST) and 16 hours of 4 °C IHHNV-VLP incubation time. For Far-Western, transfer and exposure settings were kept constant across membranes. Technical replicates were included in both assays.

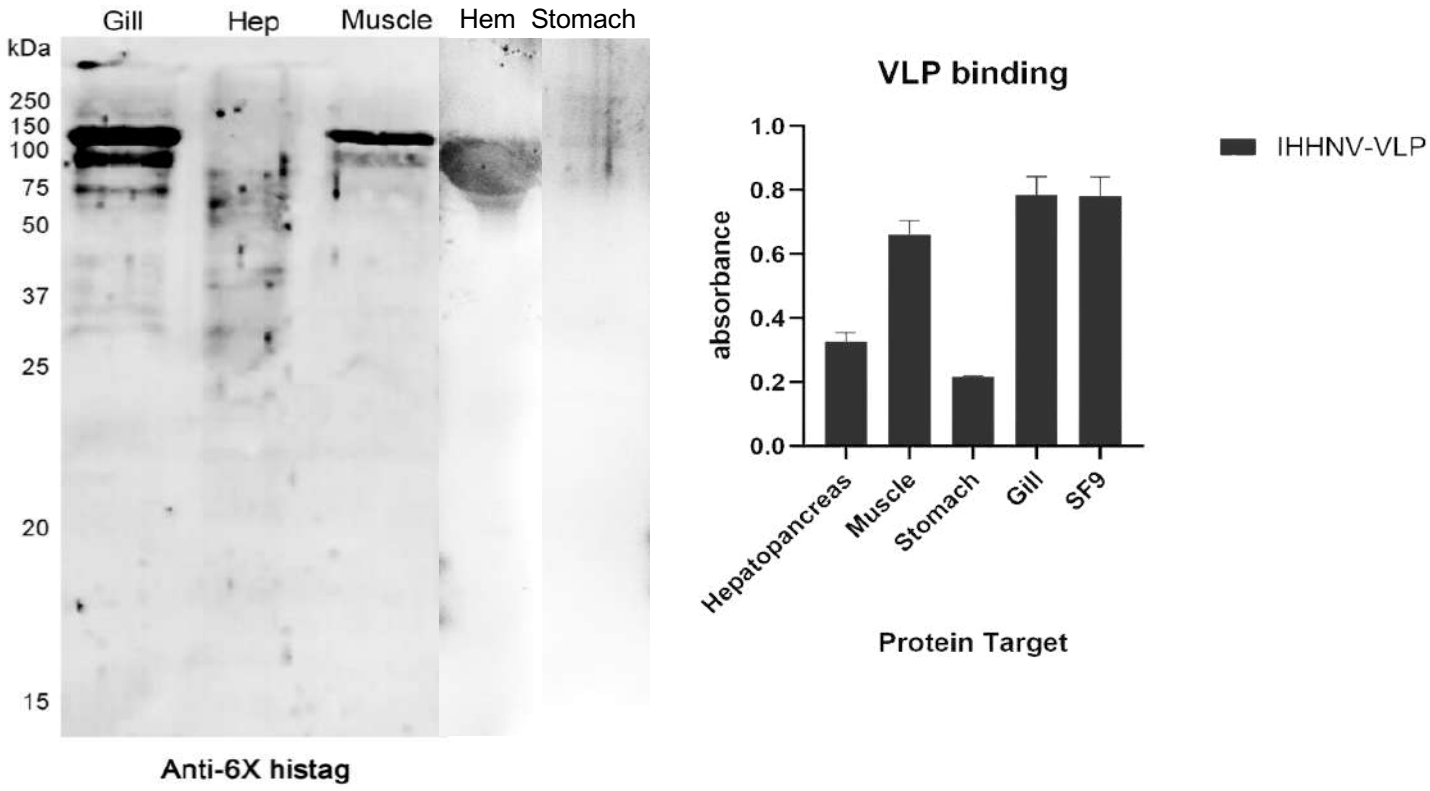

Figure. 5.7 Far-Western blot analysis of IHHNV-VLP binding to gill, Hepatopancreas (hep), Muscle, hemocytes (hem) and stomach on PVDF membrane (left). ELISA quantification of IHHNV-VLP binding to tissue lysates (gill, hepatopancreas, muscle) (right).

3. Pull-down assay

Initial binding results indicated that IHHNV-VLPs may interact with multiple protein targets in gill and muscle tissues. To further assess these interactions and to evaluate potential lectin binding or blocking effects, a pull-down assay was attempted to selectively isolate proteins of interest for subsequent experiments. Protein extracts from hepatopancreas, gill, muscle, and stomach were incubated with IHHNV-VLPs pre-bound to Ni-NTA beads (Figure 5.8). Despite multiple optimization attempts, including adjustments of imidazole and NaCl concentrations, stable binding between IHHNV-VLPs, tissue proteins, and the Ni-NTA resin could not be achieved. Consequently, subsequent experiments were conducted using native crude protein extracts.

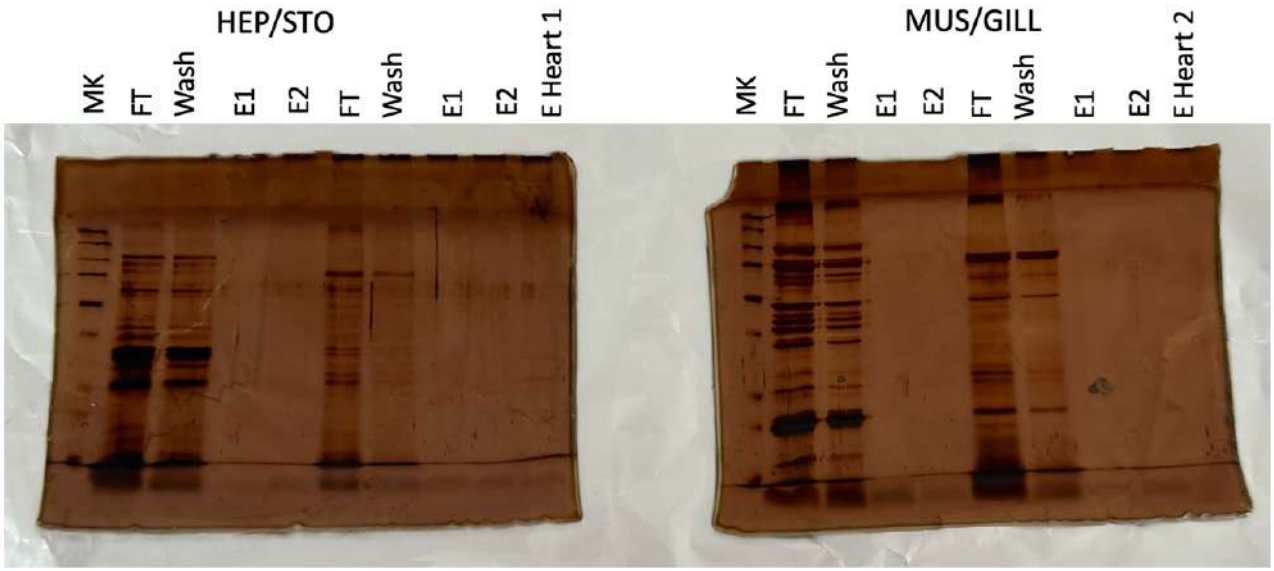

Figure 5.8. Silver staining of protein from pull-down assay. MK = protein marker, FT = Flow through, E = Elute.

4. Protein-coating titration for ELISA

Before ELISA runs, a coating titration was performed to select an appropriate protein load. Total proteins extracted from the gill and from the muscle were coated at zero, ten, twenty, fifty, and one hundred micrograms per well and probed with AAL under the standard ELISA conditions. For Gill, the absorbance rose sharply between zero and ten micrograms and reached a near-plateau by twenty micrograms, with only minor additional gains at fifty and one hundred micrograms. For muscle, a similar rise was observed, with a shallower increase between twenty and fifty micrograms and minimal change thereafter (figure 5.9). On this basis, twenty micrograms per well was selected for all subsequent assays. This load provided a strong signal while remaining within the linear working range, reduced the risk of early saturation or hook effects, and conserved the sample for replicate testing.

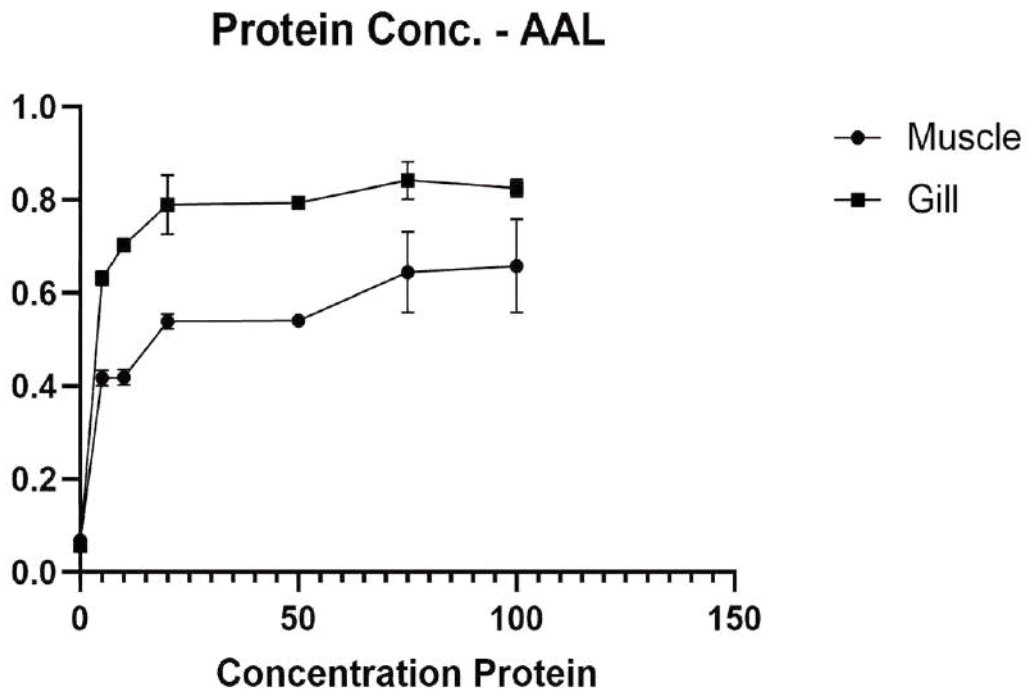

Figure 5.9. Protein-coating titration for ELISA with AAL. Gill and muscle proteins were coated onto ELISA plates at different concentrations and tested with AAL lectin. The signal increased with protein concentration and reached a stable level above ~50 µg/well.

5. Lectin profile in P. vannamei gill and muscle tissue

i. *Immunohistochemistry*

Lectin staining of muscle and gill tissues was performed under fixed exposure settings to allow direct comparison between sections (Figure 5.10A for gill; Figure 5.10B for muscle). Intense labeling by ConA and AAL was observed in both tissues, indicating abundant mannose- and fucose-containing glycans. ConA, which recognizes terminal mannose or glucose residues, showed a strong, continuous signal along muscle bundles and across gill lamellae, with hepatopancreas sections also displaying clear ConA positivity under the same imaging parameters. WGA**,** which binds *N*-acetylglucosamine, labeled both tissues and was consistently brighter in the gill than in the muscle, with accentuation along lamellar epithelia and interlamellar regions. AAL staining appeared as punctate to patchy domains in muscle and as discrete foci across gill lamellae, consistent with fucose-bearing motifs distributed over the tissue surface. RCA yielded a lower, yet reproducible signal in both tissues, compatible with the presence of β-galactoside structures such as LacNAc. In contrast, UEA-I and SNA-I produced only minimal labeling that remained close to background.

The overall intensity ranking was maintained across biological replicates: ConA was the most intense signal, WGA and AAL were intermediate, with WGA stronger in gill than in muscle, RCA was weak but detectable, and UEA-I together with SNA-I were minimal. Negative controls processed in parallel without primary lectin, and secondary-only controls, remained at baseline, supporting the specificity of the observed patterns. The spatial distribution of ConA and AAL in gill (broad lamellar coverage with discrete foci) and the heightened WGA signal in gill relative to

muscle agree with the quantitative lectin–ELISA profiles presented later, and with the glycan compositions detected by mass spectrometry.

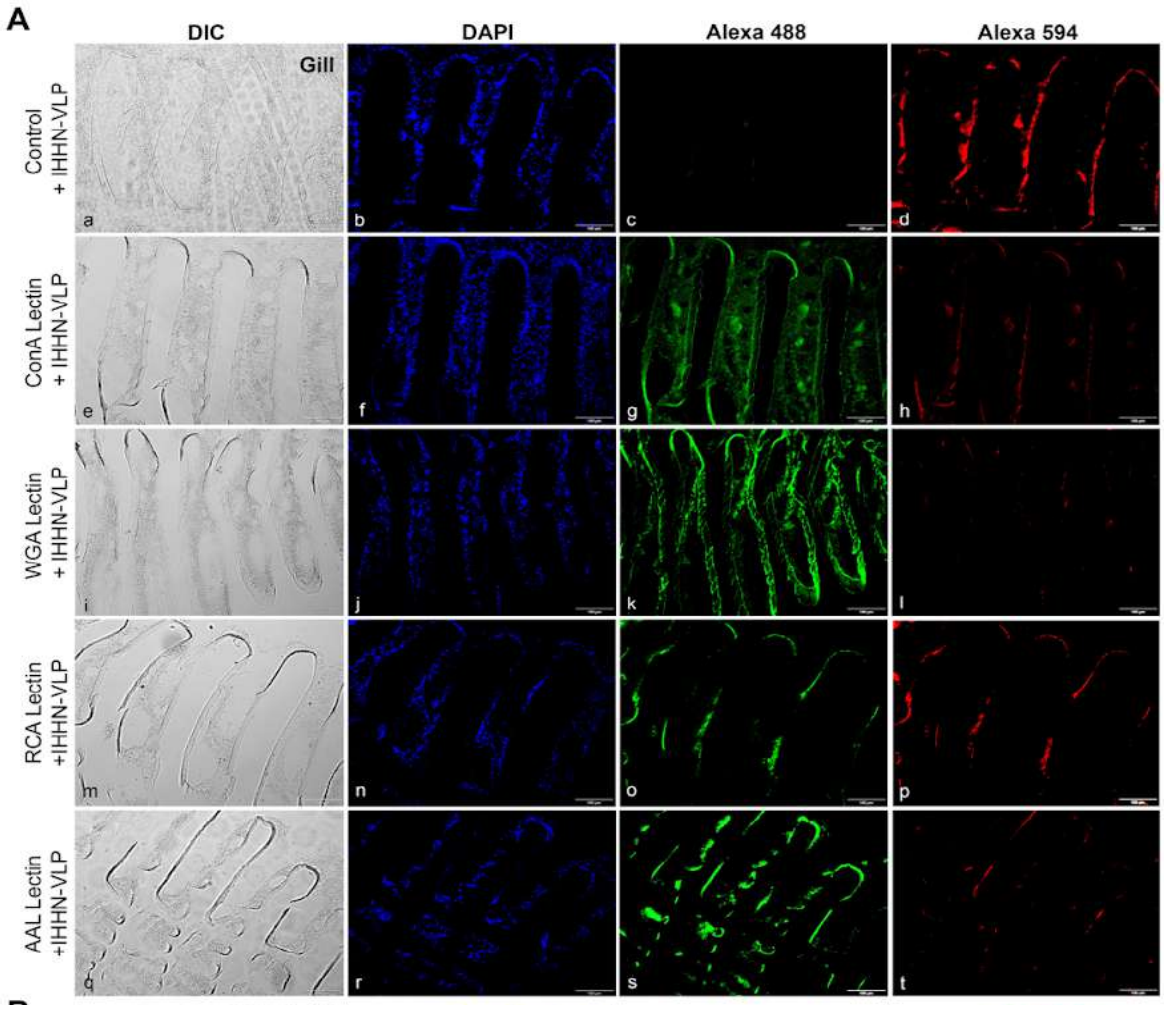

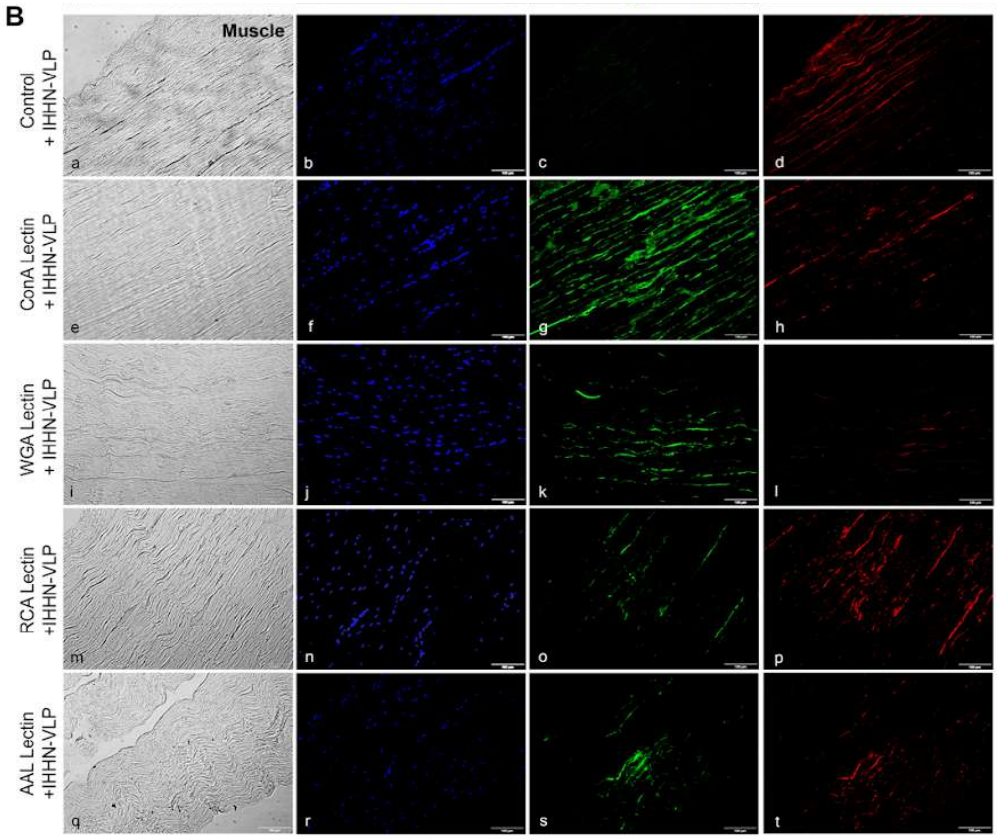

Figure 5.10 Lectin histochemistry of shrimp tissues and inhibition of IHHNV-VLP binding. Representative fluorescence images of gill (A) and muscle (B) sections stained with lectins ConA, AAL, WGA, RCA, UEA-I, and SNA-I (green, Alexa Fluor 488). Binding of IHHNV-VLP pre-incubated with corresponding lectins is shown in red (Alexa Fluor 594).

ii. *ELISA*

Lectin–ELISA was conducted on immobilized lysates to quantify relative binding. The highest absorbance values were obtained with ConA in the gill (1.411 ± 0.021 O.D.) and muscle (0.882 ± 0.046 O.D.). AAL and WGA yielded intermediate signals in gill (approximately 1.154–1.684 O.D.) and lower but measurable signals in muscle (approximately 0.599–0.916 O.D.). RCA produced weak binding in the gill (0.740 ± 0.034 O.D.) and muscle (0.313 ± 0.012 O.D.). UEA-I and SNA-I remained at minimal levels (gill 0.224 ± 0.054 and 0.179 ± 0.016 O.D.; muscle 0.214 ± 0.003 and 0.194 ± 0.007 O.D., respectively). All lectins were assayed on the same plate with matched blocking/washing conditions and a fixed substrate development time. Plate blanks and no-lectin controls returned baseline readings, confirming that measured signals reflected lectin–glycan interactions under the assay's dynamic range (Figure 5.11A).

iii. *Far-Western blot analysis*

Far-Western blots were examined to relate lectin binding profiles to capsid recognition. When membranes bearing gill and muscle proteins were probed with IHHNV-VLPs and developed with streptavidin/HRP, discrete bands were detected in both tissues, with prominent signals observed around ~150, ~100, ~75, ~40, ~35, and ~30 kDa. Membranes processed without the VLP probe (streptavidin only) showed minimal background. The molecular-weight range of the VLP-reactive bands overlapped the range in which strong lectin signals were observed in the same tissues, indicating that glycan-bearing proteins highlighted by ConA, AAL, and WGA are represented within the protein populations recognized by the capsid probe. Transfer, blocking, and exposure parameters were held constant across membranes (Figure 5.11B).

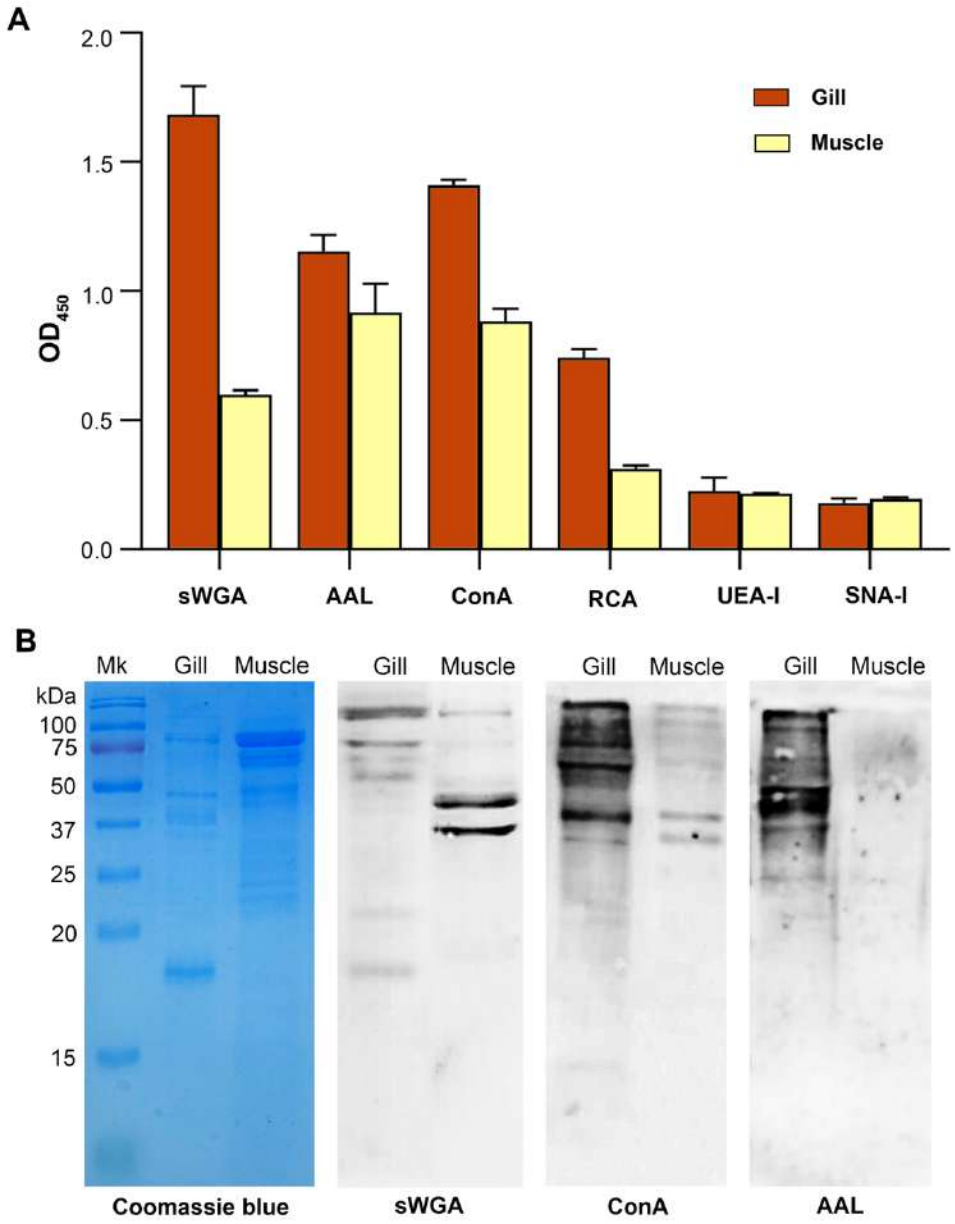

Figure 5.11 Lectin–ELISA profiling indicates mannose- and fucose-rich glycans in gill and muscle (A) ELISA assay using different lectins binding to gill and muscle protein extracts, including WGA, AAL, ConA, RCA, UEA-I, and SNA-I. (B) Far-Western blot analysis using biotin-conjugated WGA, ConA, and AAL binding to gill and muscle protein extracts on PVDF membrane

6. MALDI-MS/MS identifies oligomannose-dominated *N*-glycans and fucosylated O-glycans

For initial trials of N- and O-glycan extraction from glycoproteins, gill and muscle tissues were processed using both Triton X-100 and guanidine hydrochloride protocols. In the guanidine extraction approach, mucins were enriched by ultracentrifugation, and the resulting material was collected in fractions. Each fraction (20 μg) was loaded onto membranes for slot blot analysis. Membranes were first probed with HRP-conjugated WGA lectin, which produced positive signals across all tissues, with the strongest intensity detected in muscle. In parallel, PAS staining was performed to confirm glycan-containing fractions (Figure 5.12). Fractions testing positive for both WGA binding and PAS staining were selected for downstream N- and O-glycan release via PNGase F digestion and β-elimination.

MALDI-MS analysis of these preparations initially revealed only oligomannose-type N-glycans in both gill and muscle, while O-glycans were not detected (Figure 5.14). To improve recovery, β-elimination was subsequently applied directly to tissue lysates treated with either guanidine HCl or Triton X-100, without prior PNGase F digestion or C18 column purification. Under these optimized conditions, mass spectrometric analysis yielded composition-level glycan features consistent with the lectin-based results.

In gill tissues, O-glycans were clearly identified, with two predominant ions at m/z 953.4 (annotated as $Fuc_1Hex_1HexNAc_1$-HexNAcitol) and m/z 1127.5 (annotated as $Fuc_2Hex_1HexNAc_1$-HexNAcitol), indicating that fucosylated O-glycans represent major structural constituents (Figure 5.14). N-glycan profiles were dominated by oligomannose structures, with $Man_9GlcNAc_2$ ($[M+Na]^+$, m/z 2396.3) as the base peak. Additional peaks were detected at m/z 2192.2, 1988.1,

and 1784, corresponding to Man_8, Man_7, and $Man_6GlcNAc_2$, respectively (Figure 5.13). Furthermore, the detection of an ion at m/z 1590.9, annotated as $Fuc_1Hex_3HexNAc_3$, provided evidence of core fucosylation within the N-glycan population.

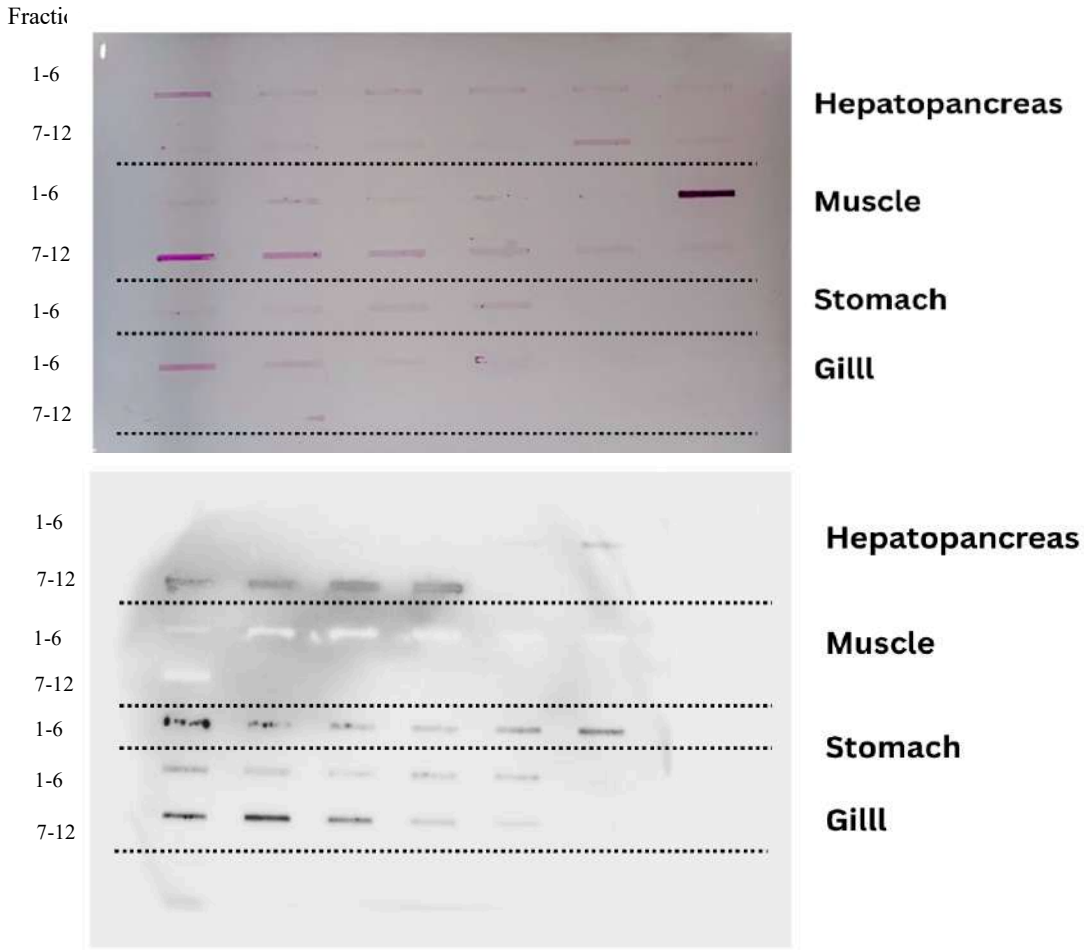

Figure 5.12 Slot blot analysis of fractionated tissue extracts probed with HRP-conjugated WGA, showing positive signals in all tissues, with the strongest binding in muscle (oversaturated white bans) . PAS staining confirmed glycan-containing fractions. Fractions positive for both WGA and PAS were selected for glycan release.

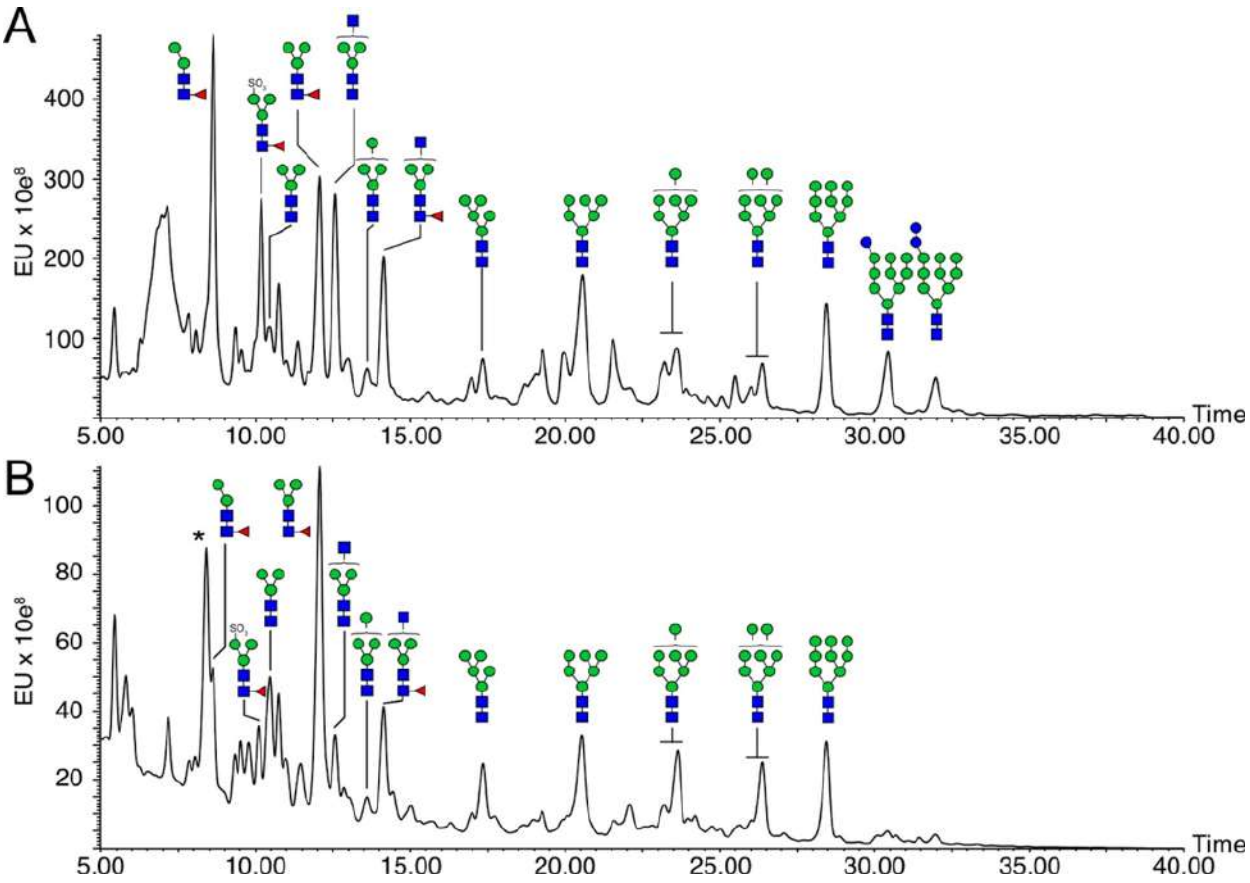
A
EU x 10e8
400
300
200
100
5.00
10.00
15.00
20.00
25.00
30.00
35.00
40.00
Time
B
EU x 10e8
100
80
60
40
20
5.00
10.00
15.00
20.00
25.00
30.00
35.00
40.00
Time

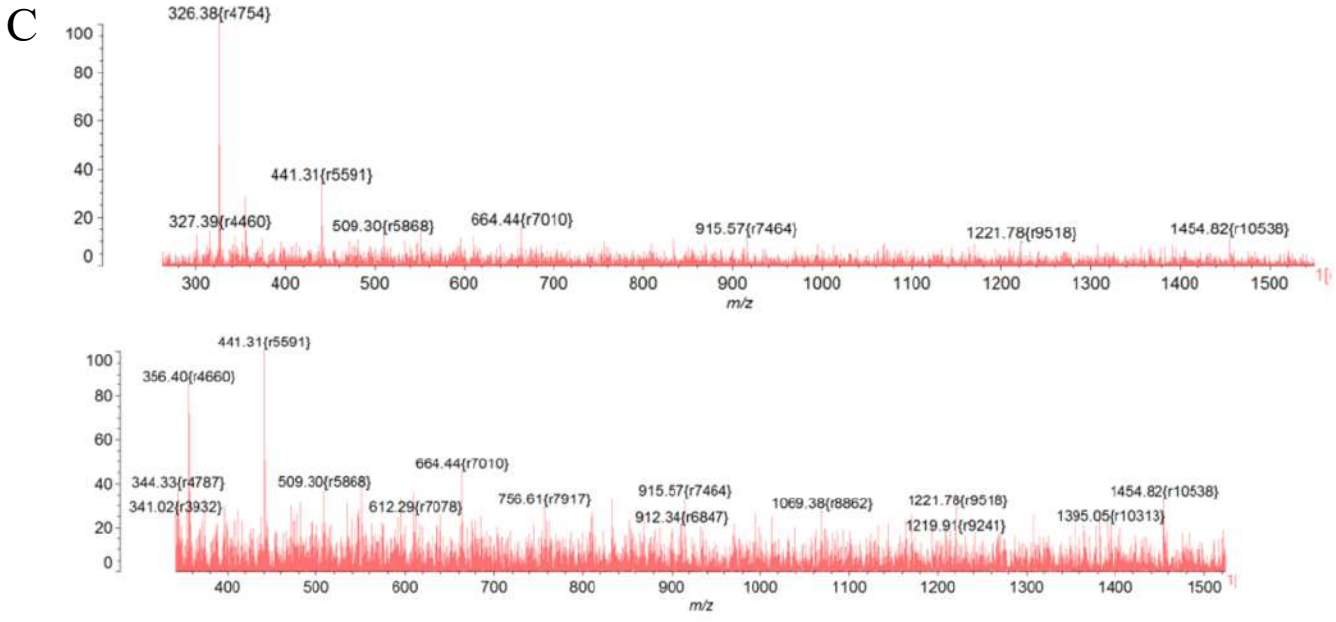
C
326.38{r4754}
441.31{r5591}
327.39{r4460}
509.30{r5868}
664.44{r7010}
915.57{r7464}
1221.78{r9518}
1454.82{r10538}
m/z
441.31{r5591}
356.40{r4660}
344.33{r4787}
341.02{r3932}
509.30{r5868}
612.29{r7078}
664.44{r7010}
756.61{r7917}
915.57{r7464}
912.34{r6847}
1069.38{r8862}
1221.78{r9518}
1219.91{r9241}
1395.05{r10313}
1454.82{r10538}
m/z

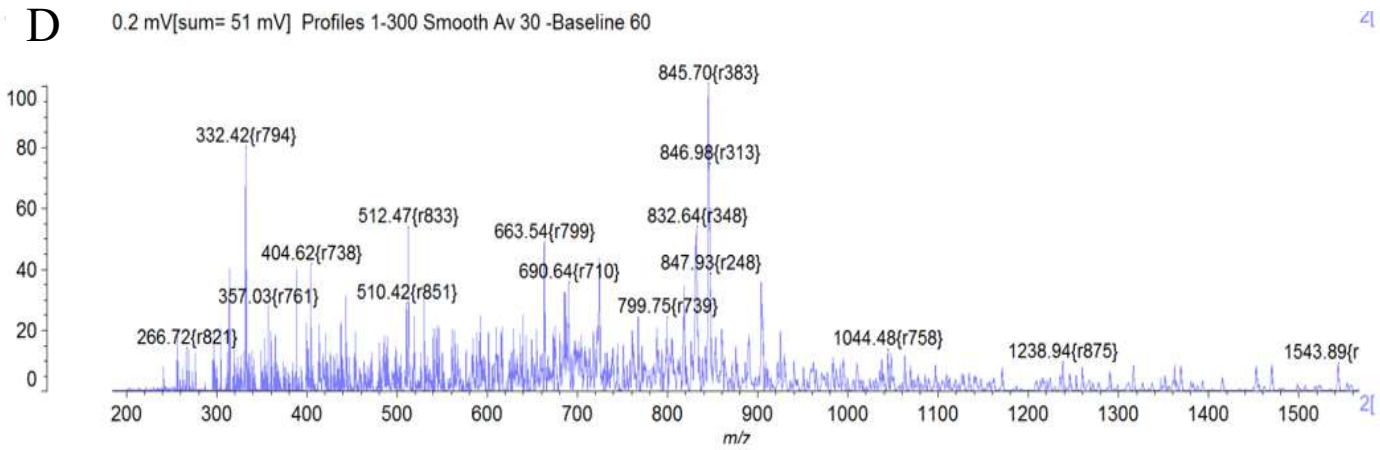

Fig 5.13 MALDI-MS spectra of glycans released from muscle, gill, hepatopancreas, and stomach . N-glycans were dominated by oligomannose structures, with $Man_9GlcNAc_2$ as the base peak and accompanying ions crresponding to $Man_{6–8}GlcNAc_2$ in muscle and gill (A,B). No specific N-glycans were found on both stomach and hepatopancreas tissues (C,D).

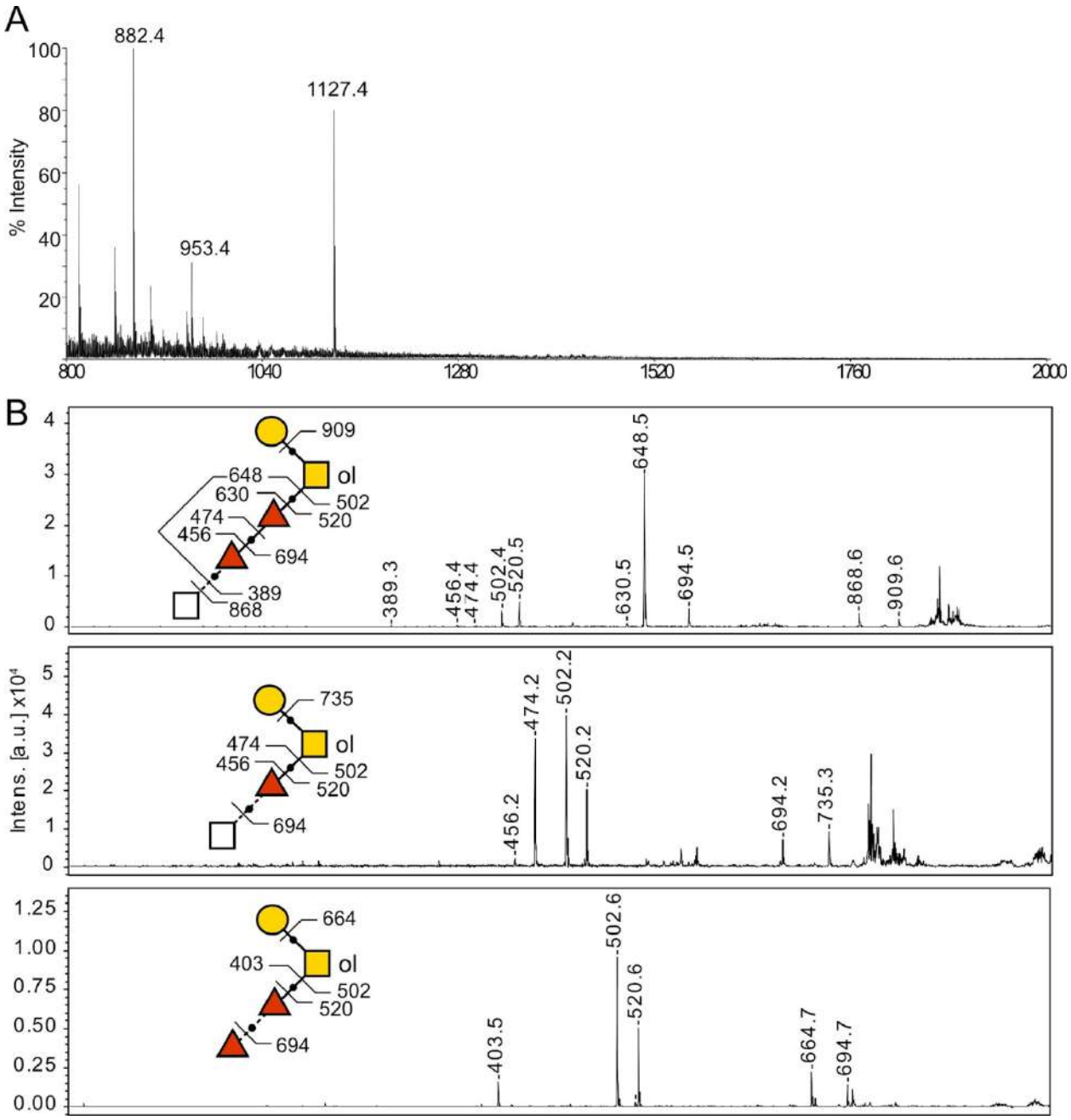

Fig 5.14 O-glycomic profiles of gill tissue analyzed by MALDI-MS(/MS). (A) MALDI-MS spectrum of permethylated O-glycans from gill extracts revealed three predominant signals at m/z 882.3, 953.4, and 1127.5. (B) MALDI-MS/MS sequence analysis of these ions is shown for m/z 882.3 (bottom), 953.4 (middle), and 1127.5 (top).

7. Lectin inhibition of IHHNV-VLP binding

i. *Immunohistochemistry*

Lectin staining was carried out on gill and muscle sections to map surface glycans. Exposure and camera gain were kept constant across slides to allow direct comparison. Secondary-only and no-lectin controls stayed at baseline. In gill, ConA produced a strong, continuous signal along the lamellae, with brighter caps at apical and marginal regions. AAL gave punctate foci distributed across the lamellar surface. WGA labelled the epithelium and interlamellar spaces more intensely than in muscle. RCA gave a low, scattered signal. UEA-I and SNA-I remained in the background. In muscle, ConA delineated myofiber bundles and the sarcolemma outline with high intensity. AAL yielded moderate, discrete puncta along fiber surfaces. WGA was present but weaker than in the gill and was confined mainly to pericellular regions. RCA was faint but reproducible. UEA-I and SNA-I stayed close to baseline under the same settings. The qualitative ranking was stable across biological replicates: ConA was highest, followed by WGA and AAL (with WGA being brighter in the gill than in the muscle); RCA was weak but detectable; UEA-I and SNA-I were minimal. DAPI was used to mark nuclei and to orient sections; overlay images showed lectin signals at cell surfaces rather than within nuclei. Panel lettering, scale bars, and imaging parameters were kept uniform so that these micrographs can be read alongside the ELISA and Far-Western results that follow.

ii. *ELISA*

Coated tissue proteins were pre-incubated with lectins at matched working concentrations and exposure times prior to the addition of IHHNV-VLPs. The panel comprised ConA, AAL, WGA, RCA, UEA-I, and SNA-I. Binding was quantified by the same indirect ELISA with fixed coating,

blocking, washing, and development parameters, and absorbance was read at 452 nanometers. In muscle lysates, pre-incubation with ConA, AAL, and WGA reduced the IHHNV-VLP signal, whereas RCA, UEA-I, and SNA-I did not change the signal relative to no-lectin controls. In gill lysates, pre-incubation with WGA, ConA, and AAL lowered the IHHNV-VLP signal, and RCA also reduced binding in this tissue; UEA-I and SNA-I showed no effect. No-lectin wells and non-inhibitory lectins remained at baseline, and plate blanks were low, indicating that the decreases observed with ConA, AAL, and WGA (and with RCA in gill) reflected specific masking of relevant glycan motifs rather than generalized surface blocking (figure 5.15).

After the verification of lectin competitive binding with IHHNV-VLP by ELISA and immunohistochemistry, far-western blot analysis was further performed to verify and visualize the blocking of IHHNV-VLP by different lectins. (b) AAL show significantly strong inhibitory effect on IHHNV-VLP binding (figure 5.16).

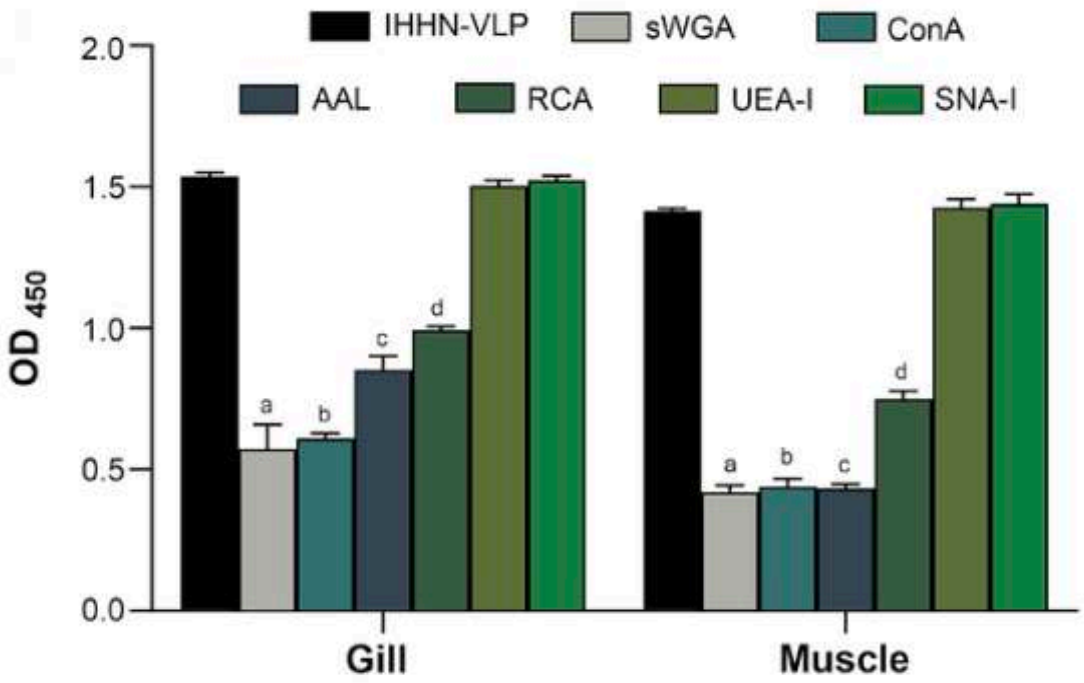

Figure 5.15 Lectin-blocking ELISA: ConA, AAL, and WGA significantly inhibit IHHNV-VLP binding, whereas UEA-I and SNA-I show no significant difference

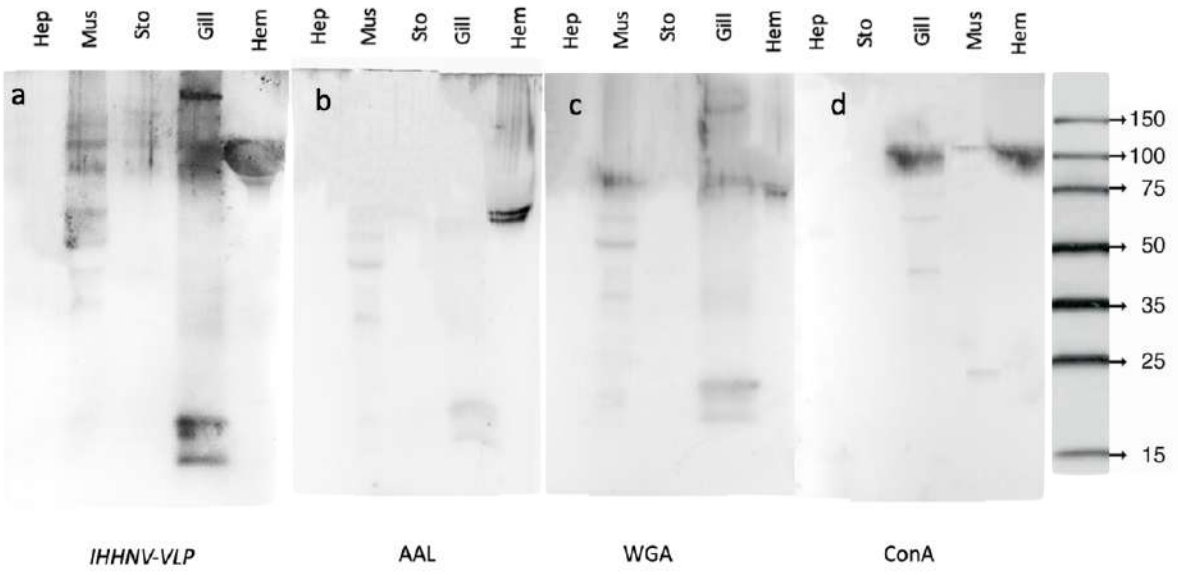

Figure 5.16 Lectin-blocking Far-western blot: AAL, WGA, ConA, significantly inhibit IHHNV-VLP binding, whereas UEA-I and SNA-I show no significant difference

8. Enzyme Digestion validation and effect on IHHNV-VLP binding

To verify enzyme activity, tissue lysates and an Sf9 insect-cell lysate were incubated overnight at 37 °C with the corresponding enzymes before being coated on ELISA plates. Activity of PNGase F was assessed by measuring WGA binding; activity of alpha-mannosidase was assessed with ConA; activity of alpha-fucosidase was assessed with AAL. A clear loss of lectin signal was observed after each matched treatment. With ConA, absorbance decreased from approximately 0.27 to 0.06 for muscle, from approximately 0.16 to 0.06 for gill, and from approximately 0.30 to 0.12 for Sf9, consistent with removal of mannose-rich *N*-glycans by alpha-mannosidase. With WGA, absorbance decreased from approximately 0.18 to 0.05 for muscle, from approximately 0.11 to 0.06 for gill, and from approximately 0.22 to 0.06 for Sf9 after PNGase F, consistent with loss of N-glycan cores. With AAL, absorbance decreased from approximately 0.55 to 0.35 for muscle, from approximately 1.30 to 0.75 for gill, and from approximately 0.85 to 0.55 for Sf9 after alpha-fucosidase, consistent with removal of fucosylated motifs. Untreated controls retained the highest signals and enzyme-treated counterparts showed reproducible decreases across replicates, confirming that the enzymes were active under the stated conditions (Figure 5.17). After validation, IHHNV-VLP binding was measured on enzyme-treated tissues. In gill, untreated wells read near 0.86 optical density units, while periodate oxidation reduced the signal to about 0.07, PNGase F to about 0.34, alpha-mannosidase to about 0.48, and alpha-fucosidase to about 0.52. In muscle, untreated wells read near 0.78, with periodate near 0.06, PNGase F near 0.47, alpha-mannosidase near 0.52, and alpha-fucosidase near 0.62. Thus, periodate produced the largest loss of binding, while the removal of *N*-glycans by PNGase F and trimming by alpha-mannosidase resulted in substantial losses, and alpha-fucosidase produced a smaller but consistent decrease. Plate blanks and no-VLP wells remained low, and buffer-only or heat-inactivated enzyme controls

did not alter the signal. These findings support a requirement for intact carbohydrate structures—especially N-linked mannose-rich and fucosylated features—for maximal IHHNV-VLP binding under the assay conditions shown

.

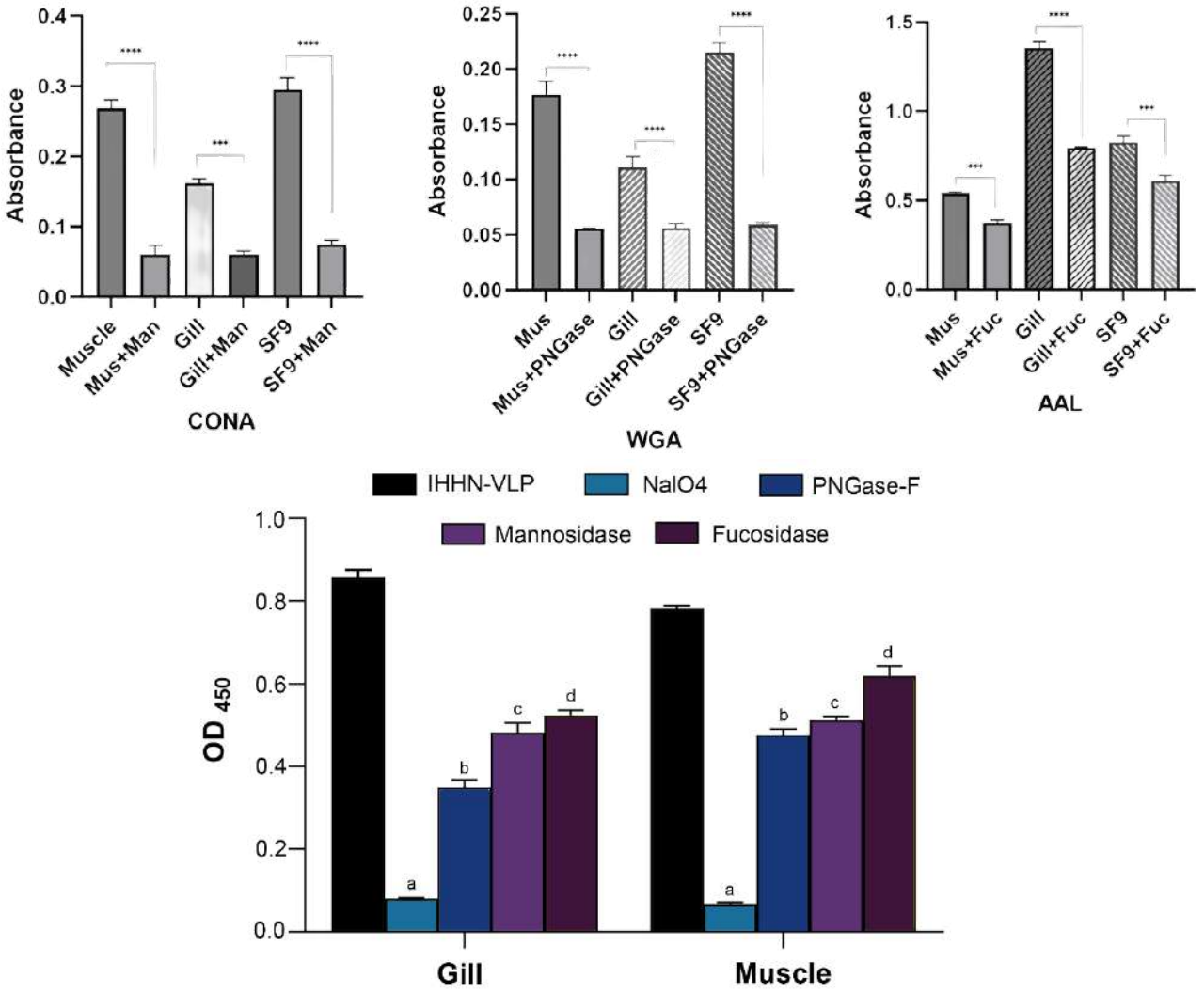

Figure 5.17 (Top) Mannosidase (man), PNGase-F, and Fucosidase (Fuc) enzyme activity testing. (bot) IHHNV-VLP binding on tissue, gill and muscle, pre-treated with different enzymes

9. Monosaccharide blocking of IHHNV-VLP binding

i. *Incubation time selection with fucose*

IHHNV-VLP was pre-incubated with fucose for thirty minutes, one hour, two hours, three hours, four hours, five hours, eight hours, sixteen hours, and twenty hours before ELISA. A progressive fall in signal was observed in both tissues as the incubation time increased. In the muscle, the absorbance declined from roughly 0.35 at thirty minutes to about 0.20 by eight hours and remained near that level at sixteen and twenty hours. In gill, the absorbance decreased from approximately 0.47 at thirty minutes to about 0.30 by eight hours and reached about 0.26 by sixteen to twenty hours. An incubation time of sixteen hours was therefore selected for subsequent blocking experiments, as it lay beyond the point at which additional incubation produced little further reduction (Figure 5.18A).

ii. *Blocking with fucose, mannose, and N-acetylglucosamine*

After sixteen hours of pre-incubation with single monosaccharides, IHHNV-VLP was allowed to bind to coated muscle, gill, and Sf9 extracts. In muscle, pre-incubation with fucose reduced the mean absorbance from approximately 0.36 to about 0.20; mannose and *N*-acetylglucosamine produced intermediate values of around 0.23 to 0.25. In gill, a more substantial effect of mannose and *N*-acetylglucosamine was observed, with means ranging from 0.16 to 0.18, compared with a baseline of around 0.51; fucose produced a reduction to approximately 0.25. In Sf9, mannose and *N*-acetylglucosamine reduced the signal to approximately 0.23 to 0.26 from a baseline of 0.39, whereas fucose produced little change, with a slight upward shift noted. Across tissues, plate blanks and no-VLP wells remained at low levels.

These results indicate that pre-occupancy of the capsid with simple sugars diminishes binding to coated targets in a sugar- and tissue-dependent manner. Mannose and *N*-acetylglucosamine produced the most consistent decreases in gill and Sf9, while fucose produced a substantial decrease in muscle and a moderate reduction in gill but little effect in Sf9. The chosen sixteen-hour pre-incubation time ensured that the observed reductions reflected near-maximal blocking under the assay conditions (Figure 5.18B).

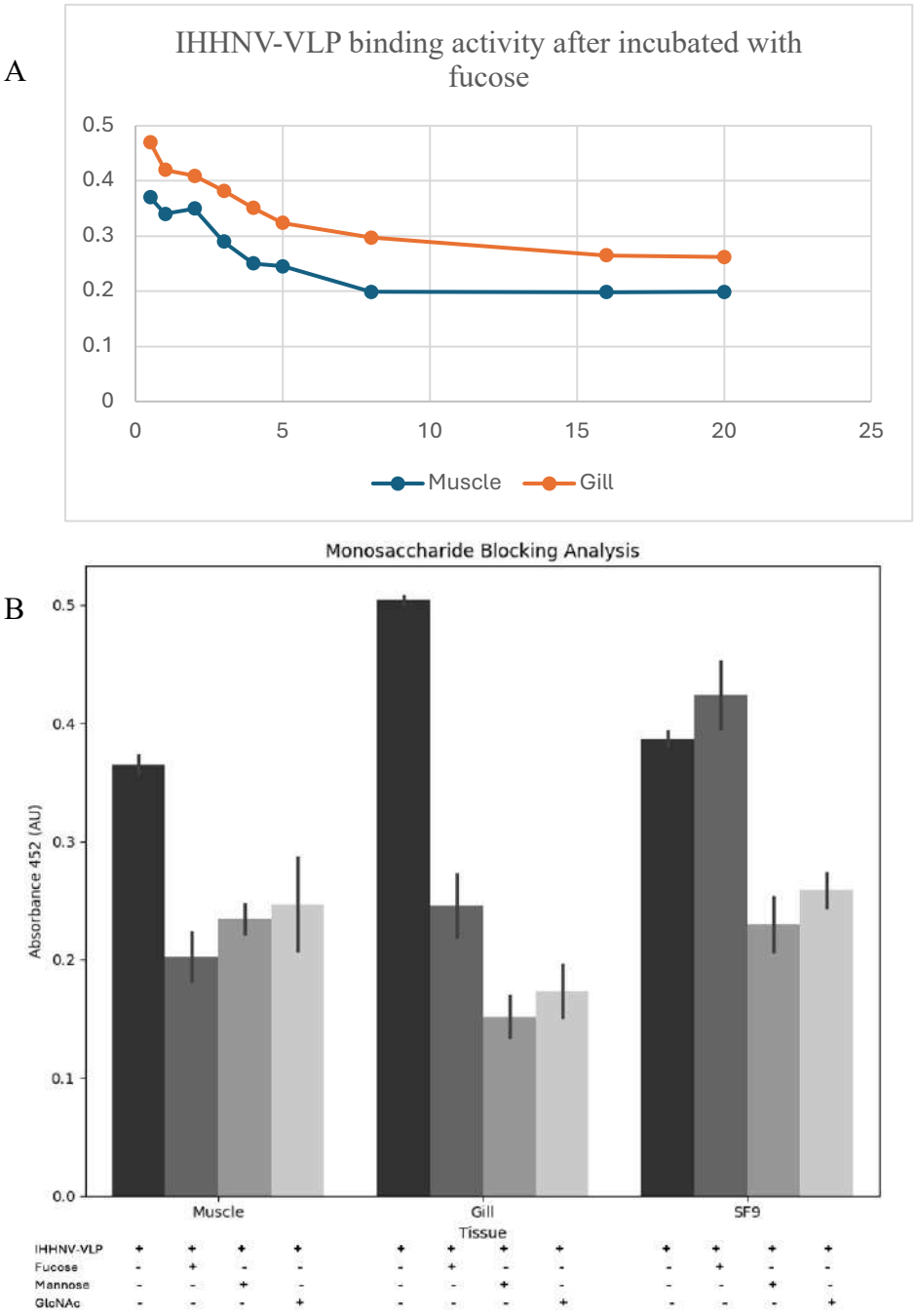

Figure 5.18 (A) Binding of IHHNV-VLPs pre-incubated with fucose for varying incubation times to muscle and gill tissues. (B) Binding activity of IHHNV-VLPs pre-incubated with different glycans for 16 hours on muscle, gill, and SF9 cells.

CHAPTER VI

DISCUSSION AND CONCLUSION

The present study provides new insights into the molecular mechanisms that govern the tissue tropism of IHHNV in Penaeus vannamei. By VLPs derived from IHHNV as a probe, we were able to dissect how glycans mediate the first steps of virus–host interaction in shrimp tissues. Our experiments consistently showed that IHHNV-VLPs bind preferentially to muscle and gill tissues, and this specificity is strongly associated with the presence of mannose- and fucose-rich glycans on these tissues. This finding not only confirms what many earlier histopathological observations suggested that IHHNV tends to infect ectodermal and mesodermal-derived tissues [63,64], but also extends our understanding by linking tissue susceptibility directly to molecular glycan motifs.

1. Glycan signatures, tissue specificity, and evolutionary concerns

Differences in glycan composition largely explain the tissue selectivity observed in our study. Glycomic profiling using lectin-based assays and MALDI-MS revealed that both gill and muscle tissues are enriched in oligomannosylated and fucosylated N-glycans. By contrast, hepatopancreas tissue expressed very low levels of fucosylated glycans, and this corresponded with minimal IHHNV binding. The correlation between glycan abundance and viral binding efficiency suggests a mechanistic link, where glycans act as the initial “landing pads” for the virus. This concept aligns with observations from other viral systems. Many parvoviruses, including canine parvovirus and adeno-associated viruses, rely on glycan moieties such as sialic acids or heparan sulfate as primary attachment factors [22]. However, attachment alone is rarely sufficient; productive infection typically requires secondary interaction with a protein receptor [36,37]. Our

far-Western blot analysis supports this two-step model: VLPs interacted with multiple glycoprotein bands of varying sizes, raising the possibility that IHHNV recognizes glycan-decorated proteins as part of a larger receptor complex. The implication is that a combination of factors dictates tissue tropism of IHHNV. Glycans provide the initial, relatively low-affinity but high-avidity interaction that concentrates virions on susceptible tissues, while proteinaceous receptors may then determine whether entry and replication occur. This layered model helps explain why hepatopancreas, though part of the shrimp's central organ system, is relatively resistant to IHHNV: the absence of appropriate glycans reduces viral docking, and additional host factors may be missing altogether.

Our findings resonate with glycan-binding phenomena reported in other crustacean viruses. MrNV, for instance, has been shown to target fucosylated N-glycans in the gills of freshwater prawns [65]. WSSV, one of the most devastating shrimp pathogens, exploits multiple glycan motifs: its envelope protein VP24 binds chitin (poly-GlcNAc) in the digestive tract, while VP37 interacts with sulfated glycosaminoglycans (GAGs) on hemocytes [66,67]. Both interactions play roles in determining the tissues WSSV can successfully infect. When we place IHHNV in this broader context, a pattern begins to emerge. Viruses that infect crustaceans often exploit carbohydrate motifs that are abundant in exposed epithelial or immune-related tissues. Gills, cuticle, and gut epithelia are repeatedly highlighted across different host–pathogen pairs. These tissues serve as natural interfaces with the environment and are rich in structurally diverse glycans, including chitin, mannose-rich N-glycans, and sulfated GAGs. From an evolutionary perspective, viruses appear to have converged on these glycans as reliable cues for host entry.Another interesting point of comparison is the degree of conservation of glycan motifs across species. Both *P. vannamei* and *M. rosenbergii* display fucosylated N-glycans in their gills, and both are targeted

by viruses that exploit these glycans. This raises the possibility that fucosylated N-glycans may serve as a conserved viral attachment factor among crustaceans more broadly. At the same time, the presence of mannose- and fucose-containing glycans in vertebrates, including humans [40], without conferring susceptibility to shrimp viruses like IHHNV, underlines that glycan recognition is necessary but not sufficient for productive infection [23, 59].

It is essential to emphasize that while glycans serve as critical attachment points, they are not the sole determinants of host specificity. The fact that vertebrate cells display similar glycan motifs but are not permissive for IHHNV infection illustrates the requirement for additional host-specific factors. In parvoviruses, these secondary factors often include protein receptors that trigger conformational changes necessary for viral uncoating. For example, adeno-associated virus serotypes can attach to glycans but require integrins or growth factor receptors for successful entry [22].

In the case of IHHNV, our data suggest that high-mannose and fucosylated glycans act as the first docking sites. However, the far-Western blot showing VLP binding to multiple protein bands hints at a more complex entry mechanism involving glycoproteins. Whether these proteins act as bona fide entry receptors or as scaffolds for viral clustering remains an open question. Further proteomic work will be necessary to identify the proteins that carry the glycan moieties recognized by IHHNV.

One question that naturally arises is why viruses such as IHHNV have evolved to target glycans as part of their infection strategy. Glycans are abundant, structurally diverse, and tissue-specific [73]. They provide viruses with a reliable way to distinguish between different host tissues and cell types. For viruses that lack large genomes or complex entry machinery, using glycans as

attachment factors may be a cost-effective solution. Parvoviruses, including IHHNV, fit this description well: they are small, non-enveloped viruses with limited coding capacity, and they rely heavily on host cell factors to complete their life cycle.

The downside of targeting glycans is that these molecules are not unique to shrimp; they are also found in other organisms. As mentioned earlier, similar structures exist in many organisms, which could lead to off-target interactions. The fact that IHHNV is restricted to crustaceans despite the widespread presence of mannose and fucose suggests that additional host-specific features possibly protein co-receptors or intracellular compatibility act as barriers to cross-species infection. This dual requirement of glycan docking and host-specific entry factors may serve as a safeguard, preventing shrimp viruses from spreading to non-crustacean hosts.

In summary, our results clearly demonstrate that the tissue tropism of IHHNV in *P. vannamei* is closely related to the glycan composition of shrimp tissues, with high-mannose and fucosylated N-glycans playing key roles as attachment factors. This mechanism aligns with a broader pattern seen in crustacean virology, where viruses target carbohydrate motifs common in epithelial and immune tissues. However, glycans do not tell the whole story; protein receptors and downstream cellular factors are likely to play essential roles. The implications of this work extend from molecular virology to practical aquaculture and even evolutionary biology. Understanding the role of glycans not only helps explain why specific tissues are infected while others are spared, but it also provides potential targets for developing antiviral agents and strategies. Future work should build on this foundation by identifying the specific glycoproteins involved, testing glycan-blocking compounds in aquaculture settings, and integrating glycomic data with proteomic and genomic approaches to deepen understanding.

2. Glycan recognition mechanisms in shrimp versus vertebrate systems

One of the notable aspects of this study is how the IHHNV–shrimp interaction resembles but also differs from glycan-mediated viral infections in vertebrates. In mammals, viruses ranging from influenza A to parvoviruses have long been known to use glycans as attachment factors. Influenza, for example, exploits sialic acid residues on respiratory epithelial cells. Avian strains prefer to bind α2,3-linked sialic acids, while human-adapted strains target α2,6 linkages [69]. This single difference in glycan linkage preference explains why avian influenza strains infect birds more effectively than humans, and why occasional cross-species infections can happen.

Similarly, parvovirus B19 uses the blood group P antigen (globoside), a glycosphingolipid abundant on human erythroid progenitors, to initiate infection [37]. Adeno-associated virus serotypes, which are non-pathogenic dependoparvoviruses, rely on heparan sulfate proteoglycans and sialylated glycans as their initial receptors [22, 36]. In all of these cases, glycans provide the virus with a convenient “handle” to attach to host cells. However, entry and productive infection almost always require additional protein receptors [73].

The situation with shrimp appears to follow a comparable logic. Our data show that IHHNV-VLPs bind mannose- and fucose-rich glycans in gill and muscle tissue, but hepatopancreas, which lacks these motifs, is largely resistant. Just as sialic acid linkages guide influenza tropism, the distribution of mannose and fucose residues in shrimp tissues appears to dictate where IHHNV can attach [74]. Yet, as we also observed, binding alone does not equal infection. The far-Western blot evidence points toward involvement of specific glycoproteins, suggesting that IHHNV may require a secondary receptor perhaps analogous to integrins, transferrin receptors, or other cell-surface proteins that parvoviruses use in vertebrates [75]. This

comparative approach is important because it shows that, despite the evolutionary gap between crustaceans and vertebrates, viruses in both groups have developed a similar two-step entry process: glycans for initial attachment and proteins for triggering entry. This similarity highlights the evolutionary value of glycans: they are plentiful, easy to access, and differ across tissues and species, giving viruses a simple yet effective way to establish host specificity [68].

The exact sequence of events during IHHNV entry still needs clarification, but our findings allow us to hypothesize based on similarities with other viruses. The initial step likely involves low-affinity, high-avidity binding of the viral capsid to multiple host glycans [24]. Our far-Western blotting results, showing interactions with multiple protein bands, suggest that IHHNV could interact with a variety of glycoprotein complexes rather than a single, defined receptor. The possibility that IHHNV recognizes both glycans and proteins cooperatively could explain why tissue tropism is precise even though glycans like mannose and fucose are widely distributed across many organisms. Future studies should focus on identifying these protein partners. Glycoprotein enrichment, followed by mass spectrometry and combined with CRISPR/Cas knockdown in shrimp cell lines (if such systems can be established), may help reveal host factors beyond glycans [76]. Without this additional layer of understanding, the complete picture of IHHNV entry remains elusive.

3. **Disease management implications**

From an applied perspective, these findings offer several interesting possibilities for disease management in shrimp aquaculture. If glycans play a crucial role in the early stages of viral infection, then strategies that disrupt glycan–virus interactions could potentially reduce the risk of infection. This concept is not new in virology: in human medicine, glycan-mimetic inhibitors and

lectins have been explored as antiviral agents against HIV, influenza, and noroviruses (87,88). For example, griffithsin (GRFT) and cyanovirin-N (CV-N) can neutralize HIV by binding to high-mannose glycans on the viral envelope [77].

Translating this approach to shrimp, one could envision testing whether glycan-blocking compounds reduce IHHNV binding to tissues in vitro. Indeed, sulfated galactans from *Gracilaria fisheri* have been shown to enhance shrimp resistance to WSSV [70], which aligns with the VP37–heparin binding mechanism described for that virus [67]. Similarly, exogenous lectins or glycan-mimicking compounds could be tested against IHHNV [56, 57]. However, such strategies would need to be carefully evaluated for toxicity, since glycans are also essential for normal host physiology. The broader implication is that glycan-focused approaches could complement existing biosecurity and selective breeding measures. They may not replace traditional strategies, but could serve as additional lines of defense, especially in hatcheries where preventing early-stage infections is critical. Understanding the glycan dependence of IHHNV infection has important implications for shrimp aquaculture. Shrimp farming, especially of *P. vannamei*, has experienced repeated disease outbreaks, with viral pathogens being some of the main causes of losses. Biosecurity measures, like water treatment, virus-free broodstock, and strict farm hygiene, are currently the main strategies used. However, once viruses enter a system, there are few, if any, treatment options. Glycan-targeted strategies might open new avenues for intervention. One option is developing feed additives that block viral binding. For instance, polysaccharides from seaweeds, such as sulfated galactans, have already been shown to protect shrimp against WSSV [54,55,61]. Similar methods could be tested against IHHNV, using compounds that either imitate mannose/fucose structures or competitively prevent viral capsids from attaching to host glycans.

Another option is selective breeding. If genetic variation exists in glycosylation pathways among *P. vannamei* populations, it may be possible to identify shrimp lines with lower expression of glycans targeted by IHHNV. Such traits could be incorporated into breeding programs alongside other disease-resistance characteristics [78]. The main challenge will be balancing viral resistance with the essential roles of glycans in shrimp physiology, including development and immunity [42,47,68]. Unlike single-gene traits, glycosylation is a complex and often pleiotropic process, making selective breeding more challenging [68]. Feed-based modulation of glycosylation presents another theoretical approach. In vertebrates, diet can influence glycosylation patterns by altering the availability of sugar precursors and metabolic pathways [79,80]. While the impact of similar dietary interventions on glycosylation in shrimp remains largely unexplored, it represents a promising area for future research. For instance, supplementation with mannose analogs or inhibitors of fucosylation could theoretically reduce the number of viral binding sites. However, the safety and feasibility of such approaches require careful evaluation. Despite these challenges, glycan-targeted strategies could complement existing biosecurity measures. For example, hatcheries might test prophylactic treatments based on glycan-blocking compounds during early larval stages when shrimp are particularly vulnerable to infection [54,55,61,70]. Farms could integrate such approaches with pathogen-free broodstock and improved diagnostic monitoring. By expanding the available tools for disease management, the industry may reduce its reliance on single strategies that often fail under sustained pressure. The knowledge gained from this study also supports ongoing efforts to enhance diagnostic tools. If IHHNV specifically recognizes mannose and fucose residues, assays that detect alterations in glycan expression could serve as early indicators of susceptibility in shrimp populations. For instance, lectin-based diagnostics could be developed to screen broodstock for glycan profiles linked to high or low susceptibility to

IHHNV [40,41,81]. This would help hatcheries make informed decisions about breeding lines, providing an extra layer of protection against outbreaks.

The discovery that IHHNV interacts primarily with mannose- and fucose-rich glycans in *P. vannamei* fits into a broader evolutionary narrative: viruses across diverse taxa have repeatedly converged on glycans as attachment factors. This convergence is remarkable because viruses are typically highly diverse in terms of structure, genome organization, and replication strategies. Yet, from influenza viruses in birds and humans to nodaviruses and parvoviruses in crustaceans, glycans consistently appear as favored entry points [25,73, 82]. From an evolutionary perspective, the explanation is simple. Glycans are universal. Every cell in every organism is covered with a dense layer of glycan structures, forming what is often called the “glycocalyx.” These structures are not random; they reflect both genetic programming and environmental factors. Importantly for viruses, glycans systematically vary between tissues, developmental stages, and species. This variation provides viruses with a ready-made molecular “barcode” that can be used to identify suitable host cells [25,73].

In the case of IHHNV, targeting mannose- and fucose-rich glycans in gills and muscle provides a reliable route to ectodermal and mesodermal tissues. This strategy is evolutionarily advantageous: gills are continuously exposed to the environment and present accessible carbohydrate structures [40,63], while muscle offers a large biomass for viral replication once infection is established. In contrast, endodermal tissues such as the hepatopancreas exhibit distinct structural and glycan compositions, which may reduce viral attachment efficiency and contribute to lower susceptibility [11,15]. This pattern mirrors observations in vertebrate viruses. Influenza viruses, for example, rely on sialic acid linkages, where subtle differences in glycan specificity can

drive major shifts in host range [26–28]. Similarly, parvoviruses demonstrate strong links between receptor recognition and tissue tropism; the emergence of canine parvovirus involved adaptation to host transferrin receptors, highlighting how receptor usage shapes host specificity. These parallels suggest that, despite the evolutionary distance between crustaceans and vertebrates, viruses are shaped by similar selective pressures. The repeated targeting of glycans reflects their accessibility, diversity, and tissue specificity, making them ideal molecular cues for viral attachment and entry."

4. Cross-species considerations: why glycans are shared but infection is not

A key puzzle in glycan-based viral recognition is the paradox of conservation. Mannose, fucose, GlcNAc, and sulfated glycosaminoglycans (GAGs) are not unique to shrimp but are widely distributed across metazoans, including vertebrates [68]. Yet shrimp viruses such as IHHNV and WSSV show no capacity to infect vertebrate hosts. This apparent contradiction can be explained by the layered nature of virus entry. Glycans typically function as initial attachment factors, concentrating virions on the cell surface through low-affinity, high-avidity interactions [21,59]. However, productive infection generally requires subsequent engagement with specific protein receptors as well as compatibility with host intracellular machinery [21,23]. In the case of IHHNV, our far-Western blot data indicate that the virus interacts with glycoproteins in addition to glycans, suggesting a cooperative recognition mechanism involving both carbohydrate and protein components. These protein factors are likely to be shrimp- or crustacean-specific, thereby restricting viral entry and replication to compatible hosts. This type of multi-layered host restriction is well documented in virology, where receptor usage and intracellular compatibility jointly determine host range and prevent cross-species transmission [23].

This layered dependency is similar to what is observed in other viral systems. Human parvovirus B19, for instance, attaches to the P antigen, which is also present in other mammals. However, productive infection occurs almost exclusively in human erythroid progenitors because secondary receptors and intracellular factors are species-restricted [37]. Similarly, avian influenza viruses can bind to human epithelial cells that display α2,3-linked sialic acids, but efficient replication requires additional host compatibility factors that are often absent [71]. In shrimp, the presence of mannose- and fucose-containing glycans in vertebrates does not imply susceptibility to IHHNV. The absence of compatible protein receptors and intracellular replication machinery likely prevents the virus from crossing into non-crustacean hosts [23]. This has important implications for biosecurity and public perception. While the aquaculture industry is concerned about the spread of viruses between shrimp species, there is no realistic risk of transmission to humans or other vertebrates, despite superficial similarities in glycan landscapes. The repeated observation that crustacean viruses exploit glycans raises the question of why these structures are such attractive evolutionary targets. One explanation is accessibility. Unlike protein receptors, which may be masked or expressed at low levels, glycans form a dense and exposed glycocalyx on the cell surface [68]. Viruses with small genomes, such as parvoviruses and nodaviruses, have limited coding capacity and therefore rely heavily on host cell factors for entry and replication [23]. Targeting glycans provides a simple yet effective strategy for initial attachment and host recognition.

Another possibility is stability. Glycan biosynthesis pathways are essential for host survival and are therefore less likely to undergo disruptive mutations compared to many protein receptors [68]. For viruses, this stability provides a relatively consistent target for attachment [25]. In contrast, protein receptors involved in immune recognition often evolve rapidly under selective

pressure, making them less reliable for long-term viral adaptation [26]. However, reliance on glycans also presents challenges for viruses. Because glycans are widely distributed across tissues and species, viruses must employ additional mechanisms to avoid non-permissive interactions. Glycan binding alone is typically insufficient for productive infection and must be coupled with specific protein receptors and compatible intracellular environments [21,23]. In the case of IHHNV, the virus does not bind indiscriminately to all glycan-rich tissues but instead shows specificity for gills and muscle while largely avoiding the hepatopancreas. This specialization likely reflects coevolutionary dynamics, where viruses adapt to target glycans that are abundant in accessible tissues yet associated with host factors that support replication. Comparative evidence supports this view. MrNV has been shown to target fucosylated N-glycans in freshwater prawn gills [65], while WSSV exploits multiple glycan interactions across host tissues, including chitin in the gut and sulfated glycosaminoglycans on hemocytes [66,67]. Each virus appears to have refined its glycan specificity through evolutionary selection to align with its replication strategy. The result is a landscape in which crustacean viruses differ in their specific glycan preferences but share a common reliance on carbohydrate-mediated attachment.

The evolutionary interaction between shrimp and their viruses can also be viewed from the host perspective. Glycans are not static features but are shaped by host genetics and environmental influences [68]. Shrimp populations under viral pressure may gradually alter glycan expression patterns in ways that reduce susceptibility, analogous to the evolution of resistance-associated variants in protein receptors in vertebrates. One possible mechanism is variation in glycosylation enzymes across shrimp populations, which can lead to subtle differences in glycan composition and structure [79]. Over time, natural selection or aquaculture breeding programs could favor variants that reduce viral binding, contributing to the development of more resilient stocks [78].

However, viruses may adapt in response by altering their capsid binding specificities, leading to a dynamic coevolutionary process. Such host–virus arms races are well documented in vertebrate systems, where reciprocal adaptation drives diversification of both host defenses and viral entry mechanisms [83]. Although less studied in crustaceans, similar dynamics are likely to occur. Cross-species comparisons among crustaceans provide additional insight. The presence of fucosylated glycans in the gills of both *P. vannamei* and *M. rosenbergii* suggests that this trait is evolutionarily conserved, likely due to its essential physiological roles [68]. Viruses such as IHHNV and MrNV have independently adapted to exploit these conserved glycan features, indicating convergent evolution toward carbohydrate-mediated attachment strategies [65]. However, differences in secondary receptors and intracellular host factors likely explain why each virus remains restricted to its specific host species.

Overall, the comparative and evolutionary perspective shows that while glycans are common across organisms, viruses such as IHHNV exploit them in highly specific ways shaped by coevolution with their hosts [73]. Glycan usage presents both an opportunity and a constraint for viruses: it provides abundant and relatively stable attachment points but also requires precise adaptation to avoid non-permissive interactions [21,23]. For hosts, glycans are essential components of cellular function, making large-scale alterations costly; however, subtle variations in glycosylation may still influence susceptibility to infection [73]. By placing IHHNV within this broader evolutionary framework, we gain insight into why tissue tropism and host specificity are structured as they are. The virus's preference for mannose- and fucose-rich glycans in gills and muscle reflects a recurring pattern observed across viral systems, from crustaceans to vertebrates. At the same time, the inability of IHHNV to infect vertebrates underscores the importance of

secondary, host-specific factors, such as protein receptors and intracellular compatibility, in defining viral host range.

Conclusion

This thesis clarifies how IHHNV initially connects with the Pacific white shrimp (*Penaeus vannamei*). A safe virus-like particle (VLP) made from the IHHNV capsid was produced and quality-checked, then used to study where and how it binds. The strongest binding occurred in gill and muscle; hepatopancreas and stomach showed weaker signals. Binding to Sf9 insect cells was also observed, suggesting some features are shared across species. Far-Western blots revealed several bands in the gill and muscle, indicating that more than one host glycoprotein is likely involved. Lectin tests were consistent: ConA (mannose), AAL (fucose), and WGA (GlcNAc) produced clear signals, while UEA-I and SNA-I were weak. When surface sugars were removed or altered (using PNGase F, alpha-mannosidase, alpha-fucosidase, or periodate), VLP binding decreased. Pre-incubating the VLP with simple sugars also reduced binding in a tissue-dependent manner. Mass spectrometry supported these findings by showing many high-mannose N-glycans, core fucosylation, and fucosylated O-glycans, especially in the gill. Overall, the data support a glycan-mediated, multivalent attachment model: mannose-, fucose-, and GlcNAc-rich motifs act as the main target for IHHNV-VLP. This suggests practical options for hatcheries—such as sugar decoys, safe seaweed polysaccharides, or gentle surface blockers—and outlines the next steps: identifying the exact host ligands and protein receotir involved, as well as testing these measures under farm conditions.

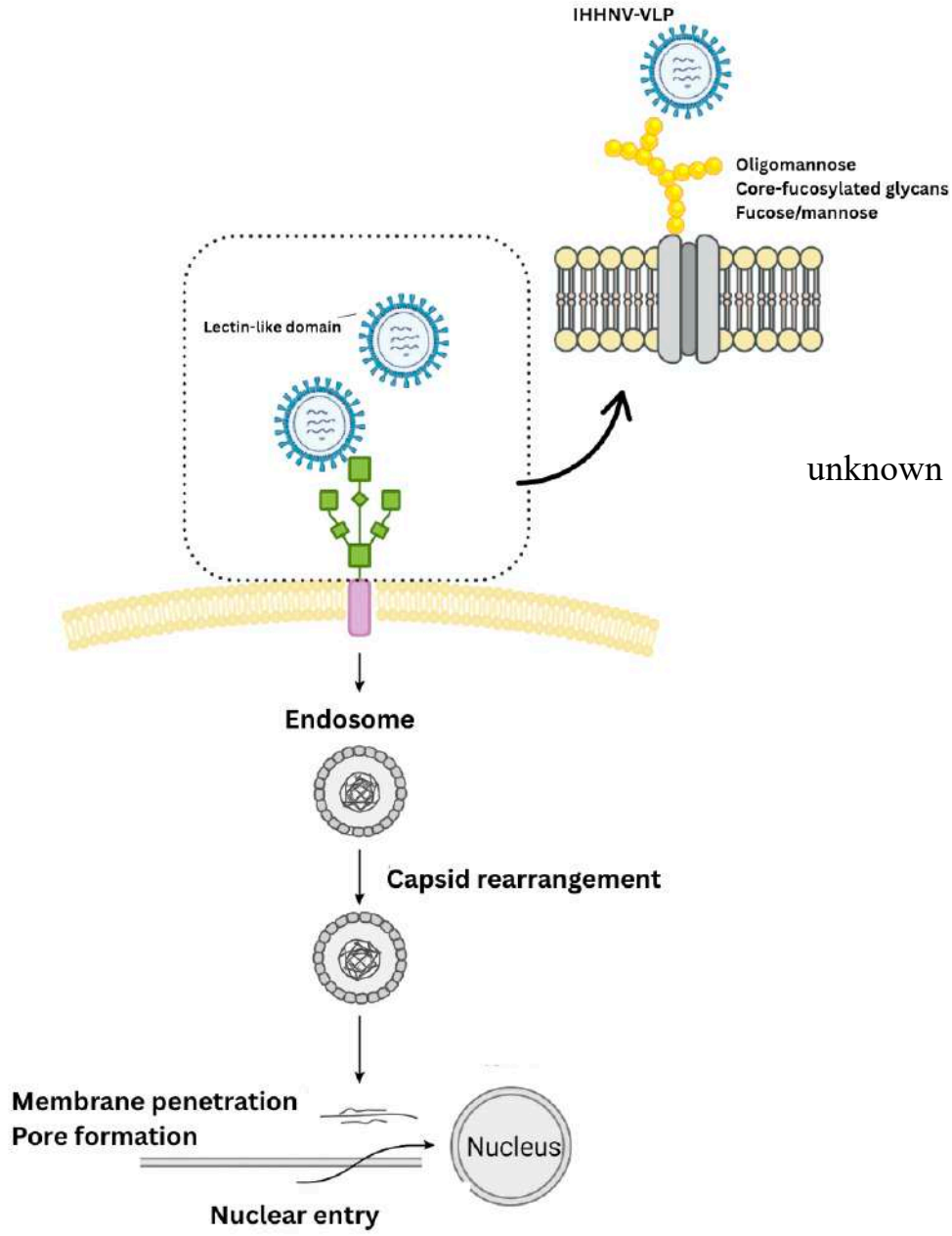

Figure 6.1 Schematic representation of glycan-mediated interactions between IHHNV-VLP and the host cell. Mannose- and fucose-containing glycans are proposed as the primary docking or attachment targets for IHHNV-VLP. The specific protein receptors required for viral internalization and subsequent replication remain to be identified.

References

1. FAO. The State of World Fisheries and Aquaculture 2024. Rome: Food and Agriculture Organization of the United Nations; 2024.
2. Stentiford GD, Sritunyalucksana K, Flegel TW, Williams BA, Withyachumnarnkul B, Itsathitphaisarn O, et al. New paradigms to help solve the global aquaculture disease crisis. PLoS Pathog. 2017;13(2):e1006160.
3. Vega-Heredia S, Mendoza-Cano F, Sánchez-Paz A. The infectious hypodermal and haematopoietic necrosis virus: a brief review of what we do and do not know. Transbound Emerg Dis. 2012;59(1):95–105.
4. Aranguren-Caro LF, Martinez-Cifuentes MA, Salmon-Mulanovich G, Palacios-Espinoza A, Gomez del Prado-Rosales C, Wille M, et al. Current status of infection with infectious hypodermal and hematopoietic necrosis virus (IHHNV) in the Peruvian and Ecuadorian shrimp industry. PLoS One. 2022;17(8):e0272456.
5. Tassanakajon A, Somboonwiwat K, Supungul P, Tang S. Discovery of immune molecules and their crucial functions in shrimp immunity. Fish Shellfish Immunol. 2013;34(4):954–67.
6. Amparyup P, Charoensapsri W, Tassanakajon A. Prophenoloxidase system and its role in shrimp immune responses against major pathogens. Fish Shellfish Immunol. 2013;34(4):990–1001.
7. Dhar AK, Roux MM, Klimpel KR. Functional characterization of putative promoter elements from infectious hypodermal and hematopoietic necrosis virus (IHHNV) in shrimp and in insect and fish cell lines. Virus Res. 2007;127(1):1–8.

8. Dhar AK, Lakshman DK, Natarajan S, Allnutt FCT, van Beek NAM. Detection and quantification of infectious hypodermal and hematopoietic necrosis virus and white spot virus in shrimp using real-time quantitative PCR and SYBR Green chemistry. J Clin Microbiol. 2001;39(8):2835–45.
9. Aiamsa-at P, Sunantawanit S, Chumroenvidhayakul R, Nakarin F, Sanguanrat P, Sritunyalucksana K, Chaijarasphong T. A novel dual CRISPR-Cas assay for detection of infectious hypodermal and hematopoietic necrosis virus (IHHNV) in penaeid shrimp without false positives from its endogenous viral elements (EVEs). Aquaculture. 2025;595:741452.
10. Lee C, Heo S, Park H, Lee WJ, Kwon MG, Soh H, et al. Detection of infectious hypodermal and hematopoietic necrosis virus (IHHNV, Decapod penstylhamaparvovirus 1) in commodity red claw crayfish (Cherax quadricarinatus) imported into South Korea. J Mar Sci Eng. 2021;9(8):856.
11. Hou ZH, Dong X, Liu L, Liu Z, Zhang X. Study of infectious hypodermal and hematopoietic necrosis virus (IHHNV) infection in different organs of Penaeus vannamei. J Fish Dis. 2023;46(9):1545–55.
12. Pénzes JJ, de Souza WM, Agbandje-McKenna M, Gifford RJ. Reorganizing the family Parvoviridae: a revised taxonomy independent of the canonical approach based on host association. Arch Virol. 2020;165(9):2133–46.
13. International Committee on Taxonomy of Viruses (ICTV). Parvoviridae: taxonomic release notes (2023/2024). London: ICTV; 2024.
14. USDA APHIS. IHHNV Pathways Assessment. Riverdale, MD: United States Department of Agriculture, Animal and Plant Health Inspection Service; 2022.

15. Arbon PM, O'Sullivan M, Landos M, Lyons R, Snow M. Determining patterns of tissue tropism for IHHNV, GAV and DIV1 in Penaeus monodon. Aquaculture. 2024;580:740657.
16. Xu F, Meng X, Wang Y, Shen J, Li J, Sun Y, et al. Prevalence of infectious hypodermal and hematopoietic necrosis virus (IHHNV) in farmed Procambarus clarkii of the middle and lower reaches of the Yangtze River in China. Pathogens. 2023;12(8):1038.
17. Bonami JR, Trumper B, Mari J, Brehelin M, Lightner DV. Purification and characterization of the infectious hypodermal and hematopoietic necrosis virus of penaeid shrimps. J Gen Virol. 1990;71(Pt 12):2657–64.
18. Dhar AK, Kaizer KN, Lakshman DK. Transcriptional analysis of Penaeus stylirostris densovirus genes. Virology. 2010;402(1):112–20.
19. Robles-Sikisaka R, Bohonowych J, McCaffrey K, Dhar AK. Genome sequence analysis of three Penaeus stylirostris densovirus (PstDNV) isolates. PLoS One. 2010;5(8):e11799.
20. Yang N, Wang L, Liu H, Qin C, Yang X, Yi G, et al. Transcriptome analysis of IHHNV infection in Penaeus vannamei at different developmental stages. Fish Shellfish Immunol. 2022;128:194–203.
21. Marsh M, Helenius A. Virus entry: open sesame. Cell. 2006;124(4):729–40.
22. Stencel-Baerenwald JE, Reiss K, Reiter DM, Stehle T, Dermody TS. The sweet spot: defining virus–glycan interactions. Nat Rev Microbiol. 2014;12(11):739–49.
23. Cotmore SF, Tattersall P. Parvoviruses: small but mighty. Annu Rev Virol. 2014;1:517–37.
24. Mammen M, Choi SK, Whitesides GM. Polyvalent interactions in biological systems: implications for design and use of multivalent ligands and inhibitors. Angew Chem Int Ed. 1998;37(20):2754–94.

25. Thompson AJ, de Vries RP, Paulson JC. Virus recognition of glycan receptors. Curr Opin Virol. 2019;34:117–29.

26. Long JS, Mistry B, Haslam SM, Barclay WS. Host and viral determinants of influenza A virus species specificity. Nat Rev Microbiol. 2019;17(2):67–81.

27. Yamada S, Suzuki Y, Suzuki T, Le MQ, Nidom CA, Sakai-Tagawa Y, et al. Haemagglutinin mutations responsible for the binding of H5N1 influenza A viruses to human-type receptors. Nature. 2006;444(7117):378–82.

28. Xu R, McBride R, Paulson JC, Basler CF, Wilson IA. Structure, receptor binding, and antigenicity of influenza hemagglutinin. J Virol. 2010;84(7):3110–7.

29. Shriver Z, Raman R, Viswanathan K, Khan AA, Sasisekharan V, Sasisekharan R. Context-specific target definition in influenza A virus hemagglutinin–glycan receptor interactions. Cell Chem Biol. 2009;16(6):674–83.

30. Doores KJ. The HIV glycan shield as a target for broadly neutralizing antibodies. Nat Rev Microbiol. 2015;13(11): 815–28.

31. Mouquet H, Scharf L, Euler Z, Liu Y, Eden C, Scheid JF, et al. Complex-type N-glycan recognition by potent broadly neutralizing HIV antibodies. Proc Natl Acad Sci U S A. 2012;109(47):E3268–77.

32. Julien JP, Sok D, Khayat R, Lee JH, Doores KJ, Walker LM, et al. Broadly neutralizing antibody PGT121 allosterically modulates CD4 binding via recognition of the HIV-1 gp120 N332 glycan. PLoS Pathog. 2013;9(5):e1003342.

33. Connell BJ, Lortat-Jacob H. Human immunodeficiency virus and heparan sulfate: from attachment to entry inhibition. Front Immunol. 2013;4:385.

34. Tan M, Jiang X. Norovirus and its histo-blood group antigen receptors: an answer to a historical puzzle. Trends Microbiol. 2005;13(6):285–93.

35. Cao S, Lou Z, Tan M, Chen Y, Liu Y, Zhang Z, et al. Structural basis for the recognition of blood group trisaccharides by norovirus. J Virol. 2007;81(11):5949–57.

36. Summerford C, Samulski RJ. Membrane-associated heparan sulfate proteoglycan is a receptor for adeno-associated virus type 2 virions. J Virol. 1998;72(2):1438–45.

37. Brown KE, Anderson SM, Young NS. Erythrocyte P antigen: cellular receptor for B19 parvovirus. Science. 1993;262(5130):114–7.

38. Nam HJ, Gurda-Whitaker B, Gan WY, Ilaria S, McKenna R, Mehta P, et al. Identification of the sialic acid structures recognized by minute virus of mice and the role of binding affinity in virulence adaptation. J Biol Chem. 2006;281(36):25670–7.

39. Kaufmann B, Simpson AA, Rossmann MG. The structure of human parvovirus B19. Proc Natl Acad Sci U S A. 2004;101(32):11628–33. (plus related MVM glycan-binding site mapping in: Kaufmann B, et al. J Virol. 2007;81(11): 5890–98)

40. Blixt O, Head S, Mondala T, Scanlan C, Huflejt ME, Alvarez R, et al. Printed covalent glycan array for ligand profiling of diverse glycan-binding proteins. Proc Natl Acad Sci U S A. 2004;101(49):17033–8.

41. Meyer B, Peters T. NMR spectroscopy techniques in glycobiology and glycomics. Chem Rev. 2003;103(2): 567–600.

42. Wang X-W, Wang J-X. Diversity and multiple functions of lectins in shrimp immunity. Fish Shellfish Immunol. 2013;34(4): 1217–27.

43. Vasconcelos AA, Pomin VH, Pereira MS, Mulloy B, Mourão PAS. The sea as a rich source of structurally unique glycosaminoglycans and mimetics. Mar Drugs. 2017;15(10):327.
44. Faria-Ramos I, Bessa LJ, Palmeira-de-Oliveira A, et al. Heparan sulfate glycosaminoglycans: (un)expected allies in infection. Biomolecules. 2021;11(2):136.
45. Kiatmetha P, Chotwiwatthanakun C, Jariyapong P, Santimanawong W, Ounjai P, Weerachatyanukul W. Nanocontainer designed from an infectious hypodermal and hematopoietic necrosis virus (IHHNV) has excellent physical stability and ability to deliver shrimp tissues. PeerJ. 2018;6:e6079.
46. Wang X-W, Wang J-X. The functional relevance of shrimp C-type lectins in host-pathogen interactions. Immunol Lett. 2020;226: 45–56.
47. Betancourt JL, García-Carreño FL, Muhlia-Almazán A. Pattern recognition receptors in Crustacea: immunological sensors of the innate immune system. Front Immunol. 2024;15:1474512.
48. Mohsen MO, Zha L, Cabral-Miranda G, Bachmann MF. Virus-like particle vaccinology, from bench to bedside. Signal Transduct Target Ther. 2022;7: 279.
49. Hou L, Wu H, Xu L, Yang F. Expression and self-assembly of virus-like particles of infectious hypodermal and hematopoietic necrosis virus in Escherichia coli. Arch Virol. 2009;154(3):547–53.
50. Weerachatyanukul W, Pooljun C, Hirono I, Kondo H, Chotwiwatthanakun C, Jariyapong P. Infectious hypodermal and hematopoietic necrosis virus-like particle (IHHNV-VLP) induces peroxiredoxin expression and activity in Fenneropenaeus merguiensis. Fish

Shellfish Immunol. 2022;121:53–61. (Corrigendum: Fish Shellfish Immunol. 2024;142:108994.)

51. Roldão A, Mellado MCM, Castilho LR, Carrondo MJT, Alves PM. Virus-like particles in vaccine development. Expert Rev Vaccines. 2010;9(10):1149–76.
52. Zeltins A. Construction and characterization of virus-like particles: a review. Mol Biotechnol. 2013;53(1):92–107.
53. Pomin VH, Mourão PAS. Marine medicinal glycomics: an overview of the current status and future perspectives. Mar Drugs. 2014;12(4): 1676–710.
54. Wei Q, Lu Q, Yue S, Wang J. Advances in research on antiviral activities of sulfated polysaccharides from seaweeds. Mar Drugs. 2022;20(5):342.
55. Ray B, Abdel-Hafiz L, Kumar D, Sahu GK, Aalinkeel R, Mahajan SD. Antiviral strategies using natural source-derived sulfated polysaccharides and heparin mimetics. Viruses. 2021;13(1):35.
56. Yu M, Li C, Shin H, Park H. Elucidating the interactions between heparin/heparan sulfate and viruses: possible antiviral strategies. Front Mol Biosci. 2021;7:628551.
57. Hoffmann M, Pohl M, Ballauff M, Landfester K. Polymers inspired by heparin and heparan sulfate for viral inhibition. *Macromolecules*. 2022;55(17):7435–48.
58. Sun L, Hickey AC, Guo H, Linhardt RJ, Dordick JS. Well-defined heparin mimetics can inhibit binding of the SARS-CoV-2 spike protein to ACE2. *JACS Au*. 2023;3(5):1293–303.
59. De Pasquale V, Pavone LM. Heparan sulfate proteoglycans in viral infection and pathogenesis. Viruses. 2021;13(2): 244.
60. Crisci E, Barcena J, Montoya M. Virus-like particles: the new frontier of vaccines for animal viral infections. Vet Immunol Immunopathol. 2012;148(3–4):211–25.

61. Immanuel G, Sivagnanavelmurugan P, Babu MM, Palavesam A. The effect of fucoidan from brown seaweed Sargassum polycystum on the immune response of Penaeus monodon and its resistance to white spot syndrome virus. Fish Shellfish Immunol. 2012;32(6): 1137–44.
62. Liu Y, Cao X, Xu L, Zhang Y, Li J, Li C, et al. A novel C-type lectin from shrimp Litopenaeus vannamei involved in antiviral defense. J Virol. 2009;83(20): 10185–96.
63. Bell TA, Lightner DV. A handbook of normal penaeid shrimp histology. Baton Rouge (LA): World Aquaculture Society; 1988.
64. Wagh K, Seaman MS, Zingg M, Fitzsimons T, Gnanakaran S, Labranche C, et al. Completeness of HIV-1 envelope glycan shield at transmission determines neutralization breadth. *Cell Rep*. 2018;25(4):893–908.e7.
65. Somrit M, Watthammawut A, Chaivisuthangkura P, Rukpratanporn S, Rojviriyapan N, Jitrapakdee S, et al. Macrobrachium rosenbergii nodavirus (MrNV) VP53 capsid protein binds specifically to shrimp hepatopancreatic glycans. J Gen Virol. 2020;101(2):207–17.
66. Li S, Meng H, Xie X, Zhang R, Zhang Y, Xu J, et al. Identification of white spot syndrome virus VP24 binding to shrimp chitin. J Gen Virol. 2016;97(12):3166–77.
67. Somsoros P, Yodmuang S, Wongprasert K. White spot syndrome virus VP37 interacts with sulfated glycosaminoglycans in shrimp hemocytes. J Gen Virol. 2021;102(4):001582.
68. Varki A, Cummings RD, Esko JD, et al., editors. Essentials of Glycobiology. 3rd ed. Cold Spring Harbor (NY): Cold Spring Harbor Laboratory Press; 201
69. Matrosovich M, Matrosovich T, Gray T, Roberts NA, Klenk H-D. Human and avian influenza viruses target different cell types in cultures of human airway epithelium. Proc Natl Acad Sci U S A. 2004;101(13):4620–4.

70. Wongprasert K, Rudtanatip T, Praiboon J. Immunostimulatory activity of sulfated galactans isolated from the red seaweed Gracilaria fisheri and development of resistance against white spot syndrome virus (WSSV) in shrimp. Fish Shellfish Immunol. 2014 Jan;36(1):52-60.
71. Taubenberger JK, Kash JC. Influenza virus evolution, host adaptation, and pandemic formation. Cell Host Microbe. 2010;7(6):440–51
72. Kaufmann B, Bowman VD, Li Y, Szelei J, Waddell PJ, Tijssen P, Rossmann MG. Structure of Penaeus stylirostris densovirus, a shrimp pathogen. J Virol. 2010 Nov;84(21):11289-96
73. Miller NL, Clark T, Raman R and Sasisekharan R (2021) Glycans in Virus-Host Interactions: A Structural Perspective. Front. Mol. Biosci. 8:666756
74. Byrd-Leotis L, Cummings RD, Steinhauer DA. The interplay between the host receptor and influenza virus hemagglutinin and neuraminidase. *Int J Mol Sci*. 2017;18(7):1541
75. Mercer J, Schelhaas M, Helenius A. Virus entry by endocytosis. *Annu Rev Biochem*. 2010;79:803–33
76. Puschnik AS, Majzoub K, Ooi YS, Carette JE. A CRISPR toolbox to study virus–host interactions. *Nat Rev Microbiol*. 2017;15(6):351–64
77. Boyd MR, Gustafson KR, McMahon JB, Shoemaker RH, O'Keefe BR, Mori T, et al. Discovery of cyanovirin-N, a novel HIV-inactivating protein. *J Biol Chem*. 1997;272(10):641–7
78. Houston RD, Bean TP, Macqueen DJ, Gundappa MK, Jin YH, Jenkins TL, et al. Harnessing genomics to fast-track genetic improvement in aquaculture. *Nat Rev Genet*. 2020;21(7):389–409
79. Stanley P. Golgi glycosylation. *Cold Spring Harb Perspect Biol*. 2011;3(4):a005199.

80. Freeze HH, Ng BG. Golgi glycosylation and human inherited diseases. *Cold Spring Harb Perspect Biol*. 2011;3(4):a005371

81. Hirabayashi J, Yamada M, Kuno A, Tateno H. Lectin microarrays: concept, principle and applications. *Chem Soc Rev*. 2013;42(10):4443–58

82. Springer SA, Gagneux P. Glycomics: revealing the dynamic ecology and evolution of sugar molecules. *J Proteomics*. 2016;135:90–100

83. Daugherty MD, Malik HS. Rules of engagement: molecular insights from host–virus arms races. *Annu Rev Genet*. 2012;46:677–700

84. Kiatmetha P, Chotwiwatthanakun C, Jariyapong P, Santimanawong W, Ounjai P, Weerachatyanukul W. Nanocontainer designed from an infectious hypodermal and hematopoietic necrosis virus (IHHNV) has excellent physical stability and ability to deliver shrimp tissues. *PeerJ*. 2018;6:e6079.

Appendix A. Extended Data Tables

1. **Table A1. An extended dataset of lectin–glycan specificity**

Tissue	Lectin	Mean_OD	SD_OD	N
Gill	UEA-I	0.224	0.054	3
Gill	aal	1.154	0.064	3
Gill	cona	1.411	0.021	3
Gill	rca	0.740	0.034	3
Gill	wga	1.684	0.110	3
Muscle	UEA-I	0.214	0.003	3
Muscle	aal	0.916	0.113	3
Muscle	cona	0.882	0.048	3
Muscle	rca	0.313	0.012	3
Muscle	wga	0.599	0.017	3
SF9	UEA-I	0.629	0.039	3
SF9	aal	0.824	0.052	3
SF9	cona	0.937	0.058	3
SF9	rca	0.207	0.011	3
SF9	wga	1.931	0.054	3

2. **Table A2. Raw ELISA absorbance values (IHHNV-VLP binding)**

Tissue	OD	Replicate
Hepatopancreas	0.300	1
Hepatopancreas	0.325	2
Hepatopancreas	0.254	3
Muscle	0.612	1
Muscle	0.685	2
Muscle	0.688	3
Gill	0.850	1
Gill	0.760	2
Gill	0.745	3
SF9	0.784	1
SF9	0.725	2
SF9	0.741	3

Appendix B. MALDI-MS Spectra

Table B1. N-glycan peak assignment table (Gill and Muscle)

m/z (Observed)	Composition	Annotation
2396.3	$Man_9GlcNAc_2$	$[M+Na]^+$, base peak
2192.2	$Man_8GlcNAc_2$	$[M+Na]^+$
1988.1	$Man_7GlcNAc_2$	$[M+Na]^+$
1784.0	$Man_6GlcNAc_2$	$[M+Na]^+$
1590.9	$Fuc_1Hex_3HexNAc_3$	Core fucosylated N-glycan

Table B2. O-glycan peak assignment table (Gill tissues)

m/z (Observed)	Composition	Annotation
953.4	$Fuc_1Hex_1HexNAc_1$-HexNAcitol	O-glycan
1127.5	$Fuc_2Hex_1HexNAc_1$-HexNAcitol	O-glycan

Appendix C. Experimental Protocols

i. *Molecular Cloning and Expression of IHHNV Capsid Proteins*

- The capsid gene (ORF3) of IHHNV was amplified using specific primers (see Appendix Table D1 for primer sequences and conditions).
- PCR amplicons were ligated into pGEM-T Easy vector and verified by sequencing.
- Verified ORF3 fragments were subcloned into pET-17b vector with a C-terminal hexahistidine tag.
- Recombinant plasmids were transformed into *E. coli* BL21 (DE3), and expression was induced with IPTG.

ii. *Protein Profiling by SDS–PAGE*

- Protein samples (10–20 µg) mixed with Laemmli buffer and heated at 95 °C for 5 min.
- Proteins resolved on 12.5% polyacrylamide gels.
- Coomassie Brilliant Blue used for staining.
- Broad-range prestained markers used for reference.

iii. *Transmission Electron Microscopy (TEM)*

- VLP suspensions (5–10 µl) placed on carbon-coated copper grids.
- Grids stained with 2% uranyl acetate.
- Images obtained using TEM at appropriate accelerating voltage.

iv. *ELISA Assays*

- 96-well plates coated with recombinant IHHNV-VLP (100 ng/well), incubated overnight at 4 °C.
- Wells blocked with 5% BSA in PBS.
- Tissue extracts or lectins added and incubated 1–2 h at room temperature.
- Detection with HRP-conjugated antibody or lectin; developed using TMB substrate.
- Absorbance recorded at 450 nm.

v. *Lectin Profiling and Blocking Assays*

- Lectins tested: ConA, RCA, PNA, WGA, SNA, MAL, UEA-I, AAL.
- Binding assays: Tissues or VLPs incubated with HRP-conjugated lectins; OD measured at 450 nm.
- Blocking assays: Samples pre-incubated with monosaccharides (mannose, galactose, fucose) prior to lectin binding.
- Binding inhibition calculated relative to untreated controls.

vi. *Glycomics and MALDI-MS Analysis*

- **N-glycans:** Released by PNGase F digestion.
- **O-glycans:** Released by reductive β-elimination.
- Purified using C18 cartridges before MS analysis.
- Spectra acquired in positive-ion mode with DHB matrix.
- Peak assignments based on theoretical glycan libraries; intensities normalized to base peak.

vii. *Enzymatic Digestion Stability Tests*

- Enzymes: Trypsin, chymotrypsin, pepsin.
- Conditions: 30 mU enzyme, 37 °C, in appropriate buffer (TBS pH 7.8 or citrate buffer pH 4.0).
- Products analyzed by SDS–PAGE; BSA used as digestion control.

viii. *Statistical Analysis*

- Data processed in Python (NumPy, Pandas, SciPy); visualized in GraphPad Prism or R.
- One-way ANOVA used for multi-group comparisons, followed by Dunnett's test ($\alpha = 0.05$).
- Results reported as mean ± SD; *p*-values indicated in figures and tables.